IMAGING THE NEUROMODULATION OF PAIN

Richard Lee-Tsong Lin

Nuffield Division of Anaesthestics
Nuffield Department of Clinical Neurosciences
University of Oxford

A thesis submitted in partial fulfillment of the requirements for the degree of Doctor of Philosophy

Balliol College
Trinity Term 2011

Imaging the Neuromodulation of Pain

Richard Lee-Tsong Lin
Candidate for the Degree of Doctor of Philosophy
Trinity Term 2011, Balliol College

Abstract

Chronic pain is a major health problem that affects approximately 20% of the adult population, but only 60% of its patients find success in managing their condition. As an alternative therapeutic tool, transcranial direct current stimulation (tDCS) has appeared promising in recent literature, with several papers using the left dorsolateral prefrontal cortex (L-DLPFC) as the stimulation target due to its inherent role in pain modulation. However, the underlying mechanisms of this treatment have never been directly investigated. The thesis intends to explore this question through the application of a combination of tDCS, functional and structural imaging, and an ongoing pain model.

The first study investigated the task-free effects of L-DLPFC tDCS by using concurrent arterial spin labeling (ASL) perfusion imaging. Anodal (excitatory) tDCS was associated with an increase in regional cerebral blood flow (rCBF) of L-DLPFC, while cathodal (inhibitory) tDCS was related to a relative decrease. Regions connected to L-DLPFC, such as thalamus and primary somatosensory cortex, also experienced significant perfusion changes. Further analyses found modulations of L-DLPFC–thalamic functional correlations, which was particularly relevant due to the importance of the thalamus in antinociceptive processing.

To understand pain neuromodulation, a robust ongoing pain model was required to serve as a platform for the investigation. Thus, electrical, thermal, and capsaicin stimuli were tested in a series of studies. The former two did not produce an ongoing pain sensation, thus failing to replicate a chronic pain experience on healthy volunteers. However, topical application of capsaicin appeared to induce such a response, which entailed a pain intensity rating between 5 and 7 on a 0-10 visual analogue scale for at least 30 minutes. Careful screening ensued to select capsaicin responders from the cohort, who served as the research volunteers for the remainder of the thesis.

Combining these two studies, rCBF changes associated with tDCS-induced pain neuromodulation were then directly investigated with concurrent ASL and the above capsaicin model. Behavioral measurements suggested a significant reduction in pain intensity for the anodal tDCS condition over the sham tDCS condition, which corroborated the results from previous pain-tDCS studies. Modulations of L-DLPFC and thalamic rCBF continued to be observed with anodal tDCS. In addition, the activity of the posterior insula, an indicator of ongoing pain intensity, was higher for the sham tDCS condition than for the anodal tDCS condition.

The final study explored the importance of L-DLPFC–thalamic connection in pain modulation with diffusion tensor imaging (DTI). Probability tractography and tract-based spatial statistics (TBSS) were used to extract the mean fractional anisotropy (FA) of the tract. As hypothesized, the mean FA values within this tract positively correlated with the pain intensity changes, which indicated that individuals with stronger structural connection enjoyed greater alleviation from L-DLPFC tDCS.

As a whole, the above studies suggest that the clinical efficacy of L-DLPFC tDCS in pain treatment may arise from the resulting top-down modulation of the thalamus. Further studies on chronic pain patients may offer further verification of the mechanism that has been proposed in this thesis.

This thesis contains approximately 34,000 words.

TABLE OF CONTENTS

Acknowledgements v
Abbreviations vi
List of Figures viii
Chapter 1 – Introduction 1
1.1 Motivation 1
1.2 Physiology and Neuroanatomy of Pain 2
1.2.1 Transduction 2
1.2.2 Transmission 2
1.2.3 Perception 4
1.2.4 Modulation 6
1.3 Pain and the Dorsolateral Prefrontal Cortex 9
1.3.1 Overview 9
1.3.2 Cognitive Studies 10
1.3.3 Clinical Studies 12
1.4 Chronic Pain 13
1.4.1 Overview 13
1.4.2 Epidemiology 16
1.4.3 Ongoing Pain Models 18
1.4.4 Changes in Brain Structure and Function 21
1.5 Treatments for Chronic Neuropathic Pain 24
1.6 Non-Invasive Neuromodulation 27
1.6.1 Transcranial Magnetic Stimulation 27
1.6.2 Transcranial Direct Current Stimulation 29
1.7 Pain and Brain Stimulation 30
1.7.1 Repetitive Transcranial Magnetic Stimulation 31
1.7.2 Transcranial Direct Current Stimulation 33
1.7.2 Transcranial Direct Current Stimulation 38
1.8 Theme 39
Chapter 2 – Methods 40
2.1 Perfusion fMRI with Arterial Spin Labeling 40
2.1.1 Basic Concept 40
2.1.2 Continuous Arterial Spin Labeling 42
2.1.3 Pulsed Arterial Spin Labeling 44
2.1.4 Pseudo-Continuous Arterial Spin Labeling 45
2.2 Transcranial Direct Current Stimulation 47
2.2.1 Overview 47
2.2.2 Local Effects 48
2.2.3 Distant Effects 50
Chapter 3 – Task-free Effects of Transcranial Direct Current Stimulation 53
3.1 Introduction 53
3.1.1 L-DLPFC tDCS 53
3.1.2 L-DLPFC rTMS 54
3.1.3 Overview 55
3.2 Methods 56
3.2.1 Subject Recruitment 56
3.2.2 Experiment Setup and Paradigm 56
3.2.3 Data Analysis 58
3.2.4 Electrode Location 60
3.2.5 Anatomical Masks 61

3.3 Results 62
3.3.1 Artefact Check *62*
3.3.2 Perfusion Activity During tDCS *62*
3.3.3 Correlation Analyses *64*
3.3.4 Perfusion Activity After tDCS *66*
3.3.5 Functional Differences Between Anodal and Cathodal tDCS *68*
3.4 Discussion 70
3.4.1 Perfusion Activity of L-DLPFC during tDCS *70*
3.4.2 Whole Brain rCBF Changes During tDCS *71*
3.4.3 L-DLPFC Functional Connectivity During tDCS *72*
3.4.4 Immediate Whole Brain rCBF Changes After tDCS *73*
3.4.5 Future Directions and Conclusions *74*
Chapter 4 – Models of Ongoing Pain **75**
4.1 Introduction 75
4.2 Electrical Stimuli 77
4.2.1 Methods *77*
4.2.2 Results *79*
4.3 Thermal Stimuli 80
4.3.1 Methods *80*
4.3.2 Results *81*
4.4 Capsaicin Model (Part I) 82
4.4.1 Methods *82*
4.4.2 Results *82*
4.5 Capsaicin Model (Part II) 84
4.5.1 Methods *84*
4.5.2 Results *85*
4.6 Discussion 86
Chapter 5 – Functional Imaging of Pain Modulation by Transcranial Direct Current Stimulation **88**
5.1 Introduction 88
5.2 Methods 90
5.2.1 Subject Recruitment *90*
5.2.2 Experiment Setup and Paradigm *90*
5.2.3 MRI Sequences *93*
5.2.4 Data Analysis *93*
5.2.5 Statistics *94*
5.2.6 Investigation of rCBF Changes Pre- and Post-Waiting Period *94*
5.3 Results 96
5.3.1 Ongoing Pain Model with Capsaicin *96*
5.3.2 Pain Ratings During tDCS-fMRI Experiments *97*
5.3.3 Questionnaire Results Between Anodal and Sham tDCS conditions *101*
5.3.4 Perfusion Activity During tDCS *102*
5.3.5 Perfusion Activity After tDCS *107*
5.3.6 Perfusion Activity Between Pre- and Post-Waiting Periods *108*
5.4 Discussion 110
5.4.1 Behavioral Changes in Pain Sensation *110*
5.4.2 Perfusion Changes Associated With tDCS *111*
5.4.3 Possibility of Cognitive-Behavioral Treatment *114*
5.4.4 Investigation of rCBF Changes Before and After Waiting Period *115*
5.4.5 Conclusion *116*

Chapter 6 – Correlation of Structural Connectivity and Pain Modulation Using Diffusion Tensor Imaging **117**
6.1 Introduction 117
6.2 Methods 121
6.2.1 Subject Recruitment *121*
6.2.2 Image Acquisition *121*
6.2.3 Image Analysis *121*
6.3 Results 127
6.3.1 Probability Tractography Between L-DLPFC and Thalamus *127*
6.3.2 Tract-Based Spatial Statistics *129*
6.3.3 Gray Matter Voxel-Based Morphometry *131*
6.4 Discussion 132
6.4.1 Probability Tractography and TBSS *132*
6.4.2 L-DLPFC–Thalamic Tract and Pain Modulation *133*
6.4.3 Conclusion *133*
Chapter 7 – Conclusion **135**
7.1 Overview of Thesis 135
7.2 Future Directions 139
7.2.1 Clinical Tests *139*
7.2.2 Roles of L-DLPFC and Thalamic Subdivisions *139*
7.2.3 Mechanism of M1 tDCS in Pain Modulation *139*
7.2.4 Current Modeling *140*
7.3 Final Conclusion 141
References **142**

ACKNOWLEDGEMENTS

A wise comic strip once taught me: in times of writer's block, "start with the acknowledgements" (Piled Higher and Deeper, 1999). While this mentality seemed to do injustice to the many who have offered me their time and effort, the suggested approach has actually allowed me to commit many hours (or perhaps days) on retrospections. No words can fully reflect my appreciation for those who have provided their assistance, and I hope they can accept my humble attempt to show my utmost gratitude.

To Irene, the most wonderful supervisor I could have wished for. A list of everything you have provided for me will surpass the word limit of this thesis, but thank you mostly for putting up with me from the very beginning. Your patience is absolutely unparalleled.

To Charlie, thank you for introducing me to the different stimulation toys and for instilling much rigor in my research. Without your impeccable scrutiny, I believe this thesis would be unreadable, both grammatically and scientifically.

To Tom and Jingyi, thank you for your guidance on the physics and analysis of ASL.

To Nico and Gwen, thank you for teaching me the intricacies of structural imaging.

To Andy, thank you for introducing me to capsaicin and other pain-inducing techniques. You are certainly the most dangerous man in the world.

To Joe, thank you for your invaluable technical assistance on literally everything.

To Katja and Asma, thank you for insightful feedbacks on the roles and localization of the prefrontal cortex.

To Stuart and Caroline, thank you for making my scans possible and for accommodating the many 8am sessions that my studies required.

To all my FMRIB friends, thank you for making me feel at home during my time here.

To the countless subjects, thank you for committing your time and body to science. My research would not have been possible without you.

To the Marshall Scholarship, while the financial assistance was valuable, I am most grateful for the wonderful friends that it has introduced me. They have helped me bear the unbearable and provided me with a crucial link to America.

To YH, wherever you are in the world right now, thank you for being yourself.

Lastly, to my parents, thank you for supporting my every endeavor, which always seemed to get more complicated and/or ambitious by the year.

Not everyone has the opportunity to study at a world-class institution and tourist attraction like Oxford. I hope my efforts here have continued the long tradition of academic excellence that its illustrious alumni have established before me.

Now back to thesis writing.

ABBREVIATIONS

ACC	Anterior Cingulate Cortex
ANOVA	Analysis of Variance
ART	Arterial Transit Time
ASL	Arterial Spin Labeling
BET	Brain Extraction Tool
BOLD	Blood Oxygen Level Dependent
BPD	Borderline Personality Disorder
CASL	Continuous Arterial Spin Labeling
CBF	Cerebral Blood Flow
CGI	Clinical Global Assessment
DOF	Degrees of Freedom
DLPFC	Dorsolateral Prefrontal Cortex
DRG	Dorsal Root Ganglia
DTI	Diffusion Tensor Imaging
EEG	Electroencephalography
EPI	Echo Planar Imaging
EPISTAR	Echo-Planar Imaging with Signal Targeting by Alternating RF Pulses
FAIR	Flow-sensitive Alternating Inversion Recovery
FEAT	FMRIB Expert Analysis Tool
FLIRT	FMRIB Linear Registration Tool
fMRI	Function Magnetic Resonance Imaging
fNIRS	Functional Near-Infrared Spectroscopy
FNIRT	FMRIB Non-linear Registration Tool
FSL	FMRIB Software Library
GABA	γ-Amino Butyric Acid
GLM	General Linear Model
GRAPPA	Generalized Autocalibrating Partially Parallel Acquisition
HbO_2	Oxyhemoglobin
HHb_2	Deoxyhemoglobin
HTM	High-Threshold Mechanoreceptors
L	Left
LT	Low-Threshold
M1	Primary Motor Cortex
MCC	Mid-Cingulate Cortex
MEP	Motor Evoked Potential
MNI	Montreal Neurological Institute
MRI	Magnetic Resonance Imaging
MRS	Magnetic Resonance Spectroscopy
MT	Magnetization Transfer
NCF	Nucleus Cuneifromis
NMDA	N-Methyl-D-Aspartate
NS	Nociceptive Specific
PAG	Periaqueductal Gray
PASL	Pulsed Arterial Labeling
pCASL	Pseudocontinuous Arterial Spin Labeling
PCC	Posterior cingulate cortex
PET	Positron Emission Tomography
PICORE	Proximal Inversion with Control for Off-Resonance Effects
PGA	Patient Global Assessment

PMN	Polymodal Nociceptors
R	Right
rACC	Rostral Anterior Cingulate Cortex
rCBF	Regional Cerebral Blood Flow
RF	Radiofrequency
ROI	Region of Interest
rTMS	Repetitive Transcranial Magnetic Stimulation
RVM	Rostral Ventromedial Medulla
SAR	Specific Absorption Rate
SD	Standard Deviation
SI	Primary Somatosensory Cortex
SII	Secondary Somatosensory Cortex
SEM	Standard Error
SICI	Short Interval Intracortical Inhibition
SMA	Supplementary Motor Area
SNR	Signal-to-Noise Ratio
SNRI	Serotonin Noradrenaline Reuptake Inhibitor
SPECT	Single photon Emission Computerized Tomography
SSRI	Selective Serotonin Reuptake Inhibitor
TBSS	Tract-Based Spatial Statistics
TCA	Tricyclic Antidepressant
tDCS	Transcranial Direct Current Stimulation
TES	Transcranial Electrical Stimulation
TE	Echo Time
TI	Inversion Time
TILT	Transfer Insensitive Labeling Technique
TMS	Transcranial Magnetic Stimulation
TR	Repetition Time
TRPV	Transient Receptor Potential Vanilloid
V1	Primary Visual Cortex
VAS	Visual Analogue Scale
VBM	Voxel-Based Morphometry
VLPFC	Ventrolateral Prefrontal Cortex
WDR	Wide Dynamic Range

LIST OF FIGURES

1.1 Spinal and supraspinal pathways of pain
1.2 Cognition-drive pain modulation
1.3 General mechanisms behind nociceptive and neuropathic pain
1.4 Average duration of chronic pain in patients
1.5 Common causes and locations of pain among chronic pain patients
1.6 Basic principles of transcranial magnetic stimulation

2.1 Basic principles of arterial spin labeling
2.2 Main principles behind CASL and PASL
2.3 Changes in motor evoked potential with tDCS

3.1 Illustrations of experiment paradigm
3.2 Sample image slices from a pilot study of concurrent tDCS-fMRI
3.3 Perfusion activity map assicoated with $Anodal_{stimulation - baseline}$
3.4 Perfusion activity map assicoated with $Cathodal_{stimulation - baseline}$
3.5 Functional correlations of L-DLPFC
3.6 Perfusion activity map associated with $Anodal_{after\text{-}effect - baseline}$
3.7 Perfusion activity map associated with $Cathodal_{after\text{-}effect - baseline}$
3.8 Contrast perfusion activity map between anodal and cathodal tDCS conditions

4.1 Setup of electrical stimuli generation
4.2 Temperature of the thermal probe during successive heat-cool cycles.
4.3 Pain intensity ratings during thermal stimulus paradigm
4.4 Pain intensity ratings in a capsaicin pilot study
4.5 Mean pain intensity ratings with topical application of 1% capsaicin cream

5.1 Illustration of experiment paradigm
5.2 Investigation of rCBF changes before and after the waiting period
5.3 Mean pain intensity ratings of the capsaicin responders
5.4 Pain ratings during inter-scan intervals
5.5 Questionnaire results on stimulation sensations after tDCS
5.6 Perfusion activity map associated with $Anodal_{stimulation - pain\text{-}only}$
5.7 Perfusion activity map associated with $Sham_{stimulation - pain\text{-}only}$
5.8 Contrast perfusion activity map between anodal and sham tDCS conditions
5.9 Perfusion activity map associated with $Anodal_{stimulation - after\text{-}effect}$
5.10 Perfusion activity maps associated with Post-Waiting – Pre-Waiting

6.1 Illustration of fractional anisotropy.
6.2 Probability tractography results and behavioral correlations with FA
6.3 Correlation between structural connectivity and functional correlation
6.4 TBSS analysis of whole brain FA skeleton against behavioral measurements
6.5 TBSS analysis of whole brain RD skeleton

CHAPTER 1 – INTRODUCTION

This chapter will review our current understanding of pain and brain stimulation. It will describe the mechanisms through which we generate pain after nociceptive input and the acute and ongoing models that we have developed to study the experience. It will summarize the commonly available pain treatments and the modulatory roles of the dorsolateral prefrontal cortex. Lastly, it will explain the basic concepts behind non-invasive brain stimulation techniques and provide an overview of their applications in pain studies.

1.1 Motivation

Chronic pain is typically defined as pain that afflicts an individual for over three months (Tracey and Mantyh, 2007). A widespread condition that affects approximately 20% of the adult population (Breivik et al., 2006), chronic pain has also burdened European and U.S. healthcare systems and impacted economic output with related annual costs of €200 billion and US$150 billion, respectively (Tracey and Mantyh, 2007). While acute pain patients can benefit from well-established pain managements and treatments, chronic pain patients have experienced greater difficulty in managing the clinical and financial aspects of their illnesses. The significance of the problem calls for new directions in the search for reliable and inexpensive ways of providing relief to chronic pain patients.

However, pain sensation is heavily dependent on the complex processes that take place in the nervous system (Tracey and Mantyh, 2007). It goes beyond a simple sensory experience, like warmth or light touch. In addition to the strength of the peripheral input, top-down influences within the central nervous system can equally alter a person's pain sensation (Bingel and Tracey, 2008). This is exemplified by studies that identified the roles of specific brain regions in modulating pain experiences (Bantick et al., 2002; Wiech and Tracey, 2009). If we can externally affect such brain regions' activity to harness this modulatory system, then we may be able to provide chronic pain patients with a superior, alternative solution to their condition besides costly and sometimes addictive pharmaceuticals.

1.2 Physiology and Neuroanatomy of Pain

A study on the neuromodulation of pain will not be complete without a review of the science behind pain. To understand the vast scope and complexity of the problem, I will begin with a background discussion on the physiology of pain. Its production, which is usually caused by nociception, involves four basic processes: transduction, transmission, perception, and modulation (Kelly et al., 2001).

1.2.1 Transduction

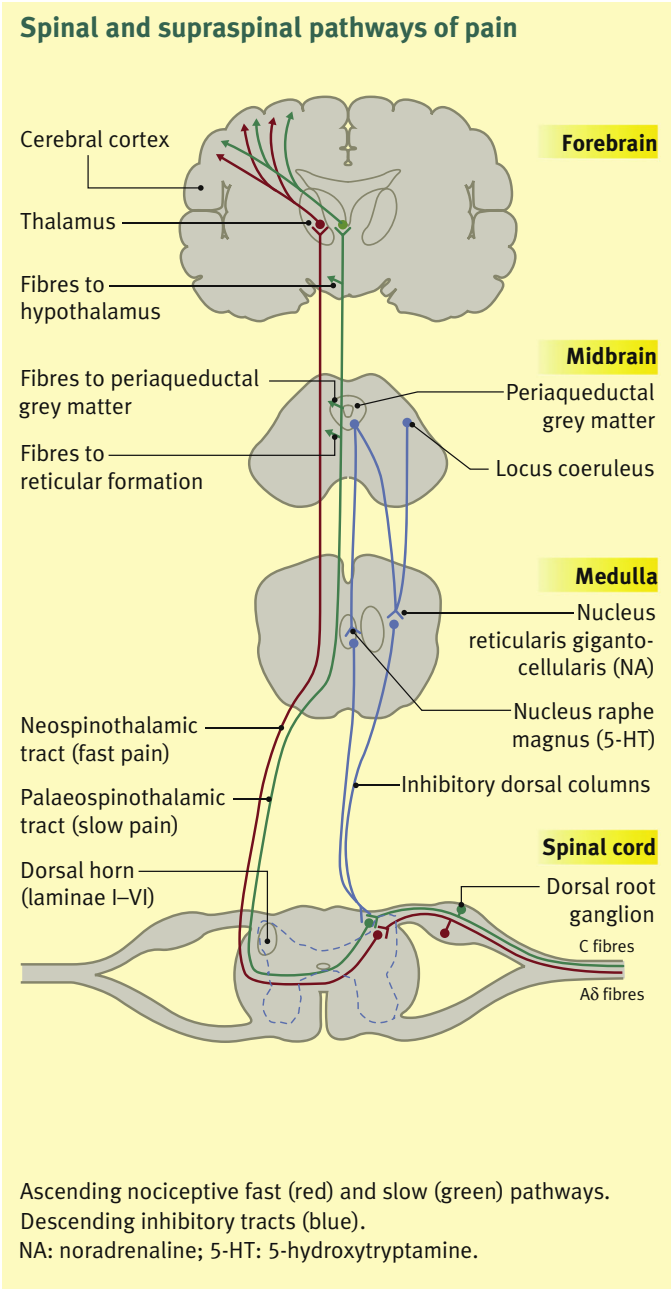
Transduction first occurs in the presence of noxious stimuli by the activation of nociceptors, a vastly heterogeneous group of receptors with different corresponding neurotransmitters, ion channels, and fiber conduction speeds (Stucky et al., 2001). Two main types of nociceptors, high-threshold mechanoreceptors (HTM) and polymodal nociceptors (PMN), are located throughout both somatic and visceral structures (Steeds, 2009). HTM respond to mechanical stimuli such as pressure, vibration, and touch, while most PMN are sensitive to chemical inputs such as substance P, prostaglandins, and bradykinin. PMN also consist of the recently discovered Transient Receptor Potential Vanilloid (TRPV) family, whose growing members include specific sensors to capsaicin (Caterina et al., 1997) and heat (Caterina et al., 1999). When irritated by a noxious agent, the corresponding nociceptors will open their voltage-gated ion channels to allow neuronal depolarization, thus triggering activation.

1.2.2 Transmission

Transmission follows shortly after transduction and proceeds in three main stages: from nociceptors to the dorsal horn in the spinal cord; from dorsal horn to brainstem; and from brainstem to subcortical and cortical structures. Primary afferent fibers, which have their cell bodies in dorsal root ganglia or trigeminal ganglion, are responsible for transmission from nociceptors to the dorsal horn and, in the main, are Aδ and C fibers (Steeds, 2009).

Aδ fibers are small, myelinated fibers that allow fast conduction speeds of 5-15 m/s before synapsing in laminae I, V, and VI of the dorsal horn in the spinal cord (Millan, 1999). These fibers can be functionally divided into types I and II based on their correspondence to mechanothermal receptors for mechanical stimuli and extreme temperatures (<-15°C and >43°C), respectively. When depolarized, Aδ fibers lead to the familiar sensations of sharp, well-localized stings and pricks in response to cuts, burns, or frostbites. In contrast, C fibers lack the myelination to permit rapid firing and instead transmit at one-tenths the speed of Aδ fibers. C fibers elicit the diffusive and dull sensation that we experience during inflammation and an extended burn. C fibers synapse in laminae I, II (external), and V of the dorsal horn. The dichotomy of response patterns between Aδ and C fibers demonstrate their differing evolutionary roles in ensuring our survival. While Aδ fibers can immediately warn us of danger, the rapid depolarization requires more time to return their neuronal potential to the resting level. Meanwhile, the slow-adapting C fibers can inform us of the continuing threats.

When the primary afferents synapse at the dorsal horn, they may target three types of second-order neurons: nociceptive specific (NS), wide dynamic range (WDR), and low-threshold (LR) (Steeds, 2009). Present in various laminae, all respond to different types of nociceptive and innocuous sensory stimuli. Activation of second-order neurons is rapidly followed by signal ascension up the spine through two phylogenetically distinct systems (Millan, 1999). The first and phylogenetically older set of tracts passes through the medial brainstem and includes paleospinothalamic, spinoreticular, and spinoparabrachial bundles. The second and more recently discovered group enters the cortex through the lateral brainstem and consists of neospinothalamic and spinocervical bundles. The spinal involvement in pain is vastly complex and lies beyond the scope of the thesis, but nonetheless forms an integral part of our nociceptive experience (Figure 1.1).



Reprinted from: Steeds C. E. (2009). 'The anatomy and physiology of pain', Surgery 27:507-511, Copyright 2009 Elsevier Ltd., with permission from Elsevier. Available at http://dx.doi.org/10.1016/j.mpsur.2009.10.013

Figure 1.1. [Adapted from Steeds] Nociceptive inputs reach the corresponding laminae in the dorsal horn through C and Aδ fibers. Several spinal pathways, such as the spinothalamic tracts, pass the signal to medulla and midbrain before it undergoes cortical processing for pain perception and modulation. The transmission process can be regulated by neuromodulators that include noradrenaline and 5-hydroxytryptamine (Steeds, 2009).

1.2.3 Perception

The development of pain perception requires our brain to process and interpret the noxious inputs. As the nociceptive signal passes up through the brainstem, it passes

through the rostral ventromedial medulla (RVM), periaqueductal gray (PAG), and thalamus, the latter of which serves as the main spinocortical relay structure (Almeida et al., 2004). The various thalamic nuclei then integrate and transfer the information to the basal ganglia and the cortex. Direct investigation of cortical changes during nociception has been difficult in humans. It was not until the advent of modern functional imaging in the early 1990s that we could advance our understanding of the brain's roles beyond what was known from the animal literature (Bushnell et al., 1999; Casey, 1999; Brooks and Tracey, 2005; Tracey and Mantyh, 2007). Using noxious heat stimuli in healthy subjects, fMRI studies have found activations in primary (SI) (Bushnell et al., 1999) and secondary (SII) somatosensory cortices (Ploner et al., 1999) as well as in anterior cingulate cortex (ACC) (Rainville et al., 1997), insula (Brooks et al., 2005), hypothalamus (Hsieh et al., 1996), and amygdala (Neugebauer et al., 2004) as well as in other regions of the limbic system (Apkarian et al., 2005). This combination of interacting structures is sometimes called the "pain matrix" because it is often activated in the presence of pain, though we do not yet know the definitive relationship between pain experiences and activity in these brain regions (Tracey and Mantyh, 2007; Tracey, 2010). In fact, altered pain perceptions resulting from changes in mood, cognition, and different contexts to the same nociceptive inputs produce, as expected, variable patterns of brain activity (Koyama et al., 2005; Wiech et al., 2008b; Wiech and Tracey, 2009; Tracey, 2010). Some core regions may often be identified as active but have altered levels of activity. Other cognitive and emotional modulations of pain perception will be further discussed in Sections 1.2.4 and 1.3.

Thus, afferent supraspinal projections of nociceptive inputs initiate the conversion of nociception into a multi-dimensional experience, which consists of sensory-discriminative and affective-cognitive components (Almeida et al., 2004). The former includes the three main aspects of stimulus localization, intensity discrimination, and

quality discrimination (Treede et al., 1999). Past literature has suggested the involvements of lateral thalamus (Lenz et al., 1994) and SI (Bushnell et al., 1999; Brooks et al., 2005; Henderson et al., 2011) in determining the stimulus site. SI is thought to be the primary site for pain localization because it has smaller receptor field sizes than the thalamus and the dorsal horn in the spinal cord (Treede et al., 1999; Brooks et al., 2005). PET studies have also found increased SI perfusion with nociceptive stimuli at multiple locations than those at only a single site (Talbot et al., 1991; Coghill et al., 1994; Derbyshire et al., 1994). SI's connection to pain discrimination is less clear, and the process may recruit contributions from other regions such as the insular cortex (Baumgartner et al., 2010). In the presence of lateralized thermal stimuli, the activity of the contralateral posterior insula has been shown to indicate pain (Owen et al., 2010).

Unlike sensory discrimination, the affective-cognitive component of pain perception addresses the different question of 'is the experience pleasant?' (Treede et al., 1999). For instance, an individual with masochistic tendencies may find a painful encounter enjoyable while others may not. Thus, our cognitive state can directly engage and change our perception. ACC, a functionally heterogeneous structure in the limbic system, shows increased activity in numerous imaging studies with acute pain stimuli (Craig et al., 1996; Rainville et al., 1997; Tracey, 2010). The region is already known for its involvements in the integration of affective and cognitive inputs (Devinsky et al., 1995), which may suggest the occurrence of deeper experiences such as suffering and torment.

1.2.4 Modulation

In response to nociceptive inputs, the brain can amend the perception through the descending pain modulatory system without any pharmacological agents (Basbaum et al., 1976; Bingel and Tracey, 2008; Wiech et al., 2008a). Through placebo studies, we have advanced our understanding of brain's involvements in cognitive pain modulation, which

included activations of ACC, insula, and thalamus (Petrovic et al., 2002; Wager et al., 2004). Other studies that applied distraction or expectation modulation with pain stimuli also provided insights into the key brain regions involved (Ploghaus et al., 1999; Tracey et al., 2002). The presence of distraction can alter behavioral ratings and elicit greater activity in ACC and prefrontal cortex than a direct summation of separate attention and pain experiments would suggest (Bantick et al., 2002; Valet et al., 2004). Also, when subjects have high expectations about the intensity of the following noxious stimulus, their subsequent pain ratings and anticipatory activity in SI, ACC, insula, thalamus, and PAG will be greater than when they have low expectations (Ploghaus et al., 1999; Porro et al., 2002). These examples illustrate the additional mechanisms through which we can modify our pain perception by manipulating key players in the descending pain modulatory system.

The region that initiates these changes, however, is most likely the prefrontal cortex because its anatomical position allows for the reception of all sensory and affective information (Figure 1.2) (Wiech et al., 2008a). Indeed, changes in dorsolateral prefrontal cortex activity has been shown to cause functional decoupling between thalamus and midbrain, which also correlated with decreased pain ratings (Lorenz et al., 2003). Due to the structure's relevance to my thesis, I will extensively explore its specific modulatory roles in the next section.

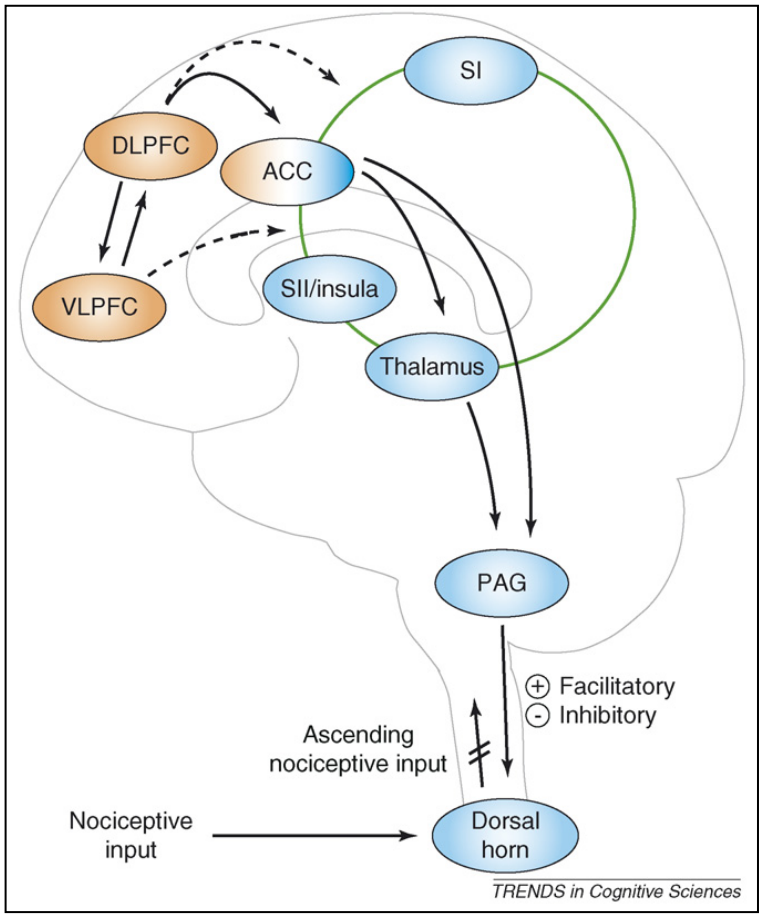


Figure 1.2. [Adapted from Wiech *et* al.] A diagram illustrating how cognition-driven pain modulation may proceed. Prefrontal areas (denoted in orange), which include ventrolateral (VLPFC) and dorsolateral prefrontal (DLPFC) cortices and part of ACC, regulate the activity of other regions in the pain matrix (denoted in light blue). Attention modulation is typically associated with increased activity in DLPFC and ACC, while expectation manipulation engages both VLPFC and DLPFC. The exact mechanism of the pain-inhibitory circuit is still under debate, but one theory suggests that DLPFC regulates ACC to change the thalamic and PAG activity (Wiech et al., 2008a).

Reprinted from: Wiech K., Ploner M. & Tracey, I. (2008a). 'Neurocognitive aspects of pain perception', Trends in Cognitive Sciences 12:306-313. Copyright 2008 Elsevier Ltd, with permission from Elsevier. Available at http://dx.doi.org/10.1016/j.tics.2008.05.005

1.3 Pain and the Dorsolateral Prefrontal Cortex

1.3.1 Overview

Previous imaging studies have shown that the dorsolateral prefrontal cortex (DLPFC) plays an important role in "keeping pain out of mind" (Lorenz et al., 2003) and pain experiences in general (Petrovic et al., 2002; Wager et al., 2004). Little is known about the roles of individual DLPFC subdivisions in pain. However, the region as a whole is postulated to influence areas that process somatosensory and affective signals (Wiech et al., 2008a). In particular, the DLPFC could provide relief through the modulation of cortical-subcortical and cortico-cortical pathways that link together SI, ACC, thalamus, and other pain-related structures. This argument is supported by our understanding of the frontal and frontal-subcortical circuits, which included strong connections between DLPFC, orbitofrontal cortex, and ACC, as well as projections of these regions to the thalamus through the basal ganglia (Tekin and Cummings, 2002). A DTI study has also shown significant white matter tracts from PAG and nucleus cuneifromis (NCF), two key pain modulatory regions, to DLPFC, though the pathway may occur through intermediary gray matter structures as well (Hadjipavlou et al., 2006).

Further investigations of DLPFC have continued to support its role in top-down pain regulation. Lorenz and colleagues used positron emission tomography (PET) to observe rCBF changes during thermal stimuli on 14 healthy subjects (Lorenz et al., 2003). Each subject received two sets of 5 scans, one with normal skin and the other with sensitized skin after 30 minutes of 1% topical capsaicin treatment on the left forearm. A thermode is attached to the left forearm to determine the heat pain threshold for both conditions before the respective scans, which then occurred concurrently with the delivery of noxious stimuli.

While the study also investigated differences in brain activity with or without allodynia, the examination of DLPFC's relationships to thalamus and midbrain is particularly

relevant to my thesis. From the scans with capsaicin-induced sensitization, the authors used a median-half-split to extract the image volumes with high left DLPFC (L-DLPFC) activity and found thalamic-midbrain decoupling and decreased pain rating in these datasets. Such changes were not observed in data blocks with lower L-DLPFC activity. Thus, they proposed that the lateralized control of L-DLPFC could disrupt bilateral thalamic connections to midbrain, which impedes signal input from the ascending nociceptive system. This pathway has been suggested from animal literature (Condes-Lara et al., 1989), where electrical stimulation of rat prefrontal cortex suppressed midbrain activity to painful stimuli on foot (Hardy and Haigler, 1985). Stimulation of cat frontal cortex also reduced medial thalamic activity during noxious input (Andersen, 1986). Supplementing these studies, our understanding about DLPFC's involvement in pain modulation has also been drawn from placebo, cognitive, and clinical imaging literature.

1.3.2 Cognitive Studies

Numerous circumstantial evidence support DLPFC's role in cognitive pain modulation, which mainly involves the ACC. Mid-cingulate section of the ACC is activated during pain experiments that incorporate concurrent distraction tasks (Davis et al., 1997; Kwan et al., 2000). The anticipation of pain, which can also alter subsequent pain rating, is often associated with rACC activity (Ploghaus et al., 1999). Further studies suggest strong projections of cingulate cortex to lateral prefrontal cortex (Devinsky et al., 1995) and the strengthening of their functional connections to the PAG and posterior thalamus during pain-distraction experiments (Valet et al., 2004). These evidence point to the involvement of DLPFC, a key region in the opioid descending pathway that partly underlies cognitive modulation of pain. This same pathway is activated during the release of endogenous opioid analgesics, which we now know occurs in contexts such as placebo (Zubieta et al., 2005).

Utilizing cognitive manipulation, placebo analgesia imaging studies provided some of the strongest evidence of DLPFC's role in pain modulation (Wager et al., 2004; Craggs et al., 2007; Wager et al., 2007). In their pain experiments, Wager and colleagues recruited healthy subjects for one control trial (without placebo cream) and one placebo trial (with placebo cream) (Wager et al., 2004). Compared to the control sessions, subjects under the placebo influence reported lower intensity ratings and produced less activation in pain-related regions, such as thalamus, insula, and ACC. Additional analyses of the anticipation phase in the placebo trials before shock pain stimuli found increased DLPFC activity that inversely correlated with rostral ACC (rACC), thalamic, and insular activity. This suggests the involvement of DLPFC in top-down pain regulation. PAG, another key region in the descending pain modulatory network, was also more active in placebo trials than in control trials.

Subsequent imaging studies have found associations between DLPFC activity and the brain's execution of placebo analgesia through opioidergic descending pain modulation (Zubieta et al., 2005; Eippert et al., 2009). A PET study compared the differences in endogenous opioid activity between placebo and pain-only sessions by measuring changes in the binding potential of μ-opioid receptors (Zubieta et al., 2005). When placebo was applied, greater activity was observed in the μ-opioid receptor-mediated neurotransmission of DLPFC, ACC, and insula in comparison to the control sessions. A follow-up study replicated the results and found two distinct activation patterns in subjects who, anticipating imminent pain, received either noxious or innocuous thermal stimuli (Wager et al., 2007). Finally, a direct fMRI investigation found significantly lower DLPFC and rACC activity in subjects who underwent placebo and naloxone (a μ-opioid receptor competitive antagonist) treatments than those who received placebo and saline infusion (Eippert et al., 2009).

1.3.4 Clinical Studies

Brain morphology studies on chronic pain patients have provided an additional perspective on the involvement of the DLPFC (Apkarian et al., 2004; Seminowicz et al., 2011). Comparing patients with chronic back pain to matched healthy control, Apkarian and colleagues found significantly lower DLPFC and thalamic gray matter density (Apkarian et al., 2004). While an earlier study with migraine patients did not find such differences (Matharu et al., 2003), the observed patterns were unlikely explained by possible confounds such as clinical depression and anxiety, each of which possesses different patterns of anatomical atrophy (Bell-McGinty et al., 2002; Almeida et al., 2003). Interestingly, later studies have shown normalization of brain morphological changes after effective treatments (Rodriguez-Raecke et al., 2009; Gwilym et al., 2010), confirmed by Seminowicz and colleagues with chronic back pain patients (Seminowicz et al., 2011). The normalization in the latter patient group was most noticeable in the L-DLPFC, as reflected by increases in cortical thickness and improvements in related cognitive functions, though the exact mechanism of this process is unclear. Follow-up sessions with a small subset (4 controls and 6 patients) of the subject cohort suggested that functional recovery preceded anatomical restoration. While structural changes were expected to take a longer time, this also indicated a non-linear relationship between cortical mass and functional competence in pain modulation. Thus, gray matter alone should not determine the magnitude of the pain modulation, and other factors, such as the strength of white matter tracts, may play key roles in the process as well.

1.4 Chronic Pain

The previous sections described how nociceptive inputs are transduced, transmitted, and processed into the pain sensations that we are familiar with. This chain of developments fittingly describes the occurrences of most acute pain episodes, but chronic pain, or pain that persists beyond normal tissue healing time (approximately 3 months), adds extra complexity to our understanding. Given the thesis's aim of potentially addressing this condition through brain modulation, I will devote this section to discuss the characteristics, epidemiology, models, and specific brain signatures of chronic pain.

1.4.1 Overview

Chronic pain conditions are vastly heterogeneous and can have little in common with each other besides imparting a lasting sensation of pain (Merskey and Bogduk, 1994). In fact, chronic pain patients often suffer from a mix of different causes that range from nerve damage to physiological hypersensitivity against noxious inputs. Broadly categorized, the disorder may be divided into nociceptive and neuropathic pain (Nicholson, 2006), though other classifications can include inflammatory and dysfunctional pain (Woolf, 2010). Nociceptive pain is driven by actual tissue damage and noxious stimuli and usually serves as a warning mechanism against irritating agents (Woolf, 2010). Depending on the physical site of the active nociceptors, the condition may lead to different pain perceptions for the patients (Figure 1.3A) (Merskey and Bogduk, 1994). Nociceptive inputs from the skin induce superficial somatic pain, while those from ligaments, bones, and muscles impart a deeper, inner ache. Nociceptive pain that originates in organs constitutes a separate category called visceral pain, which often leads to a dull, throbbing sensation. While nociceptive pain is generally acute, well-known exceptions include post-surgical pain, pain that stems from sport injuries, mechanical low back pain, and arthritic pain (Nicholson, 2006). For example, osteoarthritis induces chronic pain when normal weight bears uneven pressure on a

mechanically deformed joint to repeatedly irritate its high-threshold synovial mechanoreceptors (Torres et al., 2006).

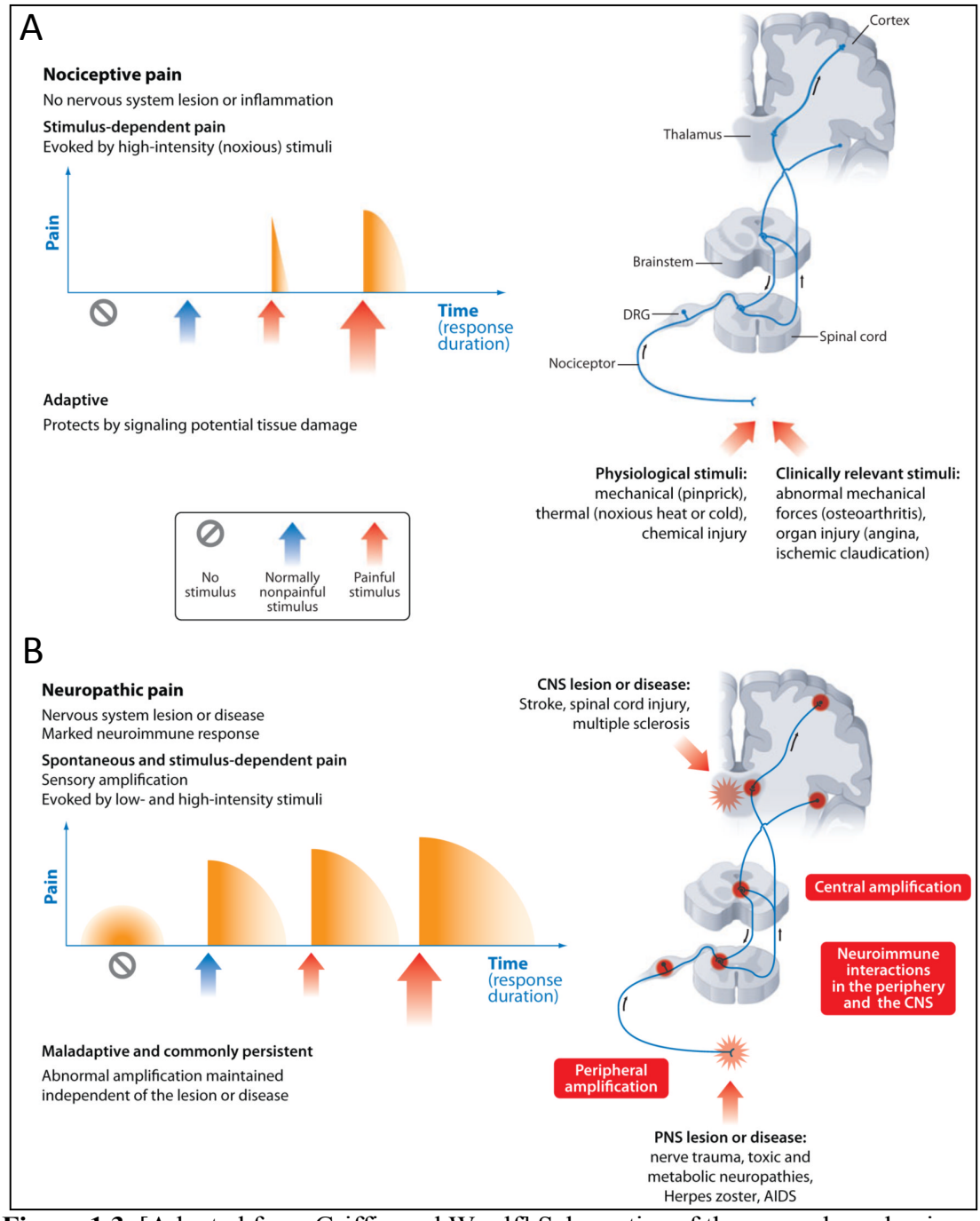


Figure 1.3. [Adapted from Griffin and Woolf] Schematics of the general mechanisms behind nociceptive and neuropathic pain. **A)** Nociceptive pain is driven by noxious stimuli or tissue damage. For the pain to enter a chronic state, the corresponding nociceptors need constant irritation. **B)** Neuropathic pain is initiated by damages to the central or peripheral nervous system. Spontaneous pain may occur as a result, or the injuries may cause sensory amplifications to turn normally innocuous sensations into perceived pain. (DRG – dorsal root ganglia) (Griffin and Woolf, 2007).

Unlike nociceptive pain, neuropathic pain can induce hypersensitivity or spontaneous pain without any noxious inputs. Rather, neuropathic pain is caused by a lesion or disease of the somatosensory nervous system and is further divided between damages to the central and peripheral nervous systems (Figure 1.3B) (Treede et al., 2008). Investigations of the neuropathic pain are difficult because the absence of noxious irritants is one of its defining traits (Costigan et al., 2009). In fact, we still know little about the underlying mechanisms of central neuropathic pain (Crown et al., 2008). Much of our current understanding of neuropathic pain has been derived from studying peripheral neuropathic pain, which has been described to impart burning, stabbing, and tingling sensations (Paice, 2003). Injured primary sensory neurons can cause ectopic transduction that then lead to spontaneous pain (Costigan et al., 2009). Axonal damage can also alter action potential generation by modifying nociceptive transmission from nociceptor to the dorsal horn. Thus, patients often suffer a sustained pain experience between medium and high intensity levels for an extended period of time (Campbell and Meyer, 2006).

Besides the occurrence of spontaneous pain, other symptoms that underlie peripheral neuropathic pain include hypersensitivities at both the sites of pain and its surrounding region (Woolf and Salter, 2000). Two phenomena characterize this – allodynia is "pain due to a stimulus that does not normally provoke pain" (Loeser and Treede, 2008), and hyperalgesia refers to a state in which noxious stimuli can cause more intense and prolonged pain. Physiological changes from neuropathic pain can also modulate the excitability of nociceptive synaptic transmission in the central pain pathway (Ji et al., 2003). The barrage of nociceptive signals from neuropathic injury alters the excitability threshold of the dorsal horn in the spinal cord, which leads to the development of central sensitization (i.e. signals become amplified) and thus secondary hyperalgesia.

1.4.2 Epidemiology

Since chronic pain has found most of its victims in developed countries, its epidemiology has been largely understood within the context of Western countries. Of the recent reviews, Breivik and colleagues have conducted the most comprehensive survey of chronic pain that covered respondents from 15 European countries and Israel (Breivik et al., 2006). This computer-assisted telephone interview study included ~46,000 willing participants (all ≥18 years of age), of whom 19% suffered pain for at least 6 months. The inclusion criteria consisted of at least two pain experiences every week for 6+ months and pain ratings above or equal to 5 on the 1 (no pain) to 10 (worst pain imaginable) numerical scale during the participant's last episode.

Among the included respondents, their conditions were generally severe. 46% suffered from constant pain, and 88% had pain experiences for at least 2 years. These numbers did not vary widely across countries (Figure 1.4). Pain-induced depression afflicted 21%, while 61% were less able or unable to continue employment outside of home. However, only one-third of these chronic pain victims were receiving treatment, and merely 2% were managed by pain specialists.

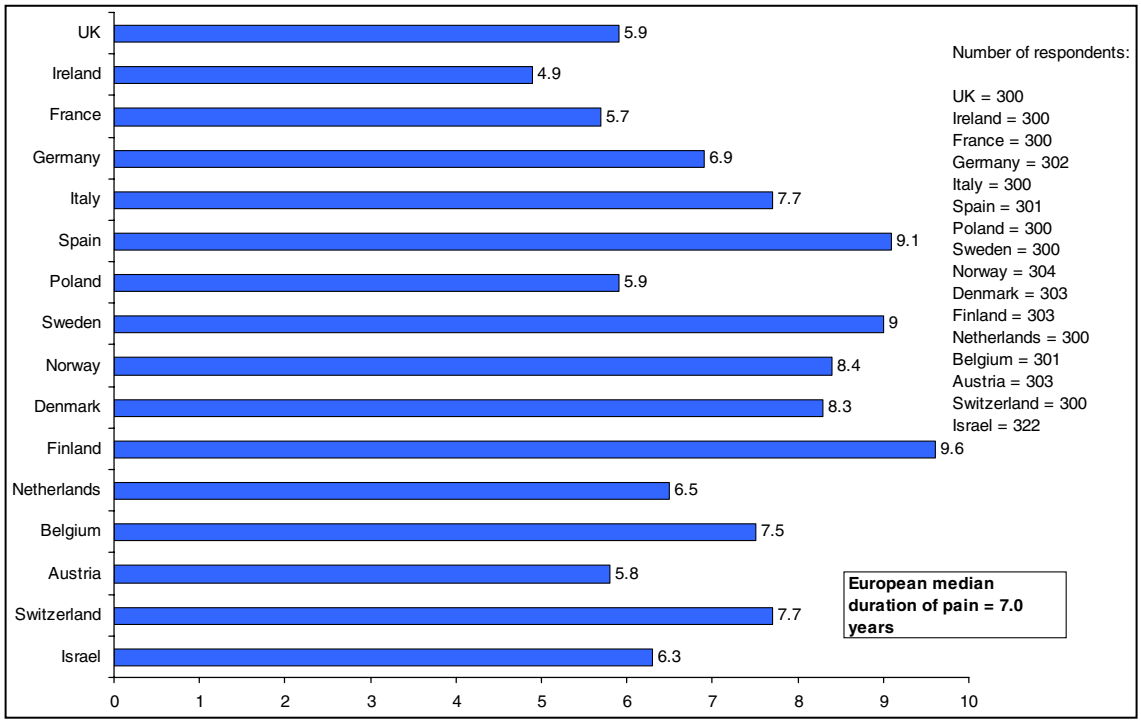
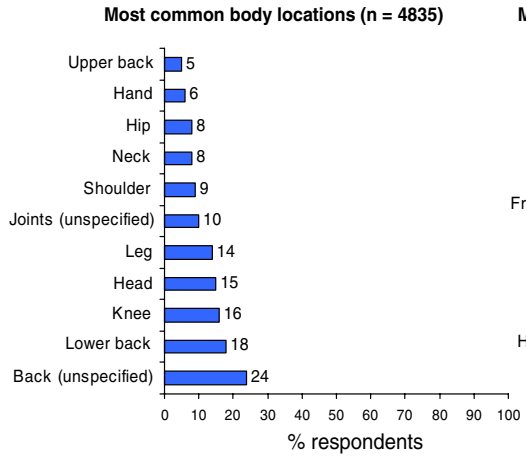


Figure 1.4. [Adapted from Breivik *et* al.] Average durations (in years) of chronic pain in patients from 15 European countries and Israel (Breivik et al., 2006).

Reprinted from: Breivik, H., Collett, B., Ventafridda,V., Cohen, R., Gallacher, D. (2006). 'Survey of chronic pain in Europe: prevalence, impact on daily life, and treatment', Eur J Pain 10:287-333. Copyright 2006 European Federation of Chapters of the International Association for the Study of Pain. Available at http://dx.doi.org/10.1016/j.ejpain.2005.06.009

Across the physical locations of pain episodes, back pain remained the most prevalent site and included 42% of respondents (Figure 1.5). Other common areas consisted of knee (16%), head (15%), leg (14%), shoulder (9%), and neck (8%). While numerous causes underlay these chronic pain conditions, 42% were attributed at least in part to some form of arthritis (Figure 1.5). Herniated or deteriorating discs were the origins of an additional 15%, and traumatic injury contributed to 12%. Migraine headaches, a common condition, afflicted 7%.



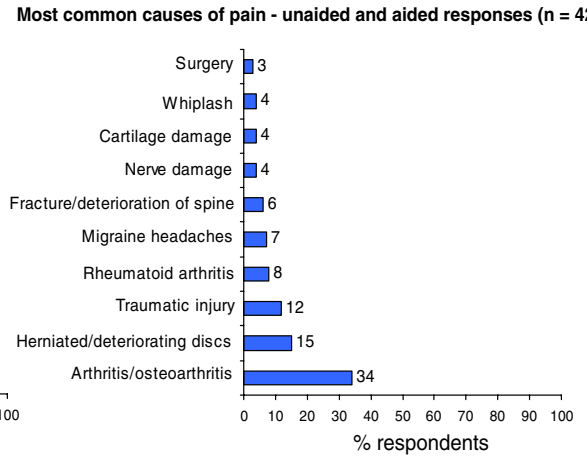


Figure 1.5. [Adapted from Breivik *et* al.] Common causes and locations of pain among chronic pain patients. The sum of the percentages may be greater than 100% because respondents may report multiple pain causes and/or locations (Breivik et al., 2006).

Reprinted from: Breivik, H., Collett, B., Ventafridda,V., Cohen, R., Gallacher, D. (2006). 'Survey of chronic pain in Europe: prevalence, impact on daily life, and treatment', Eur J Pain 10:287-333. Copyright 2006 European Federation of Chapters of the International Association for the Study of Pain. Available at http://dx.doi.org/10.1016/j.ejpain.2005.06.009

1.4.3 Ongoing Pain Models

Intuitively, chronic pain patients seem to be the most appropriate participants of chronic pain studies. However, as shown by epidemiological surveys, the condition itself is highly heterogeneous in its causes, location, and ongoing durations across the population (Breivik et al., 2006). In addition, patients may be at different stages of treatments or receiving varying pharmacological regimens at the time of their recruitment, which can bring in other confounds to the intended studies (Staahl and Drewes, 2004). At a tolerable cost in clinical relevance, a "clean" investigation of chronic pain should instead use a robust model that best mimics the experience. And if possible, the model should best replicate the symptoms of either nociceptive or neuropathic pain, though most paradigms do not make such distinctions.

In general, human pain models have been based on noxious heat stimuli (Brooks et al., 2005; Granot et al., 2006), cold stimuli (Chen et al., 1989; Hay et al., 2009; Ruscheweyh et al., 2010), electric stimuli (Klein et al., 2004; Klein et al., 2006; Geber et al., 2007), chemical irritants (Koltzenburg et al., 1994; Schmelz et al., 2000; Zambreanu et al., 2005; Geber et al., 2007; Lee et al., 2008), and hypertonic saline injections (Graven-Nielsen et al., 1997; Owen et al., 2010). Although each method utilizes different physiological bases and provides distinct sensory perceptions, establishment of an ethically allowed ongoing pain model in healthy volunteers is considerably more difficult than replications of acute pain sensations. Through a process called habituation, our body can adapt to the standard acute noxious stimuli (Rennefeld et al., 2010). For example, noxious heat probes for generating acute pain stimuli have been used extensively because they can be easily applied on and calibrated to each subject. However, if subjects receive a single, continuous thermal stimulus of medium duration (>20 seconds), they will begin to lose

pain sensitivity to the heat. Acute pain studies avoid this issue by interleaving bursts (~6 sec) of thermal stimuli with a long rest period (~1 min) (Brooks et al., 2005), but this approach cannot establish an ongoing pain experience. Granot and colleagues have suggested that repetitive-phasic stimulation, with 700ms-long stimuli and 2.5s inter-stimuli intervals in a one-minute session, can allow temporal summation of the noxious inputs and induce a continuing pain sensation (from 5 to 9 on a 0-10 VAS) (Granot et al., 2006). However, their experiments did not last longer than 1 minute, so it is unclear whether an ongoing pain experience could be maintained beyond the time frame.

Besides heat stimuli, noxious cold inputs can be used in pain models through a technique called the cold pressor test (CPT) (Ruscheweyh et al., 2010). When CPT is applied, subjects are asked to submerge a hand or a foot into a container of crushed ice and water. This imparts an intense, ongoing pain sensation that can reach VAS of 8 on a 0-10 scale and resembles characteristics of clinical pain (Chen et al., 1989; Ruscheweyh et al., 2010). However, the safety concern of frostbite prevents long-term CPT application, which is typically administered for ~1 minute before stopping. In addition, other attributes of chronic pain, such as hyperalgesia, do not appear during CPT without the complementation of pharmacological agents (Hay et al., 2009).

Electrical stimuli are another widespread and well-characterized pain model. Previous studies have demonstrated that repeated high-frequency electrical stimuli could cause allodynia and secondary hyperalgesia through long-term potentiation in spinal nociceptive pathways (Klein et al., 2004; Klein et al., 2006). However, besides these signs of central sensitization, subjects who received electrical stimuli often experienced diminishing pain sensation over time due to habituation (Condes-Lara et al., 1981). Overcoming this gradual decrease requires rapid inputs of high current stimuli. In their study, Geber and colleagues maintained ongoing pain ratings between 2 and 6 (on a 0-10

VAS) through step-wide increases in 1Hz current stimulus from 5mA to 30mA over 35 minutes (Geber et al., 2007).

Noxious chemical agents provide researchers with additional tools for investigating pain. Of the numerous irritants available, capsaicin-based models are perhaps the best understood. Topical treatment of capsaicin cream can sensitize the skin at both the site of application and the adjacent regions and cause allodynia and hyperalgesia (Koltzenburg et al., 1992). It is also known that capsaicin can target nociceptive C-fibers through TRPV1 receptors (Caterina et al., 1997) to induce secondary mechanical punctate hyperalgesia, the primary symptom of central sensitization (Magerl et al., 2001; Lee et al., 2008). In addition, human psychophysical data for mustard oil, a potent chemical irritant known to invoke similar pain experiences as capsaicin, have demonstrated a sustained pain response for at least 30 minutes (Koltzenburg et al., 1994). Long-term capsaicin application requires extra caution because the chemical could leave lasting damage to the exposed nociceptors. In fact, some chronic pain patients have used this property of capsaicin to destroy malfunctioning nociceptors (Jones et al., 2011). For healthy volunteers with repeated exposures to the compound, permanent neuronal damage can be avoided through a minimum inter-session gap of one week (Karrer and Bartoshuk, 1991).

Seeking other ways to replicate the chronic pain experience, researchers have also developed more invasive models such as hypertonic saline and intradermal capsaicin injections (Graven-Nielsen et al., 1997; Geber et al., 2007; Owen et al., 2010). The former can mimic muscle pain through saline infusion to a targeted muscle, which leads to a severe pain experience for over 15 minutes (Owen et al., 2010). This can be coupled with local anesthetics on the insertion site to remove cutaneous pain as an experimental confound (Graven-Nielsen et al., 1997). Intradermal capsaicin injection combines an injection model with capsaicin to induce neuropathic characteristics such as central

sensitization in addition to the pain sensation (Lee et al., 2008). While subjects experience severe pain (maximum VAS of 8 on the 0-10 scale) for the first 5 minutes after infusion, the sensation then undergoes habituation following the fatigue of the involved Aδ nociceptive fibers (Geber et al., 2007). This subsequent decrease in pain (often to ~2 on a 0-10 VAS) hinders the development of a robust, ongoing pain experience. However, primary and secondary hyperalgesia can readily last for over 30 minutes, so researchers with an interest in these aspects of neuropathic pain can still use the intradermal capsaicin model (Lee et al., 2008).

1.4.4 Changes in Brain Structure and Function

Before discussing how brain modulation may achieve pain alleviation, we need to first understand the differences in brain activity and structures between chronic pain patients and healthy controls. While we have addressed the anatomical transformations associated with chronic pain in Chapter 1.3.4, an understanding of the functional changes can answer another basic question of how the condition affects regional activity and vice versa. Such examinations require imaging tools such as MRI and PET and hence remain bounded by the techniques' limitations (Owen et al., 2008). For example, BOLD fMRI is an ideal tool for investigating changes in brain activity during high-frequency tasks such as a train of acute noxious stimuli. Through this setup, we have identified the brain regions involved in the perception of acute pain, but we cannot directly associate the same pattern with chronic pain. Despite their similarities, onset and maintenance of pain are dependent but separate processes that may recruit different brain structures. Indeed, recent studies have suggested that another main contributor to the brain activations observed in acute pain fMRI experiments could be stimulus saliency, which is a cognitive recognition of the stimulus's relevance and novelty (Iannetti et al., 2008; Legrain et al., 2011). By contrast, PET is better suited for extended pain experiences yet

suffers from technical challenges, such as poor temporal and spatial resolutions, radiation exposures, and the need for invasive procedures (Becerra et al., 1999).

To investigate changes in brain activity due to tonic, low-frequency ongoing pain stimuli, perfusion fMRI using arterial spin labeling (cf. Chapter 2.1) appears to be the ideal technique for addressing this question. Owen and colleagues first used ASL in 2008 to examine functional changes from 5 alternating, 1-minute blocks of nociceptive and warm thermal inputs to the left hand of 14 healthy volunteers (Owen et al., 2008). In the study, they found increased activity on the order of ~5% from baseline rCBF in bilateral insula, SII, cingulate cortices, and supplementary motor area (SMA), as well as contralateral SI and ipsilateral thalamus during pain blocks. While I would not consider the 1-minute duration of their noxious stimuli as particularly ongoing, the authors demonstrated the technical feasibility of ASL in detecting pain-related rCBF changes, which usually vary by small percentages from the resting baseline (Coghill et al., 1994; Derbyshire and Jones, 1998).

In their follow-up study, Owen and colleagues combined ASL with a hypertonic saline (5% NaCl) pain model on the left arm of 11 healthy volunteers, which allowed a ~15-minute block of ongoing pain (mean VAS of 5.9±0.6 on a 0-10 scale) (Owen et al., 2010). The average perfusion map of the pain condition showed increased rCBF in bilateral insula (anterior and posterior), thalami, and anterior mid-cingulate cortex and decreased rCBF in bilateral SI and precuneous cortex. In contrast, the control group (injected with 0.9% NaCl solution) had increased activity in bilateral anterior insula and decreased activity in precuneous and mid-cingulate cortices. The authors then proceeded to plot the mean time courses to explore the temporal rCBF changes of ROIs that intersected between anatomical structures and regions of significant functional change. In the pain group, activity of ipsilateral insula, bilateral thalami, and mid-cingulate cortex peaked

within 3 minutes of the pain commencing before fading to baseline for the remainder of the ongoing pain block. While contralateral posterior insula activity showed a similar peak, its activity never returned to baseline but remained heightened at an rCBF of ~4%. This finding suggests this region's key role in the maintenance, rather than just the onset, of pain.

While these studies relied on ongoing pain models that may not fully replicate chronic pain experiences, recent work applied ASL to investigate rCBF changes in pre- and post-surgical pain showed comparable results (Howard et al., 2011). Recruiting 16 male volunteers due for molar extractions, Howard and colleagues compared the subjects' rCBF before and after dental surgery. Of the widespread increases observed, the main changes occurred in pain-related regions such as insula, the jaw region in SI, SII, and thalamus.

1.5 Treatments for Chronic Neuropathic Pain

While acute pain patients can generally benefit from localized treatment regimens that can target the specific causes of their condition, neuropathic pain patients lack such options (Costigan et al., 2009). Instead, they mostly rely on medications that globally modulate the nervous system to gain relief, which can lead to negative side effects such as drowsiness and dizziness (Moulin et al., 2007). Given this clinical need and my interest in utilizing neuromodulatory networks for pain alleviation, chronic neuropathic pain should be the most ideal and appropriate target group for my approach. Thus, we will present in this section a brief overview of the existing treatments, though an extensive discussion will be beyond the scope of my thesis.

Chronic neuropathic pain requires pharmacological intervention when it has sufficiently exacerbated to undermine a patient's quality of the life. The treatment regimen is divided into four lines of analgesics, which are determined by the clinical efficacy, ease of use, potential risks, and cost-effectiveness of each class of drugs (Moulin et al., 2007). Antidepressants and anticonvulsant constitute the first line of pain management. Although the exact mechanism is unclear, tricyclic antidepressants (TCAs) are thought to induce analgesic effect by blocking sodium channels and inhibiting the reuptake of serotonin and noradrenaline (Kingery, 1997), which are two key neurotransmitters in endogenous analgesic transmission (Mease, 2009). Studies have found similar clinical efficacy with TCA in treating neuropathic pains of different underlying conditions (McQuay et al., 1996). Among the anticonvulsants, gabapentin and pregabalin comprise the primary candidates and induce pain relief by binding to presynaptic, voltage-gated calcium channels in the dorsal horn (Taylor, 2004). This reduces the release of excitatory neurotransmitters such as glutamate and substance P and weakens the strength of the ascending nociceptive transmission.

If the first-line analgesics are ineffective or unsuitable, second-line pharmaceutics of serotonin noradrenaline reuptake inhibitors (SNRIs) and topical lidocaine can be deployed instead (Moulin et al., 2007). SNRIs are more specific than general antidepressants at inhibiting the reuptake of serotonin and noradrenaline, though side effects such as prolonged hypertension can force a subject off SNRI treatment. This class of medication has demonstrated clinical efficacy against conditions such as painful diabetic neuropathy in multiple randomized controlled trials (Goldstein et al., 2005; Raskin et al., 2005). Topical lidocaine is a sodium channel blocker that is useful for treating localized peripheral neuropathic pain. Often prepared in the form of patches or gel, lidocaine can provide relief to postherpetic neuralgia and other focal neuropathic syndromes (Rowbotham et al., 1995).

Third-line analgesics consist of tramadol and opioid analgesics (Moulin et al., 2007). Tramadol expresses low-affinity binding for μ-opioid receptor and inhibits the reuptake of noradrenaline and serotonin (Moulin et al., 2007). The treatment has led to significant improvements in patients with painful diabetic neuropathy and mixed neuropathic pain syndromes (Finnerup et al., 2005) and resulted in fewer negative side effects than other weak opioid analgesics. However, the improved efficacy also means higher costs for eligible patients. For those who seek other third-line medications, they can take strong opioid analgesics, such as oxycodone and morphine, which have a strong track record in alleviating neurpathic pain (Eisenberg et al., 2005). Unfortunately, these powerful analgesics carry a nontrivial risk of drug addiction by the patients, so they are generally prescribed when other solutions have proved ineffective.

The last line of analgesics mainly consists of drugs that have shown great clinical promise and efficacy but have yet been fully validated and accepted by the pain management establishment. For example, cannabinoids demonstrated great analgesic

properties in animal models (Moulin et al., 2007), though applications of dronabinol produced modest improvements in central pain symptoms of multiple sclerosis patients (Svendsen et al., 2004). Methoadone, a synthetic opioid analgesic, may alleviate chronic pain conditions, though the conducted randomized controlled trials have been limited in scale (Gagnon et al., 2003; Morley et al., 2003). Selective serotonin reuptake inhibitors (SSRI) is another type of fourth-line analgesics that specifically inhibits serotonin reuptake. While modestly effective in randomized controlled trials of painful diabetic neuropathy (Sindrup et al., 1990), SSRIs appear to be less potent than closely-related compounds, such as TCAs or SNRIs.

Thus, a multitude of pharmaceutical treatments for chronic neuropathic pain currently exists on the market. While some are more effective than others, most are costly medications with multiple negative side effects, from drowsiness to constipation. These shortcomings underlie the need for alternative, non-pharmacological treatments. Given our understanding of the brain's endogenous pain modulatory functions, we may be able to utilize this network to assist chronic pain patients.

1.6 Non-Invasive Neuromodulation

Past imaging studies have associated pain modulation with brain regions. If we can externally harness their faculty, we could provide novel, non-pharmacological treatment alternatives for chronic pain patients. This may be achieved through non-invasive brain interference techniques, a method of modulating neocortical activities through electrical and magnetic stimulations. To date, its two most prominent examples are transcranial magnetic stimulation (TMS) and transcranial direct current stimulation (tDCS).

1.6.1 Transcranial Magnetic Stimulation

TMS was first developed by Barker and colleagues in 1985 (Barker et al., 1985) and has since been used in various clinical treatments (Pascual-Leone et al., 1996; Fregni et al., 2005a; Khedr et al., 2005a; Khedr et al., 2005b; Passard et al., 2007). The device works by sending a pulse of high current through a coil of wires over the subject's head, thus inducing a magnetic field that passes perpendicularly to the plane of the coil (Hallett, 2007). The change in magnetic flux then induces a current within the brain, which moves in a parallel but opposite direction as the current in the magnetic coil (Figure 1.6). This magnetic field can reach 2T in strength under the coil center and usually lasts ~100μs per pulse. If the regions of interest are parallel to the electric field, the stimulation strength will simply vary as a function of distance. If they are not, TMS's neuromodulation of equidistant regions will no longer be uniform.

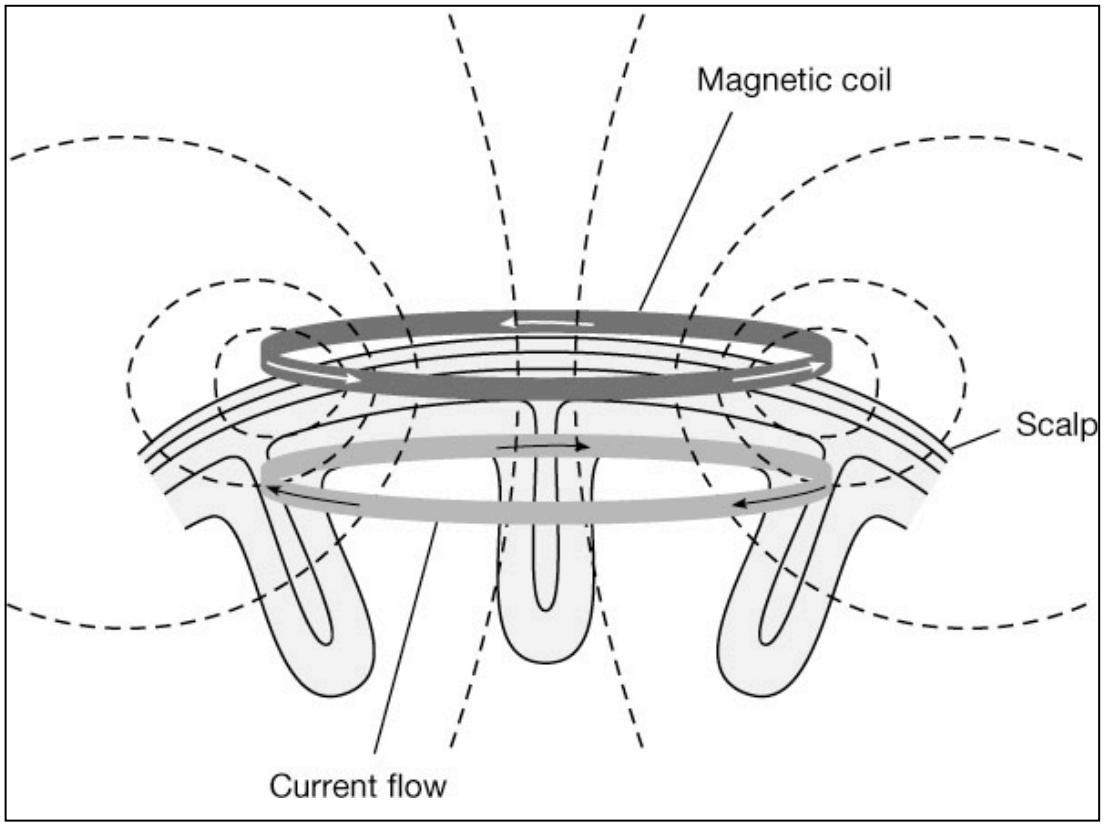


Figure 1.6. [Adapted from Hallett] The magnetic coil of TMS is placed above the targeted cortex. Electric current in the magnetic coil generates strong magnetic flux through the plane of the coil, which induces current of opposite direction in the underlying cortex. This basic mechanism allows TMS to interfere with brain activity (Hallett, 2000).

Reprinted by permission from Macmillan Publishers Ltd: Hallett, M. (2000). 'Transcranial magnetic stimulation and the human brain', Nature 406:147-150. Copyright 2000 Macmillan Magazines Ltd. Available at: http://dx.doi.org/10.1038/35018000

Several designs of magnetic coils have been utilized to date (Hallett, 2007). The figure-of-eight coil is the most focal, inducing the strongest electric field at the underlying cortex of the coil center. This power can be further increased if the components are placed at an angle to each other. The H-coil has intricate windings that allow a smaller drop in magnetic field strength with increasing distance.

While studies involving timed stimulus paradigms can find single-pulse TMS useful, this method is severely restricted when the subject is required to perform motor or cognitive tasks (Priori et al., 2009). The bulkiness of the device, along with the challenge of maintaining coil position, renders online stimulations difficult. Thus, repetitive pulses of TMS, or rTMS, are used instead to pursue such studies through offline stimulations. The

technique typically applies 500 to 10,0000 pulses per session at a frequency between 1Hz (inhibitory) and 20Hz (excitatory). Since most task-related rTMS experiments happen after stimulation, the technique relies on the assumption that the after-effects of rTMS will be strong enough to influence task executions.

1.6.2 Transcranial Direct Current Stimulation

While also a brain stimulation technique, tDCS differs from TMS in that tDCS directly applies electric current to targeted regions in the underlying cortex through large electrodes (Nitsche and Paulus, 2000). The device's technical requirements are minimal, requiring only electric cables, electrode pads, and a direct current generator akin to standard AAA batteries. By passing weak current of positive or negative polarity through targeted brain regions, tDCS has been able to influence human behaviors, physiology, and functions such as memory processing (Chi et al., 2010) and motor learning (Nitsche et al., 2003b). Anodal stimulation is thought to have an excitatory effect on the affected cortex, while cathodal stimulation is inhibitory (Nitsche et al., 2008). Due to the technique's relative youth, the pain-tDCS literature is significantly smaller than that of pain-rTMS. The results are nonetheless promising; since 2006, tDCS has also been safely, repeatedly, and successfully applied in pain studies with both patient and healthy subject groups (Fregni et al., 2006a; Fregni et al., 2006b; Boggio et al., 2008a; Boggio et al., 2009; Soler et al., 2010; Borckardt et al., 2011). Further details about the underlying principles of tDCS will be covered in Chapter 2.2.

1.7 Pain and Brain Stimulation

The rapidly growing literature on brain stimulation applications of pain modulation illustrates the widening clinical interest in the technique and underlies the need for a review on the topic. In 2001, Lefaucheur and colleagues presented the first clinical application of non-invasive brain interference techniques in pain with rTMS (Lefaucheur et al., 2001b; Lefaucheur et al., 2001a). While rTMS has continued to be used in the field ever since, the tool suffers from practical considerations in clinical settings that dampen its implementation as a pain treatment tool (Edelmuth et al., 2010). The large and clumsy device requires a trained technician to operate and costs in the five-digit range. If improperly handled, rTMS can be potentially hazardous to both the patient and the surrounding electrical equipment because of its ability to generate a train of 2-tesla magnetic pulses with a single click. These drawbacks render point-of-care treatments with rTMS all but impossible for most chronic pain patients and help bring tDCS into limelight.

Thus, while the following section will describe a few rTMS studies in pain modulation, it will focus more on a review of tDCS-pain literature instead. In addition, out of the favored stimulation sites of M1 and DLPFC (Fregni et al., 2007), I will place greater emphasis on the latter because the pain modulatory mechanisms of DLPFC are better understood than that of M1. In contrast, M1 became a target due to encouraging clinical results from early invasive motor cortex stimulation (MCS) work, which used invasive electrical stimulation to increase M1 activity, and found corresponding pain decreases in chronic pain patients (Hosobuchi, 1993; Meyerson et al., 1993; Tsubokawa et al., 1993). While the proposed rationale for this analgesia is that the interference of sensory processing helps relieve pain (Boggio et al., 2008a), this hypothesis remains a theory and still requires substantial experimental support. In fact, several acute pain studies have shown increased activity in the motor cortex during noxious stimuli without the presence

of any relief (Tracey et al., 2000; Brooks and Tracey, 2005). Coupled to possible links with basal ganglia dopaminergic systems, M1 does likely have considerable relevance in nociception. However, given a lack of clarity regarding the its role in pain modulation, the DLPFC is better suited as a stimulation target than M1 for my investigation, which focuses more on neuro-mechanisms than on the magnitude of clinical efficacy.

1.7.1 Repetitive Transcranial Magnetic Stimulation

In 2001, Lefaucheur and colleagues reported the first use of a figure-of-eight rTMS on chronic pain relief by stimulating the M1 that corresponds to the painful area (Lefaucheur et al., 2001b; Lefaucheur et al., 2001a). Since then, several clinical studies have been published in this area, including chronic migraine (Brighina et al., 2004; Conte et al., 2009), visceral pain (Fregni et al., 2005a), and fibromyalgia (Sampson et al., 2006). The overall success differs for each study (Fregni et al., 2007). On a 0-to-10 VAS, the group mean effects of chronic pain patients have been reduced by as much as 2.20 or increased by 0.10.

Brighina and colleagues published the first rTMS work that uses DLPFC stimulation for pain alleviation (Brighina et al., 2004). The randomized, double-blinded pilot study recruited 11 chronic migraine patients and separated the cohort into sham (N=6) and active rTMS (N=5) groups. The coil of sham rTMS was placed perpendicular to the head surface and underwent the same stimulation schedule as active rTMS. All patients experienced headaches for at least 15 days per month for the preceding 3 months and found at least 3 preventive medications to be ineffective. With the exception of one subject, all others received prophylactic treatment for at least 2 months and remained doing so during the rTMS study. Twelve active or sham rTMS sessions on the L-DLPFC were given every other day excluding weekends. Each session consisted of 10 trains of 20-Hz (excitatory), 2-second stimulations with an inter-stimulus interval of 30 seconds.

The patients were asked about their migraine attack frequency, pain intensity ratings, and number of consumed abortive medications at three time points: immediately before treatment (T0) and 1 month (T1) and 2 months (T2) after treatment. In the study, the author reported significant decreases in all three indices at both T1 and T0 compared to T0 for the active rTMS group. The sham rTMS group observed modest decreases, but the values were not significantly different from pre-treatment ratings. L-DLPFC's negative modulation of central supraspinal pain pathways was suggested as a likely mechanism for the clinical efficacy of the rTMS treatment.

A separate study by Sampson and colleagues used rTMS for alleviating fibromyalgia pain (Sampson et al., 2006). The double-blinded, crossover study recruited four female subjects with depression, fibromyalgia, and borderline personality disorder (BPD). All were diagnosed with fibromyalgia for 4 to 10 years, but the actual durations of the related symptoms were unknown. The patients satisfied the authors' recruitment criteria of possessing the ability to give consent and scoring at least 20 on the 28-item Hamilton Rating Scale for Depression. During the study, the subjects continued to consume the different medications that they were each prescribed previously, such as gabapentin and fluoxetine. The authors did not specify the exact locations of their subjects' pain.

Daily rTMS treatment from Monday to Friday was given for 4 weeks at a frequency of 1 Hz and through two 800-second sets of stimuli with a 60-second interval time in-between. The inhibitory rTMS was approximately targeted at the R-DLPFC, a position 5 cm anterior of the optimal motor cortex stimulation site. Only one of the four subjects received sham treatment, which lasted for the first two weeks of her trial. This patient experienced no pain relief during this period. The authors measured pain intensity on an 11-point Likert scale (0 being "no pain" and 10 being "the worse ever") and recorded the score as given by subject surveys before and after the 4-week trials. The treatment

efficacy was evaluated by subtracting this difference. The pretreatment pain averaged 8.2 (7 to 9.5), which diminished to 1.5 (0 to 3.5) afterwards.

1.7.2. Transcranial Direct Current Stimulation

In 2006, Fregni and colleagues performed the first tDCS study on pain (Fregni et al., 2006a). Their randomized, double-blinded, sham-controlled, parallel-group trial included 17 patients with spinal cord injury that culminated in central pain. For the recruitment criteria, all subjects 1) suffered from a traumatic spinal cord injury; 2) experienced stable chronic pain for at least the past 3 months; 3) scored at least 4 on VAS (0 to 10 scale), though the average baseline scores were ~6; 4) possessed conditions that persisted despite at least two drug prescriptions for 6 months; and 5) could not attribute their pain to other causes. The authors excluded patients with unstable clinical or mental conditions, a record of substance abuse, neuropsychiatric co-morbidity, and implanted devices for pain alleviation. During the trial, the subjects did not stop their routine medication regimens, which varied between patients. They also experienced different sensations of pain at different parts of their body.

Daily 2-mA, 20-minute session of active or sham tDCS was given for 5 consecutive days. The authors applied anodal stimulations on the contralateral primary motor cortex (M1) for patients with asymmetric pain and on the dominant left M1 for those with symmetric pain. Out of the 17 subjects, eleven received active tDCS stimulations. The remaining subjects received sham stimulations, in which the tDCS was turned off after 10 seconds of stimulation. The authors also monitored the subjects' mental stability with Beck Depression Inventory and a VAS for anxiety. The pain results were regressed against these depression and anxiety indicators to minimize the effects of these confounders.

Pain was primarily evaluated through patient surveys of their VAS scores, which were taken 1) daily in the two weeks prior to treatment to form the baseline value; 2) twice everyday during the 5-day study; and 3) once in the follow-up period 16 days after the conclusion of the trial. In every survey, the subjects were asked to rate their pain sensations during the previous 24 hours. The authors also assessed the pain with the clinical global assessment (CGI) and the patient global assessment (PGA). CGI is a two-item scale that clinicians used to rate 1) the severity of the illness on a 7-point scale (1 being "very much improved" and 7 being "very much worse") and 2) the subjects' improvements relative to baseline. PGA is a survey that asked patients to estimate their overall change in pain relative to their personal baseline on a 7-point scale. CGI and PGA were taken on days 2, 3, 4, and 5 and follow-up. Through these three evaluation methods, the authors noted a significant reduction in pain by the active group at the end of day 5 (mean VAS score of 2.6) in comparison to both its baseline scores (mean VAS score of 6.2) and the placebo group. The pain relief effect lessened, but still persisted at a mean VAS score of 3.9, after the follow-up period.

Fregni and colleagues then performed a follow-up study with fibromyalgia subjects (Fregni et al., 2006b). The double-blinded, sham-controlled, parallel trial recruited 32 female patients who maintained a mean pain score at least 4 on VAS (0 to 10 scale) during the 2 weeks prior to the trial and did not have uncontrolled clinical disease. Subjects were not asked to discontinue their medication regimens, but they must have received stable doses of analgesics for at least 2 months before the study began. The authors did not specify the exact locations of their patients' pain.

The tDCS protocol did not differ significantly from the methods used in Fregni's previous study on central pain. The authors gave daily 2-mA, 20-minute session of active or sham anodal tDCS for 5 continuous days. Twenty-two subjects were evenly divided to

receive active treatment on L-DLPFC or M1, while another ten obtained sham stimulation. However, one M1 subject backed out of the study after experiencing redness and itching at the electrode site. The authors primarily assessed pain through patient surveys of their VAS scores, which were taken at the same time points as in their previous study, though the follow-up period has been extended from 16 to 21 days. In addition, the authors included evaluations with CGI and PGA, which were taken on days 2, 3, 4, and 5 and follow-up. Through these three metrics, the authors noted a significant reduction in CGI and PGA scores by the M1 active group in comparison to both its baseline scores and the control group. The effect of pain alleviation subsided for the M1 subjects throughout the follow-up period, but these patients still reported lower VAS scores than baseline. The authors observed a smaller analgesic effect with L-DLPFC stimulation. The DLPFC group's overall CGI scores across time were statistically lower than those of the sham condition, but significant decreases were not observed with the PGA scores. Thus, the authors suggested that fibromyalgia patients might benefit more from M1 tDCS, though L-DLPFC stimulation would still be clinically useful.

Anodal tDCS of L-DLPFC has also been used to alleviate chronic neuropathic pain (Arul-Anandam et al., 2009) and post-endoscopy pain after endoscopic retrograde cholangiopancreatography (ERCP), an interventional technique for detecting abnormalities in the pancreatic ductal system (Borckardt et al., 2011). The former was a case study involving a 51-year-old woman with both clinical neuropathic pain and major depressive disorder (MDD). The patient received five sessions of sham tDCS followed by ten sessions of active 2mA stimulation on alternate weekdays. Each session lasted 20 minutes. While she was blinded to the treatment allocation, the patient only reported pain improvement after the active treatments began. The authors recorded a decrease in pain from 7 (before the commencement of anodal tDCS treatment) to 4 (after 5 sessions of active tDCS) on a 0-10 VAS, even though they primarily used tDCS to treat her MDD.

The patient found the improvements, which persisted in the 1-month follow-up, to be similar to the effect of the spinal block analgesia that she was given 3 years ago. Since her depression condition also responded to the stimulation, this progression could have confounded her pain perceptions. However, given the large magnitude of the analgesic effect, L-DLPFC tDCS remained a likely contributor to the pain improvement.

The post-ERCP study by Borckardt and colleagues was a larger study involving 21 patients, which were randomly separated into real and sham tDCS conditions (Borckardt et al., 2011). All subjects received one session of 20-minute, 2mA stimulation and reported their pain ratings 4 hours afterwards using a VAS and upon discharge from the hospital using a questionnaire. The tDCS protocol was similar to that of previous studies, though the authors placed the reference (cathodal) electrode over the gut representation of the right sensory cortex instead. While the differences were not statistically significant, the pain ratings, as assessed by VAS after 4 hours, showed a decreasing trend in all measured indices such as "pain on average," "pain at its worst," and "pain unpleasantness" from real to sham tDCS conditions. Followed up with a questionnaire, the patients who received anodal stimulation reported significantly less throbbing pain and pain interference with sleep at the time of their discharge than those with sham treatment.

In addition to the initial clinical studies, Boggio and colleagues applied experimental pain models to explore the possible modulatory mechanisms of pain by tDCS (Boggio et al., 2008a; Boggio et al., 2009). In a double-blinded, randomized, and cross-over trial, they tested the changes in sensory perception thresholds and pain thresholds of 12 subjects during anodal 2mA tDCS of L-M1, L-DLPFC, occipital cortex, and sham tDCS (Boggio et al., 2008a). Each stimulation session lasted 5 minutes, which has a brief (<5 minutes) after-effect (Nitsche and Paulus, 2000). Thus, the tDCS sessions were spaced

by 50 minutes, during which the authors performed baseline measurements to ensure the absence of long-lasting changes and for comparisons against the values recorded during tDCS. To gather the individual thresholds, the authors used an electrical model on the right index fingers that increased stimulation intensity in a step-wise (0.1mA) manner from 0mA. The sensory perception threshold equaled the current intensity at which subjects first detected the stimulus sensation. This same judgment was applied for determining the value of the pain threshold.

During M1 tDCS, the subjects reported significantly higher (6.5%) sensory perception than baseline. This pattern was not observed with L-DLPFC, V1, and sham stimulations. For pain threshold changes, significant increases from baseline were only associated with L-DLPFC (10.0%) and M1 tDCS (8.5%). The authors attributed these modulations to the regions' regulation of thalamus and brainstem through cortical-subcortical connections. They suggested that M1 tDCS might have produced the analgesic effect by modifying sensory aspects of pain, while L-DLPFC stimulation could alter pain sensation through affective networks without interfering with our sensory perception. Regardless of the possible explanations, L-DLPFC tDCS does appear to be an effective tool for providing pain relief.

A follow-up study by Boggio and colleagues seemed to support this notion that L-DLPFC stimulation can influence pain-related affective functions (Boggio et al., 2009). The authors recruited 23 healthy subjects and applied an almost identical paradigm as the previous study, though emotionally aversive images of human pain replaced the electrical pain model. The subjects were then asked to rate the unpleasantness and level of emotion discomfort from the images. Only L-DLPFC tDCS resulted in significant decreases in the two indices from baseline, while M1, V1, and sham stimulations were not associated with significant changes.

1.7.3. Summary

Recent meta-analyses underlined the heterogeneity of brain stimulation literature with pain applications (Leung et al., 2009; O'Connell et al., 2010). Most experimental factors varied between studies, including patient size, number of stimulation sessions, polarity, electrode size, and active and reference electrode placements. From the wide range of protocols, a Cochrane review on the pain application of brain stimulation techniques (TMS, tDCS, and cranial electrotherapy stimulation) only found one study with low risk of bias (O'Connell et al., 2010). The overall diversity underscores the relative youth of this field, where pioneer scientists are still exploring the best ways to apply brain stimulation tools for the treatment of various pain conditions. Consequently, the existing studies focus mainly on eliciting the highest clinical efficacy rather than on repeating previous studies or in-depth investigations of the underlying scientific principles. Some shortcuts, especially in subject blinding or the use of a control group, were occasionally taken to allow for the testing of different experiment methods or patient groups .

In the context of this thesis, the above studies are most useful in their consensus that brain stimulation techniques can alleviate the pain condition when applied (excitatory) to M1 or DLPFC. Thus, I can build upon these works to study the neuro-mechanisms behind tDCS and its top-down pain modulation. By using a standard protocol and a healthy cohort with an ongoing pain model, I can minimize the experimental confounds in my own investigation.

1.8 Theme

Combining pain-related successes of tDCS applications with our understanding of the DLPFC, I plan to use functional MRI to investigate the mechanisms behind this resultant pain modulation throughout this thesis. Chapter 2 will provide a detailed overview of arterial spin labeling and tDCS. Chapter 3 will investigate task-free functional changes during and after both anodal and cathodal tDCS of L-DLPFC. Chapter 4 will describe various attempts at establishing an ongoing pain model to simulate the experience of chronic neuropathic pain patients in healthy subjects. Chapter 5 will combine my understandings from Chapters 3 and 4 and use fMRI to determine the brain regions affected by tDCS in the presence of an ongoing pain model. Chapter 6 will apply diffusion tractography imaging and other structural analyses to explore the possible correlations between structural differences and behavioral changes across subjects. Lastly, Chapter 7 will conclude my thesis and suggest directions for future studies.

CHAPTER 2 – METHODS

To achieve its aims, the study requires the incorporation of neuromodulatory, imaging, and pain-related tools. Some have been well characterized in published lists of works over the course of decades, while others much less so. In this chapter, I will begin with a review of arterial spin labeling and transcranial direct current stimulation, two key but young techniques, to help readers understand their pertinence for this thesis.

My study utilizes four main techniques: quantitative whole brain perfusion fMRI, tDCS, diffusion tensor imaging, and capsaicin-induced tonic pain. Of these, the first two are relatively novel tools that only gained prominence in recent years. To better justify their usage, this chapter will summarize the techniques' background and respective relevance to the study.

2.1 Perfusion fMRI with Arterial Spin Labeling

2.1.1 Basic Concept

Arterial spin labeling (ASL) perfusion imaging uses arterial blood as the endogenous tracer to derive blood flow measurements without the radioactive agents typically needed by other modalities, such as positron emission tomography (PET). The concept was originally applied to observe intraluminal flow in arteries and veins (Singer and Crooks, 1983; Sardashti et al., 1990). ASL works on the principle that the volume of perfused blood to a region equals the difference between the arterial inflow and venous outflow (Kety and Schmidt, 1948). Thus, electromagnetically-labeled water can be used instead of injected radiotracer to track the CBF over time. Radiofrequency (RF) pulses can first label the arterial blood at the common carotid arteries, followed by a second scan to locate the distribution of the tagged blood flow throughout the whole brain (Williams et al., 1992b; Golay et al., 2004). This process is then repeated for a control scan, in which the arterial blood is not magnetically tagged (Figure 2.1). By finding the difference in perfusion profiles between the labeled and control volumes, it is possible to determine the rate and volume of rCBF at that time point.

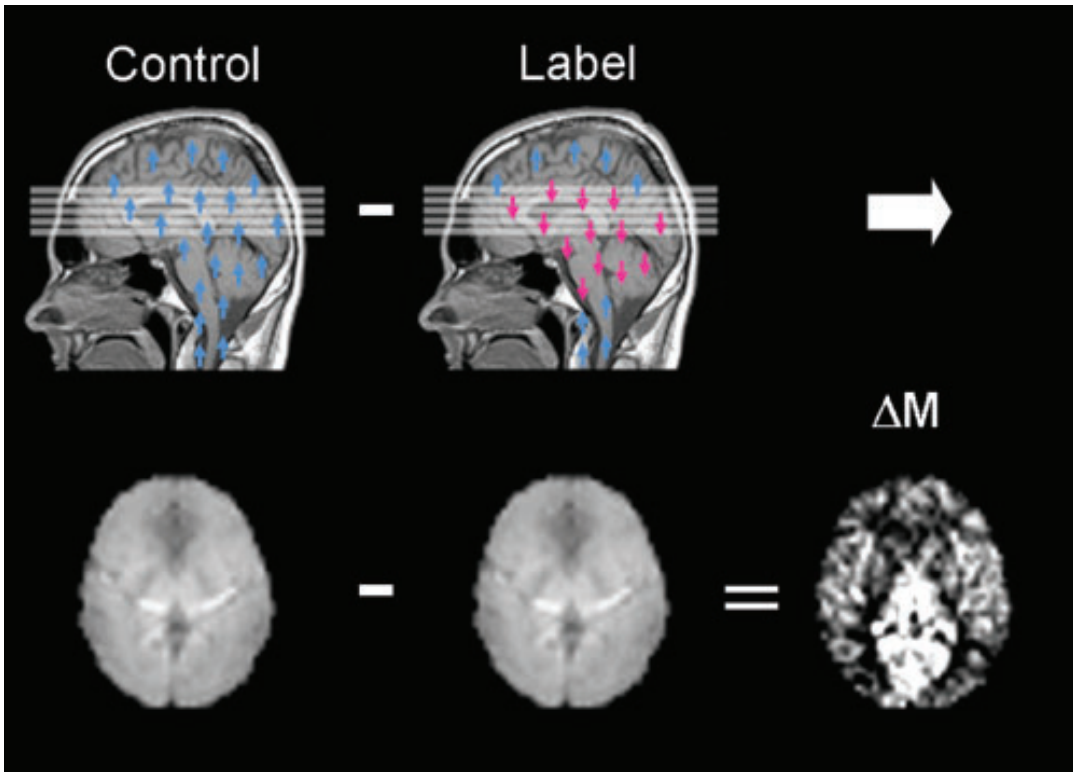


Figure 2.1. [Adapted from Petersen *et* al.] A schematic describing the basic principles of arterial spin labeling. The technique acquires two subsequent images, one without ("Control") or one with ("Label") arterial inversion. The acquisition process is repeated throughout the entire ASL scan. Pair-wise subtraction between the control and labeled volumes occurs during data analysis to derive the perfusion map (ΔM) (Petersen et al., 2006).

In 1992, Williams and colleagues used anaesthetized rats to demonstrate the first application of ASL perfusion MRI (Williams et al., 1992a). Scanned with a 4.7T MRI, rat brains' baseline perfusion maps were first acquired as a control in the absence of any arterial labeling. In the subsequent volume, the researchers inverted and thus "tagged" the spins of ^{1}H protons in the arterial blood at the neck with an RF pulse before obtaining a second image. A pair-wise subtraction between the two images yielded measures of cerebral blood flow across whole brain. This process was repeated multiple times for all rats to improve the accuracy of the final measurements, which agreed with previously reported values and correlated with individual pCO_2 data. The method also revealed the expected flow abnormalities when it was applied to rats with freeze-injured brains. Since

the approach relied on long, continuous RF pulses to perform arterial inversion, it was later named continuous arterial spin labeling (CASL) (Figure 2.2a).

2.1.2 Continuous Arterial Spin Labeling

Despite CASL's initial success, the continuous inversion of arterial magnetization requires the long RF pulses at frequencies off-resonant to that of the imaging region (Golay et al., 2004). Because large macromolecules in tissues have broad resonance frequencies, they inevitably become saturated as well and will exchange their magnetization with adjacent ^{1}H protons in a process called magnetization transfer (MT). This leads to an overestimation in the perfusion quantification, which posed significant challenges for ASL's pioneers. One solution is to replicate the MT effects in the control volumes by including a labeling sequence that targets a distal location. This is successful if one acquires a small region of interest that is evenly balanced between the labeling planes of the control and label volumes. However, slice-dependent effects of MT problems will remain in whole brain perfusion imaging. Another approach uses a separate coil for arterial inversion so that its localized magnetic field will restrict RF saturation of other tissues (Silva et al., 1995; Zhang et al., 1995). While the correction is effective, the implementation requirements are too specific and demanding for most standard multi-purpose MRI centres. Lastly, the continuous transmission of RF pulses required for CASL is often restricted by the hardware restrictions on most MRIs and the specific absorption rate (SAR) limit, thus affecting the sequence's SNR (Golay et al., 2004).

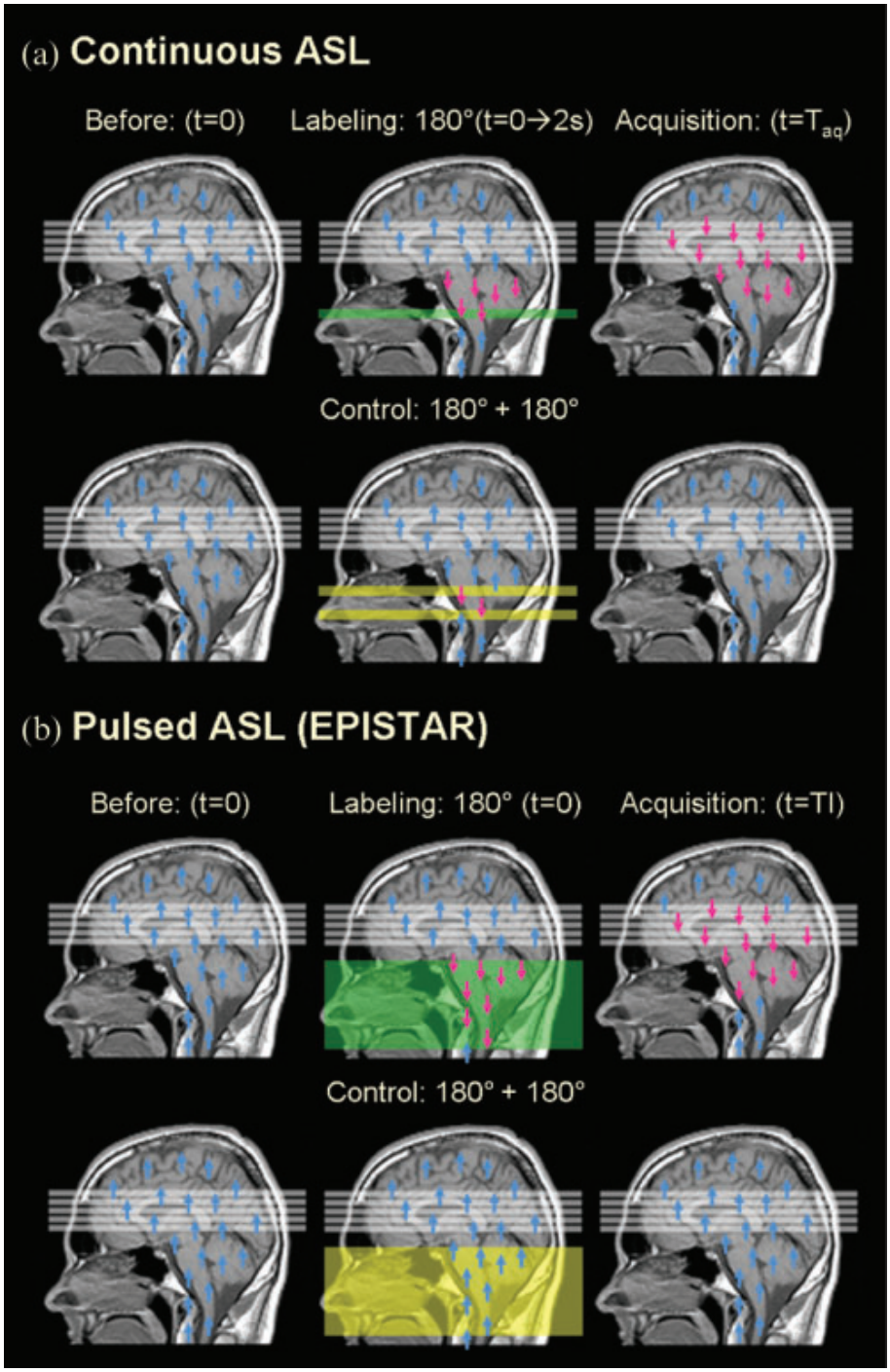


Figure 2.2. [Adapted from Petersen *et* al.] Schematic diagrams that depict the main scientific principles behind the two primary types of ASL. **a)** Continuous ASL (CASL) first tags the arterial blood with a long block of RF pulse to a narrow labeling plane (denoted by the green highlight) on the neck. To allow labeled blood some time to perfuse throughout the brain, the sequence then proceeds with a post-labeling delay that equals the arterial transit time (ART) before performing image acquisition. This waiting period is also referred to as the inversion time (TI) because it equals the waiting time before inversion recovery occurs. In the control volumes, minimal arterial inversion may take place (denoted by the yellow labeling plane) in order to replicate the magnetization transfer (MT) effect, though little arterial tagging should happen. **b**) This illustration is more relevant to the asymmetric pulsed ASL (PASL) sequence, but it is still informative for understanding the general concept of the PASL technique as a whole. Pulsed ASL (PASL) relies on a large labeling plane (denoted green) to compensate for the short RF

pulse, which provides background tissues with less time for the excitation and helps reduce the MT effect. While this circumvents possible hardware limitations in RF emission and human's specific absorption limit (SAR), it also complicates ART estimation because arterial blood in different vessels will take various times to arrive in the imaging plane. Thus, the eventual TI that one applies for the sequence may be suboptimal. In the control volumes (denoted with the yellow labeling plane), PASL also attempts to imitate the MT effect by incorporating a labeling sequence, much like the approach used in CASL (Petersen et al., 2006).

2.1.3 Pulsed Arterial Spin Labeling

In the end, it was a related technique called pulsed arterial spin labeling (PASL) that successfully brought the field to human applications (Detre et al., 1994). Unlike CASL, PASL does not require long durations of RF excitation pulses and therefore reduces the MT effect (Figure 2.2b). Instead, PASL applies an instantaneous inversion pulse over a larger slab, which typically overlaps with parts of the brain, and inevitably tags the arterial blood as well as some background tissue (Golay et al., 2004). This circumvents the problems of SAR limit and potential hardware restrictions, but it also prevents accurate estimations of arterial transit times (ART) because the arterial blood will be located in different blood vessels of varying sizes and orientations when tagged. Consequently, the labeled blood will reach the imaging plane at a wide range of time points, which makes it difficult to know when to start the image acquisition. Overall, the technique can be categorized by the two most common sequences of symmetric and asymmetric PASL, which are distinguished by the locations of the labeling planes in respect to the imaging volumes.

The original concept of symmetric PASL was proposed by Kwong and colleagues (Kwong et al., 1995) and was later referred to as flow-sensitive alternating inversion recovery (FAIR) (Golay et al., 2004). In this sequence, magnetic labeling occurs in both tag and control volumes but without a slice-selection gradient in the latter. Thus, the perfusion signal is derived from the absence of arterial inversion in the slice-selective volumes compared to those without slice selections. Since both sequences use the same

RF pulses to acquire images, MT effects would be offset at the middle slice. In addition to the use of short RF pulses, this approach can significantly minimize the MT effect and therefore the problem of perfusion overestimation that CASL faces.

Besides symmetrical PASL, an asymmetric variety has also been developed based on an EPISTAR (echo-planar imaging with signal targeting by alternating RF pulses) sequence (Edelman et al., 1994). Similar to CASL, both tag and control sequences perform arterial labeling at proximal and distal locations, respectively, to the image acquisition plane. However, symmetrical PASL requires large labeling slabs to compensate for the brief RF pulses. While MT effect will remain due to the slice-select gradient, the short labeling pulses will help minimize it in contrast to CASL, though the region of interest will need to be narrow and balanced between the labeling planes (Golay et al., 2004). To improve the technique, variants of asymmetric PASL have since appeared and included sequences such as PICORE (proximal inversion with control for off-resonance effects) (Wang et al., 2011) and TILT (transfer insensitive labeling technique) (Golay et al., 1999).

2.1.4 Pseudo-Continuous Arterial Spin Labeling

While both CASL and PASL have been used in many organs such as brain, lung (Mai et al., 2001), and heart (Williams et al., 1993), their respective technical shortcomings have made whole brain imaging difficult and thus impeded their use for fMRI. Fortunately, the recent development of pseudo-continuous ASL (pCASL) has helped break this barrier. Its overall scheme is similar to a standard CASL sequence in its use of flow-driven adiabatic inversion, but the continuous spin inversion is replaced by a train of RF pulses with identical phases for the tag volumes and alternated for the control volumes (Wu et al., 2007). This allows the use of lengthy arterial inversion pulses on a narrow slice of the neck without being bounded by hardware and SAR limits, which increase the tagging efficiency and the SNR without sacrificing the accuracy of ART estimation. In addition,

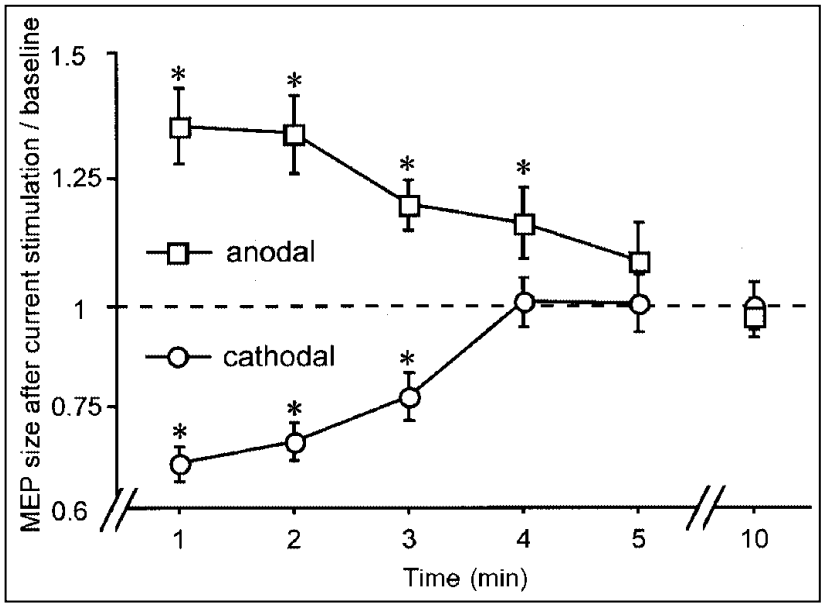
the control volumes can apply the same gradient-select profile as the tag volumes because the control volumes experience net-zero magnetic tagging. Since the RF trains are applied at the same location, subsequent subtraction of the two sessions can theoretically remove most MT effects. Thus, the imaging plane no longer needs to be centered between the labeling planes of tag and control volumes and paves the way for whole brain acquisition. With these advantages in mind, I pursued pCASL as the sequence of choice for my fMRI studies.

2.2 Transcranial Direct Current Stimulation

2.2.1 Overview

Transcranial direct current stimulation was coined in 1998 (Priori et al., 1998), though the exact method of its modern usage was established later in 2000 by Nitsche and Paulus (Nitsche and Paulus, 2000). Early works on electrical stimulation were pioneered in animal and human studies throughout the 1960s and 70s (Paulus, 2004). In cat, anodal tDCS was shown to increase, and cathodal tDCS to decrease, the excitability of motor and visual cortices (Kupfermann, 1965). Similar observations were found in rat models, in which the modulatory effect outlasted the simulation period (Creutzfeldt et al., 1962). However, pilot stimulation paradigms in humans often used small EEG electrodes, which led to a high current density and subsequent scalp burns without discernible behavioral or physiological changes (Stagg and Nitsche, 2011).

Modern tDCS gained prominence after it successfully altered motor evoked potential (MEP), a quantitative measure of motor-neuronal activity that serves as an indicator for M1 cortical excitability, through anodal and cathode stimulations of the motor cortex (Figure 2.3). Since tDCS only needs to apply a weak direct current, its design is remarkably simple. The components required to build a tDCS involve only a battery, a direct (0 Hz) current regulator, and a pair of electrodes.



Reprinted with permission from: Nitsche, M.A., Paulus, W. (2000). 'Excitability changes induced in the human motor cortex by weak transcranial direct current stimulation', The Journal of Physiology 527 Pt 3:633-639. Copyright 2000 M. A. Nitsche & W. Paulus. Available at http://dx.doi.org/10.1111/j.1469-7793.2000.t01-1-00633.x

Figure 2.3. [Adapted from Nitsche and Paulus] Changes in motor evoked potential (MEP) after 5 minutes of 1mA tDCS of the motor cortex. MEP size increased for 5 minutes after anodal stimulation and decreased after cathodal stimulation (Nitsche and Paulus, 2000).

The technique's simplicity helped expand the technique's repertoire of applications in recent years to include depression (Boggio et al., 2008b), stroke rehabilitation (Hummel et al., 2005), smoke craving reduction (Fregni et al., 2008), memory enhancement (Fregni et al., 2005b), and alleviation of acute (Antal et al., 2008; Terney et al., 2008) and chronic pain (Fregni et al., 2006a; Fregni et al., 2006b; Soler et al., 2010). Standard tDCS paradigms typically involve 5 to 20 min of stimulation with 5 to 15 seconds of ramp-up and ramp-down periods (Nitsche et al., 2008). The current applied varies between 1 and 2mA over two electrode pads with an area of 25cm^2 or 35cm^2 each.

2.2.2 Local Effects

The physiological basis of tDCS has been explored through pharmacological, neurophysiological, behavioral, and spectroscopy studies (Stagg and Nitsche, 2011). During stimulation, the effects of both anodal and cathodal tDCS seem to depend only on the modulation of membrane potential without affecting the synaptic signaling. For anodal tDCS, calcium and sodium channel blockers were found to reduce and eliminate the physiological changes, respectively (Nitsche et al., 2003c). However, the same

calcium and sodium channel blockades did not affect physiological responses from cathodal stimulation, in agreement with the standing theory that hyperpolarization occurs under the cathodal electrode. Neither NMDA nor GABA receptor antagonists, which respectively prevented the binding of glutamate (an excitatory neurotransmitter) and GABA (an inhibitory neurotransmitter), altered physiological changes for both stimulation modes (Nitsche et al., 2003c; Nitsche et al., 2004c).

The after-effect of anodal tDCS also appears to depend on membrane depolarization (Nitsche et al., 2003c). Similar to intrastimulation observations, sodium and calcium blockers could abolish the physiological responses from the stimulation. However, synaptic modulation does seem to also occur. Application of NMDA receptor antagonists can eliminate post-stimulation increases in intracortical facilitation (as measured by TMS (Nakamura et al., 1997)), which mainly reflects glutaminergic interneuron activity (Nitsche et al., 2004a). Additional TMS work also found a decrease in short-interval cortical inhibition (a quantitative measure of intracortical inhibitory circuits (Kujirai et al., 1993)) following anodal tDCS, which suggested the involvement of GABAergic interneurons (Nitsche et al., 2005). This is supported by a magnetic resonance spectroscopy (MRS) study that observed a decrease in GABA concentration after 10 minutes of anodal tDCS (Stagg et al., 2009b).

For cathodal tDCS, the contribution of membrane hyperpolarization to its post-stimulation effects has not been established. Calcium and sodium channel blockers did not appear to alter physiological responses, which corresponded to the intrastimulation observations (Nitsche et al., 2003c). However, modulation of glutamatergic synapses does seem to take place in the post-stimulation period. Significant decreases in glutamate concentration were observed in the after-effect period (Nitsche et al., 2005; Stagg et al., 2009b), though applications of NMDA receptor antagonists found conflicting evidence

(Nitsche et al., 2004a). As for the role of GABAergic interneurons, both short-interval cortical inhibition (an indicator of GABAergic interneuron activity) and GABA concentration seemed to increase after stimulation (Nitsche et al., 2005; Stagg et al., 2009b).

2.2.3 Distant Effects

To further elucidate the task-free effect during and after tDCS, past studies have employed modalities such as positron emission tomography (PET) (Lang et al., 2005), electroencephalography (EEG) (Garcia-Larrea et al., 1999; Ozen et al., 2010), and BOLD fMRI (Baudewig et al., 2001; Kwon et al., 2008; Stagg et al., 2009a; Antal et al., 2011). The first investigation of this kind used BOLD fMRI on healthy subjects during finger tapping tasks after stimulation on the motor cortex (M1) (Baudewig et al., 2001). Compared to volunteers who received sham tDCS, those stimulated cathodally experienced a 38% and 28% decrease in the total number of activated voxels within 0-5 and 15-20 minutes of terminating a 5-minute, 1mA stimulation, respectively. However, none of the reduction occurred in the hand area of the primary motor cortex. For the subjects with anodal tDCS, an insignificant 5% increase in activated voxels was observed without regional biases. Based on these results, the authors suggested that tDCS exerts its influence over cortico-cortical connections rather than the primary sensorimotor input itself. Further, BOLD fMRI studies attempted at investigating the tDCS effect during, rather than after, stimulation without any task. Dechent and colleagues were not able to detect any baseline activity, though they did find a reduction in BOLD response for both anodal and cathodal M1 tDCS when the stimulation occurred during a voluntary motor task (Dechent et al., 2010). A separate study by Kwon and colleagues used an unconventional tDCS paradigm and found single voxels of activation in the primary motor cortex for only one of four 21-second anodal M1 tDCS sessions (Kwon et al., 2008), though Antal *et* al. found no activity at all (Antal et al., 2011).

Besides BOLD fMRI, PET and EEG studies have provided different information on how electrical stimulation can affect neuronal activity. Lang and colleagues used PET to investigate task-free regional cerebral blood flow (rCBF) changes after 10 minutes of both anodal and cathodal tDCS on the left M1 (Lang et al., 2005). Widespread increases and decreases in rCBF were observed across the whole brain without significant polarity-specific differences. Active regions included the premotor cortex, posterior parietal cortex, insular cortex, superior temporal gyrus, lateral prefrontal cortex, cerebellum, and thalamus. The lack of spatial specificity in the effect of electrical stimulation was supported by EEG studies, which also reported widespread cortical changes (Garcia-Larrea et al., 1999; Ozen et al., 2010).

A recent study by Zheng and colleagues found promising tDCS-related rCBF changes using perfusion fMRI with ASL (Zheng et al., 2011). Since this imaging modality is significantly less vulnerable to low-frequency drifts than BOLD fMRI, it is better suited for investigating the effects of the tonic tDCS blocks. Fourteen healthy subjects were recruited for the resting, concurrent ASL-tDCS scans, in which 6 subjects received only anodal or cathodal stimulation and 2 subjects underwent both stimulation polarities. The active electrode was located at the right M1 and the reference electrode was placed over the left supraorbital ride. Using an unconventional tDCS paradigm, the authors designed each scan to consist of four 10-minute, tDCS-off blocks that were interleaved with three 7-minute, tDCS-on blocks. The current was applied through a pair of $20cm^2$ electrodes and ranged between 1.0mA and 1.7mA for anodal stimulation and between 0.8mA and 2.0mA for cathodal stimulation. The authors found significant increases in rCBF during both anodal and cathodal tDCS, though the magnitude was larger with anodal stimulation. The blood flow then dropped to sub-baseline levels immediately after current cessation.

A trend was also observed between percent changes in rCBF and current strength, which was positive for anodal tDCS ($p<0.05$) and negative for cathodal tDCS ($p=0.16$).

Although the above studies have offered insights into the neuromodulations that occurred during and after tDCS, each is limited by its respective techniques or experimental designs. PET is a radioactive, costly, and invasive method that requires large spatial smoothing with low temporal resolution (Brooks et al., 2005), while EEG provides even less spatial information. BOLD fMRI may have seen considerable success in countless applications, but it is not suited for experimental designs with long stimulus blocks due to low-frequency scanner drifts (Wang et al., 2003). A combination of factors such as cerebral metabolic rate, blood volume, and regional cerebral blood flow also contributes to the final BOLD signal, thus lowering its accuracy to reflect neuronal activity. The only tDCS-ASL study demonstrated the technical feasibility of using an MRI approach that specifically targets low-frequency tasks (Zheng et al., 2011). However, its unusual tDCS paradigm limits its relevance to clinical studies, which typically used single, 20-minutes stimulation blocks.

In addition, the existing human imaging and electrophysiological literature placed greater focus on M1 stimulation and presented more data on post-stimulation than intrastimulation effects, but they reached conflicting conclusions. Functional MRI investigations (Baudewig et al., 2001; Antal et al., 2011; Zheng et al., 2011) suggested that M1 tDCS has localized effects during and after stimulation in contrast to the results from PET (Lang et al., 2005) and EEG studies (Ardolino et al., 2005). They also did not agree on whether concurrent tasks were required for the modalities to detect any neuronal changes. These uncertainties hinder us from inferring the effects of DLPFC tDCS using these approaches alone.

CHAPTER 3 – TASK-FREE EFFECTS OF TRANSCRANIAL DIRECT CURRENT STIMULATION

Before studying the effects of L-DLPFC tDCS on pain modulation, I needed to first understand the functional changes in the brain from such stimulation in the absence of noxious inputs. The previous chapters have underscored the dearth of information on this topic, thus requiring separate experiments for this investigation. Using concurrent tDCS-fMRI with arterial spin labeling, we studied the changes in brain perfusion activity and functional connectivity during and after stimulation from baseline.

3.1 Introduction

Before investigating the neuromodulation of pain, I need to first understand the stand-alone effects of L-DLPFC tDCS on brain activity. The literature provides little information about this topic, and I will proceed to review the existing work available in the following section.

3.1.1 L-DLPFC tDCS

I performed an exhaustive literature search on task-free L-DLPFC tDCS in Pubmed and did not find any related human MR studies. The closest example found involved a resting EEG experiment that examined the post-stimulation changes in regional electrical activity (Keeser et al., 2011). Keeser and colleagues recruited 10 healthy subjects and applied one 20-minute session of 2mA anodal tDCS and one session of sham stimulation. The active electrode was placed over the F3 position in EEG 10/20 system, and the reference electrode over the right supraorbital ridge. Within 5 to 10 minutes after each session of stimulation, the researchers placed a 32-electrode EEG cap onto the subjects and recorded their resting EEG signatures for 10 minutes. Experimental analysis separated the data across five frequency bands: delta (1-4 Hz), theta (4-8 Hz), alpha (8-12 Hz), and gamma (30-40 Hz). Significant decreases in the delta wave amplitudes were observed in the frontal cortex after anodal tDCS in comparison to sham, which suggested less inhibitory activity. Increased alpha and gamma waves were also recorded. Although

these differences were not significant, they were greater in the first 5 minutes of the resting EEG recording than in the overall mean.

In a separate study, Merzagora and colleagues used functional near-infrared spectroscopy (fNIRS) to examine changes in oxyhemoglobin (HbO_2) and deoxyhemoglobin (HHb_2) concentrations in the prefrontal cortex after tDCS (Merzagora et al., 2010). The authors recruited 12 healthy subjects for one session of real stimulation and one session of sham stimulation. The active (anodal) and reference (cathodal) electrodes were placed over Fp2 and Fp1 positions, respectively. The 1mA stimulation lasted for 10 minutes per each session, followed by a 20-minute fNIRS recording. Merzagora and colleagues found significant [HbO_2] increases under the anodal electrode compared to sham, though a negligible increase was also observed under the cathodal electrode. The matching directionality of [HbO_2] changes from tDCS of opposite polarities was unusual, especially given the mirrored locations of Fp1 and Fp2 across the hemispheric divide.

3.1.2 L-DLPFC rTMS

Apart from the tDCS studies, I expanded the literature search to include task-free rTMS of L-DLPFC, which helped to provide additional information about the resulting neuromodulatory effects. Speer and colleagues published the first paper on how rTMS can alter cerebral blood flow to the L-DLPFC (Speer et al., 2000). Recruiting 10 depression patients as their subjects, they used PET to observe increases in L-DLPFC rCBF after excitatory (20 Hz) rTMS and decreases after inhibitory (1-5 Hz) stimulation. These findings were verified by Loo *et* al. with single photon emission computerized tomography (SPECT) (Loo et al., 2003) and again by Speer *et* al. in a separate study (Speer et al., 2009), though Knoch and colleagues have suggested that the rCBF changes could vary depending on other rTMS parameters such as train speed and intensity of stimulation (as a percentage of motor threshold) (Knoch et al., 2006). Differing opinions

are prevalent in the discussion on the activity of DLPFC-connected structures. For example, while Speer *et* al. found global increases in many cortical and subcortical structures during excitatory rTMS (Speer et al., 2000), Loo *et* al. only observed highly localized effects and some rCBF decreases (Loo et al., 2003). The heterogeneity of rTMS parameters in the studies above may explain the differing results. However, a consensus appeared evident that DLPFC rCBF was increased with excitatory rTMS and decreased with inhibitory rTMS.

3.1.3 Overview

The limited knowledge on the effect of L-DLPFC tDCS underlines the need for a separate investigation on this topic. Given the tonic nature of tDCS paradigms, perfusion fMRI with arterial spin labeling (ASL) becomes an ideal modality for this study. The pair-wise subtractions between control and tag volumes throughout an experiment (Figure 2.1) can theoretically remove any low-frequency contaminations and allow the imaging of long stimulus blocks like a tDCS session. In addition, ASL imaging can potentially measure rCBF changes with greater sensitivity and resolution than PET without the need for invasive procedures or radioactive tracers (Ye et al., 2000). With these advantages in mind, I sought to investigate the task-free effects of tDCS across the whole brain by using ASL fMRI. While L-DLPFC is anatomically and functionally connected to many cortical and subcortical regions (Cummings, 1993; Tekin and Cummings, 2002), I will be particularly interested in the effect of L-DLPFC tDCS on thalamus and midbrain, two key regions for the modulation of pain.

3.2 Methods

3.2.1 Subject Recruitment

I recruited a cohort of 14 healthy subjects to participate in the study(4 females, all right-handed, mean ± SD age: 26.4 ± 4.9 years). Two of the subjects withdrew due to discomfort in the scanner environment and were there excluded in the data analysis. In adherence to ethical regulations from the U.K. National Research Ethics Service and the Declaration of Helsinki (1996), all research participants were fully informed of the techniques used and gave written consent to participate in the study. Besides observing MRI safety guidelines, I further screened for possible contradictions to tDCS as reported in previous literature (Nitsche et al., 2008), thus minimizing the safety risks for the participants.

3.2.2 Experiment Setup and Paradigm

An MR-compatible tDCS kit (DC-Stimulator MR, Magstim, Cardiff, UK) was used, which was fitted with a pair of 5 kΩ resistors by the electrodes (7cm x 5cm) to prevent the occurrence of eddy current or significant electrode heating in an MR setting. The active electrode was centered at the F3 position in EEG 10/20 system, the location for L-DLPFC used in previous tDCS-pain studies (Fregni et al., 2006b; Boggio et al., 2008b; Boggio et al., 2008a). An Omega-3 oil pill (Ultra-Pure Omega-3 Fish Oil, Purity Products, Plainview, NY, USA) was placed above the electrode center in order to visualize the electrode's location in MR images. The reference electrode was located above the contralateral supraorbital ridge to complete the electrical circuit. To minimize the contact resistance between the scalp and the electrodes, high-chloride EEG gel (Abralyt HiCl, EasyCap, Herrsching, Germany) was used as a conducting medium.

The subject cohort received sessions of anodal and cathodal tDCS that were counterbalanced in order across the group. A gap of at least one week was spaced for

every subject between the two experimental sessions. Prior to each session of tDCS, subjects were given approximately 15 seconds of stimulation in order to familiarize themselves with the sensation. tDCS of such short duration has been shown to exert no lasting after-effects (Nitsche et al., 2008). During the experiment, stimulation of 1mA was applied for 20 minutes between two 10-second ramp-up and -down periods. To increase the likelihood of detecting adverse events, the first 15 seconds of the stimulation were used to ensure that the subjects were comfortable before scanning began, but I continued scanning without informing the subjects when the stimulation ended.

Using a 3T MRI scanner (Magnetom Verio 3T, Siemens, Germany) and a 32-channel head coil, I performed perfusion imaging with a pseudo-continuous ASL sequence that utilized GRAPPA (factor of 2) and applied a gradient-echo EPI readout (TR=3.21s, TE=11ms, 7/8 k-space). This sequence is similar to the non-selective cycles described in Okell *et* al. (Okell et al., 2010) and has been previously applied (Bridge et al., 2010). Whole brain coverage was provided for each subject with 28 axial slices, all acquired in ascending order through the brain (4x4x4.6mm^3 voxels) with an inter-slice gap of 0.46mm. Through a time-of-flight scan of the neck, the optimal labeling plane was chosen at approximately 8 to 10cm inferior to the center of the axial slices. Each labeling pulse lasted 1.4s and was followed by a post-labeling delay of 900ms. The high-resolution (1x1x1mm^3 voxels) structural scans were acquired with a standard T1-weighted sequence (TR=2.04s, TE=4.68ms) and contained 192 axial slices.

The experiment paradigm is illustrated in Figure 3.1. Once a subject had been fully prepared, I proceeded with a 10-minute scan to record his or her baseline rCBF map. Prior to initiating tDCS, I made sure that the subjects were comfortable with the tingling sensation of the stimulation. Concurrent tDCS-fMRI for 20 minutes was then performed, followed by a final 10-minute scan of the tDCS after-effect. Subjects did not carry out

any task during the scans and were asked to remain motionless and awake. Participants were not informed about the polarity of their stimulation sessions, although there are no reported differences in the sensations of anodal and cathodal tDCS (Gandiga et al., 2006).

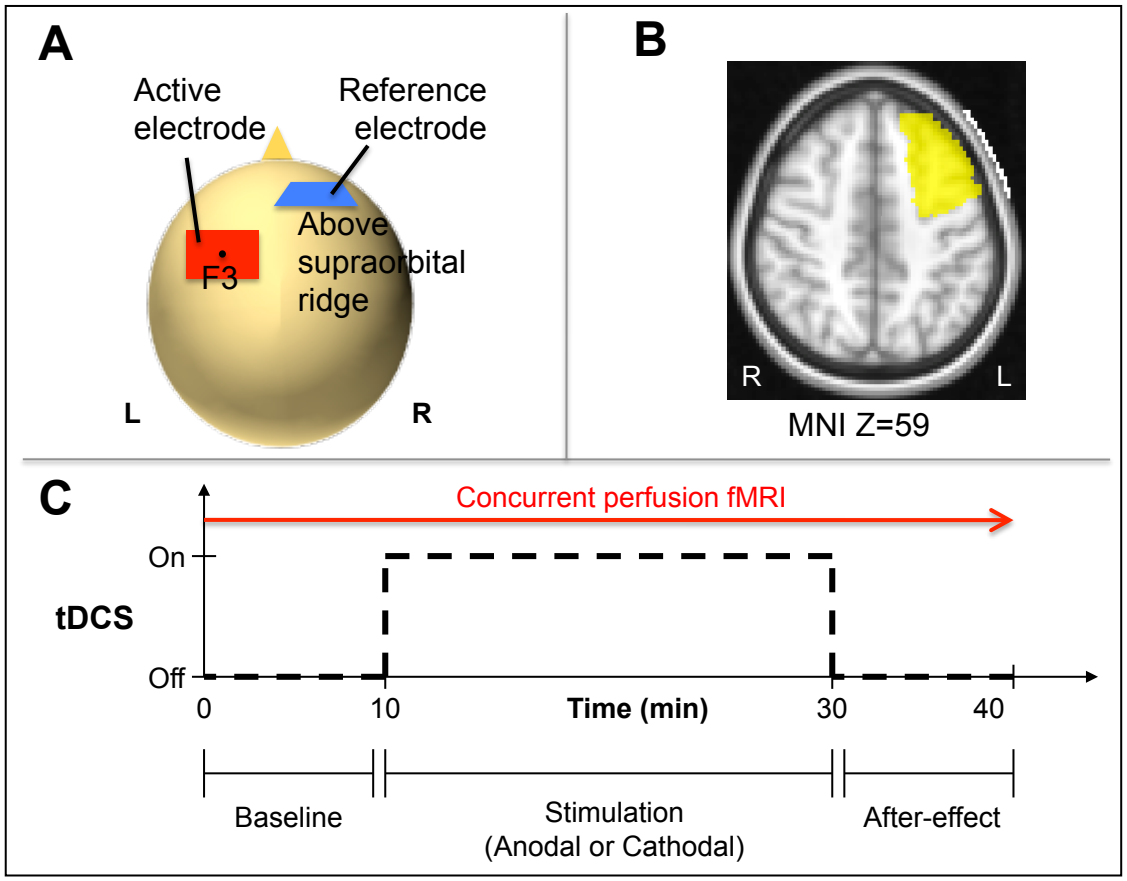


Figure 3.1 – Illustrations of the experiment setup and design. **A)** The center of the active electrode was placed over the F3 coordinate in the EEG 10/20 system, while the reference electrode was placed on the right forehead above the supraorbital ridge. **B)** The active and reference electrodes (shown as a white line along the outside of the skull) provided coverage of the L-DLPFC (in yellow). The location of the active electrode was acquired by registering the coordinates of the fish-oil pills to standard space, while that of reference electrode was established above the supraorbital ridge. Both the background image and the specified slice numbers are presented in MNI standard space (2mm resolution). **C)** The experiment paradigm lasted for 40 minutes from beginning to end in an MR setting. Electrodes were secured to the participants before they entered the scanner. The first 10 minutes constituted the baseline ASL scan with the tDCS not switched on, followed by 20 minutes of concurrent tDCS-ASL fMRI, and then a 10-minute scan to observe the after-effect of tDCS. The participants did not perform any tasks during the scan and were simply asked to remain still and keep a blank mind.

3.2.3 Data Analysis

Separate first-level analyses of baseline, stimulation, and after-effect scans were carried out with FMRIB software library (FSL) version 4.1.7 (http://www.fmrib.ox.ac.uk/fsl) (Wager et al., 2004; Woolrich et al., 2009). For each scan, the functional data first underwent motion correction with a six-parameter affine algorithm (Jenkinson et al., 2002). Skull removal was then performed with the Brain Extraction Tool (BET) in the FSLtools (Smith, 2002), followed by manual extraction to ensure thoroughness and precision. I used non-linear high-pass temporal filtering (sigma of 200s) to remove scanner drifts and BOLD contaminations (Chuang et al., 2008) and applied spatial smoothing (full-width half-maximum of 8mm). The perfusion subtraction of the ASL data was modeled with a boxcar regressor by using the TR (3.21s) as the duration of each on or off period. Finally, functional data was registered to the respective high-resolution T1 structural scan, which was subsequently registered to the Montreal Neurological Institute (MNI) standard brain.

The second-level analysis used a paired t-test to perform intra-subject comparisons between baseline, stimulation, and after-effect periods. These individual analyses were submitted to a third and final level of analysis for the averaged group comparison in rCBF across periods (mixed effect; $Z>2.0$, cluster corrected at $p<0.01$). This sequence of analyses allowed us consideration of both the intra-scan and intra-subject variances, thus minimizing the bias from any single session or participant.

To explore tDCS-induced changes in functional coupling between L-DLPFC and the rest of the brain, I conducted functional connectivity analysis by using the time course of the demeaned perfusion-subtracted signal, which was acquired by using the perfusion subtraction function in FSL (Smith et al., 2004; Woolrich et al., 2009). Since the size of the electrodes was quite large, the mean time course was extracted from the whole L-DLPFC as the regressor to acquire correlation maps for individual baseline, stimulation,

and after-effect periods. For each period, the standard L-DLPFC mask (see below for anatomical limits) was registered to the structural space to generate subject-specific masks, followed by a subsequent registration to the respective functional space. Similar to my analysis of rCBF changes, I first found the functional connectivity map for each period. I then employed fixed-effect analysis for an intra-subject comparison followed by a final group average (mixed effect; $Z>2.0$, cluster corrected at $p<0.01$).

To corroborate the functional connectivity maps, I also performed Pearson correlation tests between the activity within the L-DLPFC and thalamus, midbrain, and right cerebellum lobule VI. Lobule VI was used as a control due to its lack of anatomical and functional connection to L-DLPFC (Krienen and Buckner, 2009). For the different periods, the mean perfusion-subtracted time courses were extracted for all areas of interest. The respective Pearson correlation coefficient was then calculated between the specified pair of regions for each period and averaged across subjects. Using the mean coefficient values from the baseline period as a reference, I tracked how they were changed by the subsequent stimulation.

3.2.4 Electrode Location

The location of the active electrode was determined from the fish-oil pill in the structural scans. The center of the active electrode was found by marking the coordinates of the pills, which were then registered to MNI standard space and averaged across subjects. An area of 35 cm^2 that clung along the standard head was drawn around this center to delineate the electrode location. Little inter-subject variation was found in the standardized positions of the fish-oil pill centers; the standard error means of the mean pill location in MNI x-, y-, and z-directions were ~2.6mm, ~2.9mm, and ~4.6mm, respectively. For the reference electrode, its location was established by a 35-cm^2 area above the right supraorbital ridge. After overlaying the electrode locations on the

standard head, I used this as the background image for the final activity and correlation maps. This allowed for easy determination of whether the changes in activity or functional connectivity occurred near the sites of stimulations.

3.2.5 Anatomical Masks

The region-of-interest masks were determined from anatomical demarcations or structural atlases. The midbrain mask was initially drawn from the MNI-converted Talairach atlas, part of which overlapped with the ventricles, and then overlaid with a thresholded (20%) brainstem mask from the Harvard-Oxford probabilistic atlas to derive the final midbrain mask. The M1 mask was based on demarcations used in previous literature (Stagg et al., 2009a). The standard DLPFC mask covers Brodmann areas 8A, 46 and 9/46, all of which consist of similar cytoarchitectonic features with a well-developed layer 4. Nearby regions of areas 9 and 8B, located on the dorsal most and medial aspect of the prefrontal cortex, were not included because their sparse granular layers differ from those found in the other areas (Petrides and Pandya, 1999). In addition, area 9 encompasses the medial surface above the paracingulate sulcus, thus making it more appropriate for the dorsomedial prefrontal cortex instead (Croxson et al., 2005). Further details of the DLPFC demarcations can be found in the study by Petrides and Pandya (Petrides and Pandya, 1999). All other anatomical masks were derived from the Harvard-Oxford probabilistic atlas after a 20% threshold cutoff.

3.3 Results

3.3.1 Artefact Check

Before data collection, a pilot scan was performed on one subject to check for possible image artefacts from the electrical equipment or the current. I used the same pCASL sequence as the rest of the study, but applied a higher resolution (3x3x4 mm^3 voxels) to better discern any possible distortions along the outer edges of the brain. Visual examinations of the structural and functional images as well as temporal SNR maps did not reveal any artefacts, even in the presence of electrical stimulation (Figure 3.2).

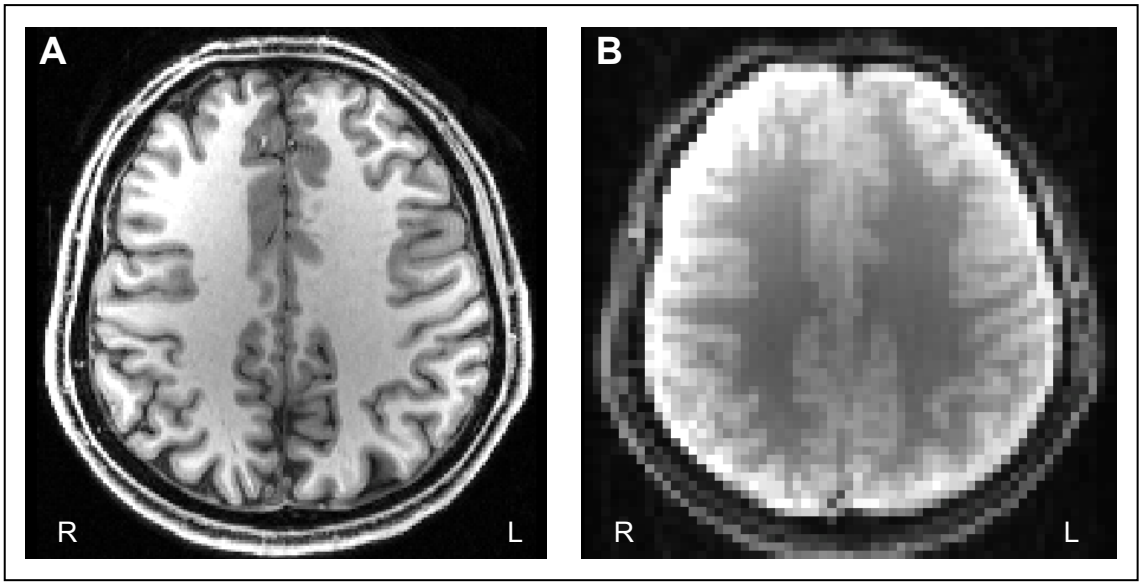


Figure 3.2 – Sample image slices at the same axial level as the electrodes were taken from a pilot study of concurrent tDCS-fMRI. **A)** The structural volume was acquired with electrodes attached but without current input. **B)** The functional volumes were taken during concurrent stimulation. No image artefacts were observed in either condition.

3.3.2 Perfusion Activity During tDCS

After I verified the absence of image distortions, imaging data was collected across the cohort of 12 healthy subjects and used to derive perfusion activity maps to infer changes in gray matter activity across the whole brain. The existing literature suggests that excitatory stimulation should increase rCBF and inhibitory stimulation should decrease it (Speer et al., 2000; Wachter et al., 2011). During anodal tDCS over L-DLPFC, there was an increased rCBF in L-DLPFC, left SI, mid-cingulate cortex, and paracingulate cortex

compared to baseline (Figure 3.3). While the effect was quite lateralized to the stimulated hemisphere, cortical regions that underlie the reference electrode (e.g. the frontal pole) also experienced higher activity.

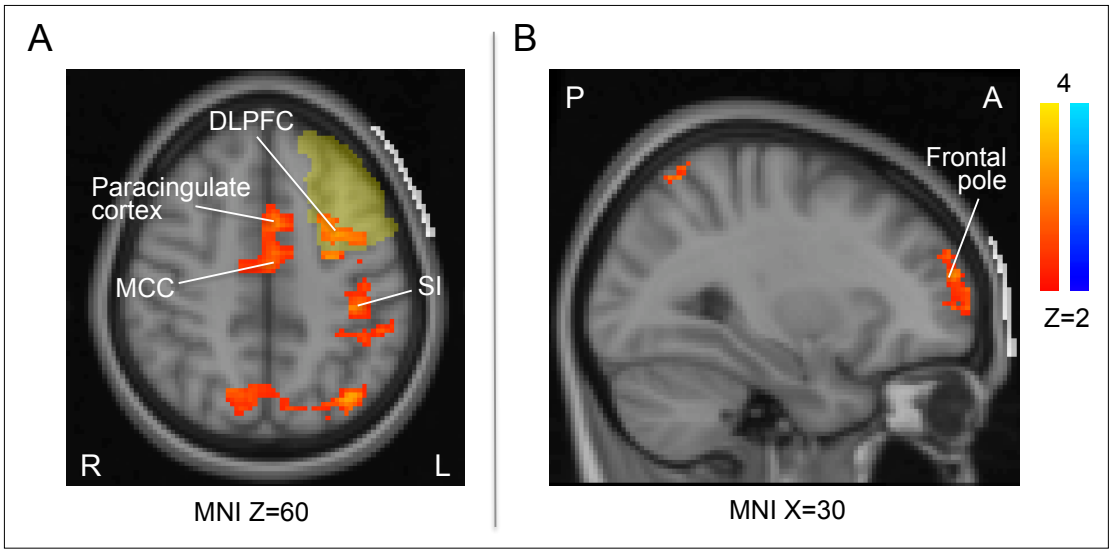


Figure 3.3. Perfusion activity map of gray matter associated with $Anodal_{stimulation - baseline}$ (mixed effects; Z>2, cluster corrected at p<0.01). White linings along the skull delineate the locations of the electrodes. **A)** L-DLPFC (denoted by the yellow mask) and its connected regions, such as MCC, and SI, showed increased rCBF during stimulation from baseline. These changes were mainly lateralized, suggesting that they were caused by L-DLPFC tDCS. **B)** In addition, increased rCBF was observed in the right frontal pole underneath the reference electrode, which did seem to have an effect. (MCC = mid-cingulate cortex; SI = primary somatosensory cortex; DLPFC = dorsolateral prefrontal cortex)

In comparison, the activity map of cathodal tDCS showed markedly different patterns that did not resemble those of anodal tDCS (Figure 3.4). While changes in L-DLPFC did not survive the statistical thresholds, rCBF decreases were observed in the thalamus and the right temporal lobe across Wernicke's area and the medial and inferior gyri. No other regions experienced significant rCBF changes.

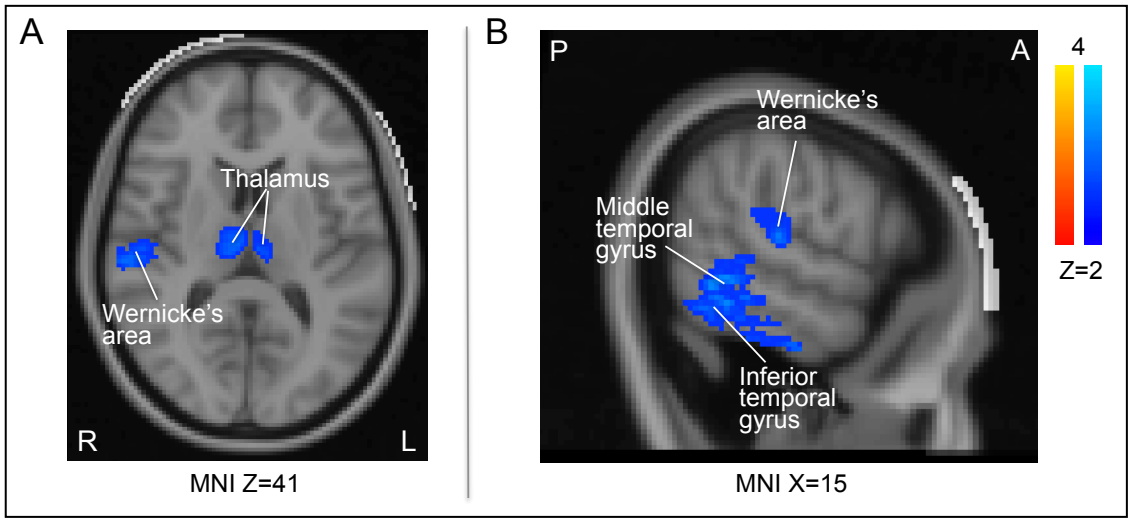


Figure 3.4. Perfusion activity map of gray matter associated with $Cathodal_{stimulation - baseline}$ (mixed effects; Z>2, cluster corrected at p<0.01). White lines along the outside of the skull delineate the locations of the electrodes. A) Decreased rCBF was observed in the thalamus and Wernicke's area. B) Activity in the right temporal lobe, including the middle and inferior temporal gyri, also decreased.

Since tDCS modulates cortical activity through large electrodes, I suspected that the activity of L-DLPFC as a whole (rather than just subregions) might be altered. Thus, the analysis was extended to investigate the region's relative rCBF changes. The mean perfusion signals were calculated from L-DLPFC to compare rCBF across the baseline and stimulation periods for both anodal and cathodal tDCS. The data showed higher perfusion in L-DLPFC during anodal stimulation (2.05 ± 1.43%; mean ± SEM) than during cathodal stimulation (-1.72 ± 1.28%), a difference that was marginally significant (p=0.067). There were no significant difference between stimulation and baseline periods for both anodal (p=0.26) and cathodal (p=0.20) tDCS.

3.3.3 Correlation Analyses

Besides changes in perfusion activity, L-DLPFC tDCS may alter the functional connectivity of L-DLPFC to connected regions. tDCS has been shown to modulate functional connectivity after M1 stimulation (Polania et al., 2011), though this has not yet been explored with L-DLPFC tDCS. To determine the functional connectivity of L-DLPFC with gray matter across the whole brain, the region's mean perfusion-subtracted

time course was used as the seed to generate correlation maps. In comparison to the baseline period, there was a relative reduction in the L-DLPFC connectivity to bilateral thalami and an increase to the caudate nucleus and the paracingulate cortex during anodal stimulation (Figure 3.5A). Deeper brain structures, such as the midbrain, also became less functionally coupled from L-DLPFC than before stimulation (Figure 3.5B). Given that the *a priori* interest is in thalamus and midbrain, I also sought to verify these findings with separate Pearson correlation tests. The mean perfusion-subtracted time courses of both thalamus and midbrain were extracted from anatomical masks and correlated with that of L-DLPFC. Between baseline and stimulation periods for anodal tDCS, I found significant decreases in time course correlations from L-DLPFC to thalamus ($p<0.02$) and midbrain ($p<0.01$) (Figure 3.5C). This pattern of functional coupling was not observed for cathodal tDCS and began to recover after the cessation of anodal tDCS. As a control, the correlation coefficients between the time courses of L-DLPFC and right cerebellum lobule VI were used due to their structural and functional separation (Krienen and Buckner, 2009). These values did not significantly change between periods for both stimulation polarities.

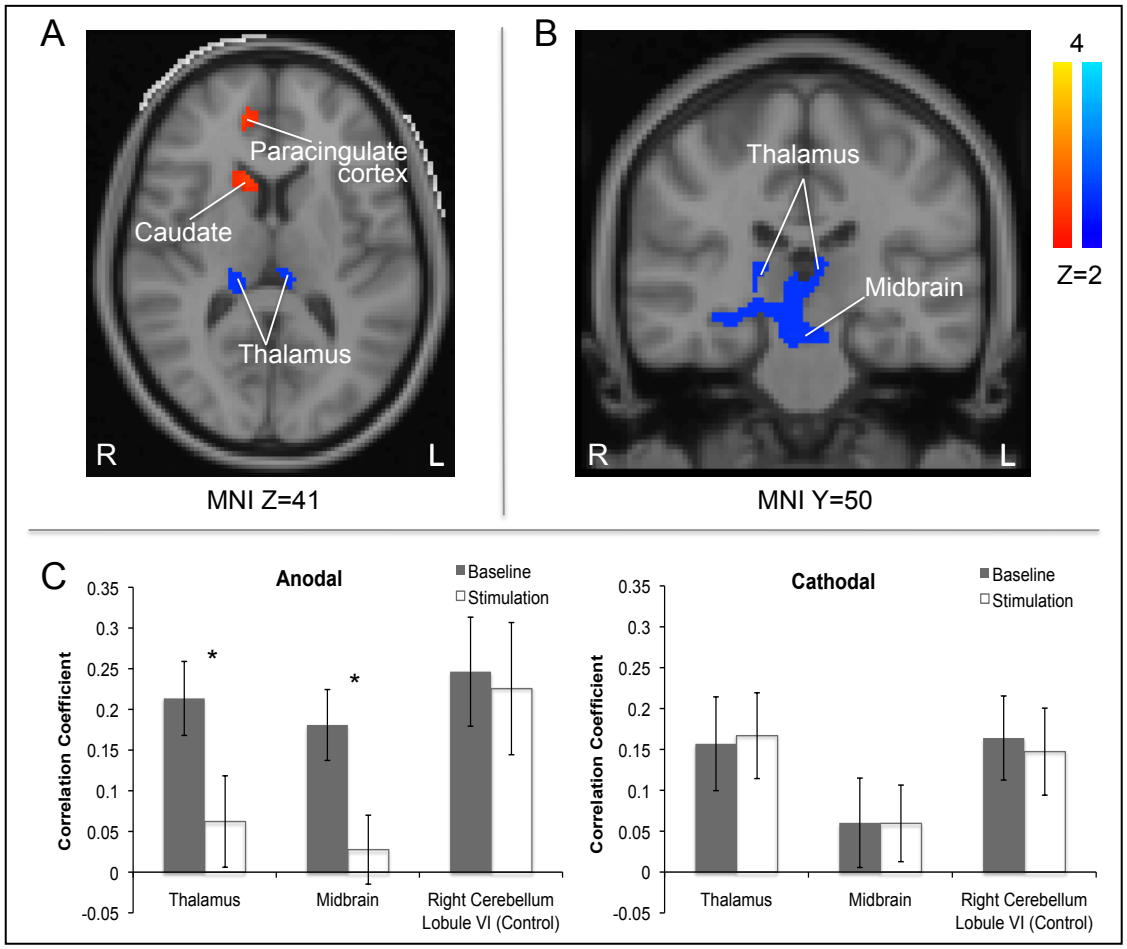


Figure 3.5. **A)** Functional connectivity map of L-DLPFC to gray matter during anodal tDCS (mixed effects; Z>2, cluster corrected at p<0.01). The specified slice numbers are presented in MNI standard space (2mm resolution). The mean time course of the whole L-DLPFC was used as the seed because of the large size of the electrode. Correlation of L-DLPFC to paracingulate cortex and caudate nucleus increased while that to bilateral thalami decreased during stimulation. The latter suggests that anodal tDCS on L-DLPFC interrupted its ability to communicate with the rest of the body. **B)** The decrease in functional connectivity is also extended to the midbrain, a deep brain structure with key roles in pain modulation. **C)** I also tested our *a priori* hypothesis on changes in L-DLPFC connectivity to thalamus and midbrain by calculating the Pearson correlation coefficients between the regions' mean perfusion-subtracted time courses, which were extracted with anatomical masks. As suggested by the functional connectivity maps, I observed a significant decrease in respective correlations to thalamus ($p<0.02$) and midbrain ($p<0.01$) from the baseline period to the stimulation period. These changes were not observed during cathodal tDCS. I used right cerebellum lobule VI as a control because of the region's weak structural and functional links to DLPFC (Krienen and Buckner, 2009). The functional connectivity between cerebellum lobule V and L-DLPFC did not significantly vary from the baseline period to the stimulation period. Error bars denote the standard error means across subjects.

3.3.4 Perfusion Activity After tDCS

In addition to intra-stimulation changes, I explored the immediate after-effects of L-DLPFC tDCS and found significant differences to baseline for both anodal and cathodal stimulations. Within the 10 minutes after the anodal stimulation stopped, widespread rCBF decreases were observed across the whole brain, which included thalamus, ACC, PCC, and, lingual gyrus (Figure 3.6). The right frontal pole, an area covered by the reference electrode, also showed increased rCBF. Changes in L-DLPFC activity did not survive statistical thresholds.

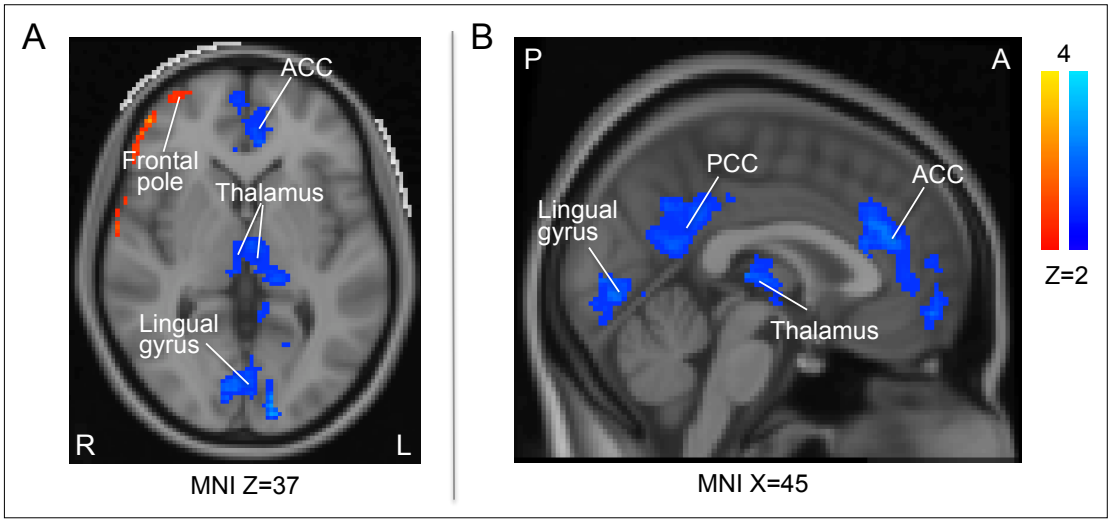


Figure 3.6. Perfusion activity map associated with $Anodal_{after\text{-}effect - baseline}$ (mixed effects; Z>2, cluster corrected at p<0.01). White lines along the outside of the skull delineate the locations of the electrodes. **A)** Widespread decreases in rCBF were observed after anodal tDCS relative to baseline. Regions with functional and/or anatomical connections to L-DLPFC, including ACC and bilateral thalami, were affected. Activity underneath the reference electrode decreased from the intra-stimulation period. While rCBF changes in L-DLPFC were observed during stimulation from baseline, these changes no longer survived the statistical thresholds in the after-effect period. **B)** A sagittal view of the perfusion activity map. Besides ACC, PCC also experienced lower activity after the stimulation stopped. (ACC = anterior cingulate cortex; PCC = posterior cingulate cortex)

Similar to anodal tDCS, widespread rCBF decreases from the baseline was observed after cathodal tDCS (Figure 3.7). Larger regions in bilateral temporal lobes, such as Wernicke's area, showed lower activity. The rCBF of paracingulate cortex, precuneous cortex, ACC, lingual gyrus, and left caudate nucleus had also decreased from baseline levels.

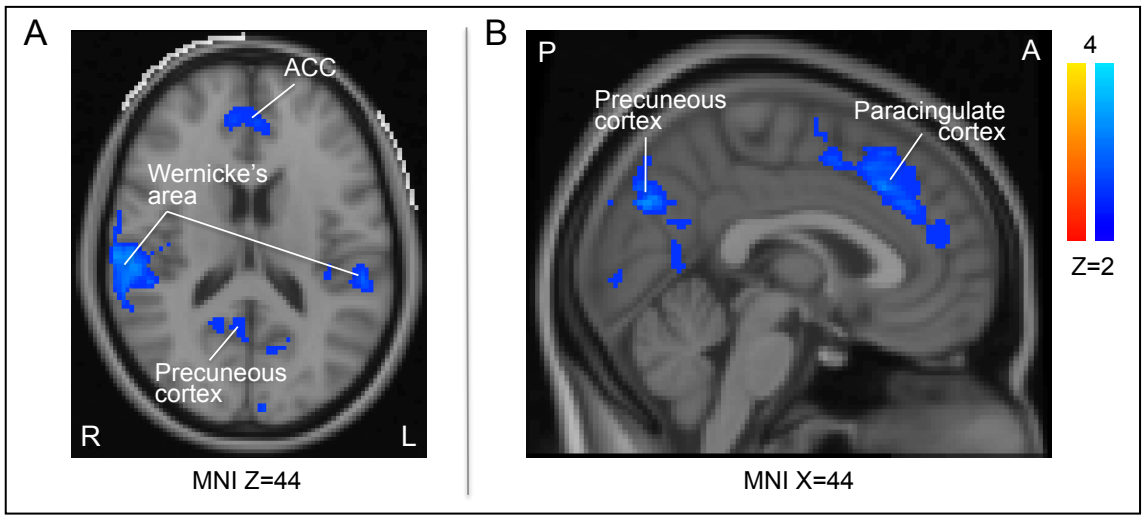


Figure 3.7. Perfusion activity map associated with $Cathodal_{after\text{-}effect - baseline}$ (mixed effects; Z>2, cluster corrected at p<0.01). White lines along the outside of the skull delineate the locations of the electrodes. **A)** Like anodal tDCS, further rCBF decreases after cathodal tDCS were observed compared to the intra-stimulation period in most regions, such as Wernicke's area, precuneous cortex, and ACC. However, functional changes in the thalamus no longer survived statistical thresholds. **B)** On a sagittal view, activity changes in precuneous and paracingulate cortices can be prominently observed. (ACC = anterior cingulate cortex)

3.3.5 Functional Differences Between Anodal and Cathodal tDCS

The perfusion activity maps of both anodal and cathodal tDCS showed activity in numerous regions in the brain, most of which are anatomically and/or functionally connected to L-DLPFC. To determine whether these effects were specific to one particular polarity or whether they were associated with tDCS in general, I performed contrasted between $Anodal_{stimulation - baseline}$ and $Cathodal_{stimulation - baseline}$ (Figure 3.8A) and between $Anodal_{after\text{-}effect - baseline}$ and $Cathodal_{after\text{-}effect - baseline}$ (Figure 3.8B). For the former, L-DLPFC and the paracingulate cortex were the only regions that showed significantly different rCBF changes and were more active during anodal tDCS than during cathodal tDCS. Between the after-effect periods, cathodal tDCS was associated with significantly lower activity in the middle and superior temporal gyri and Wernicke's area.

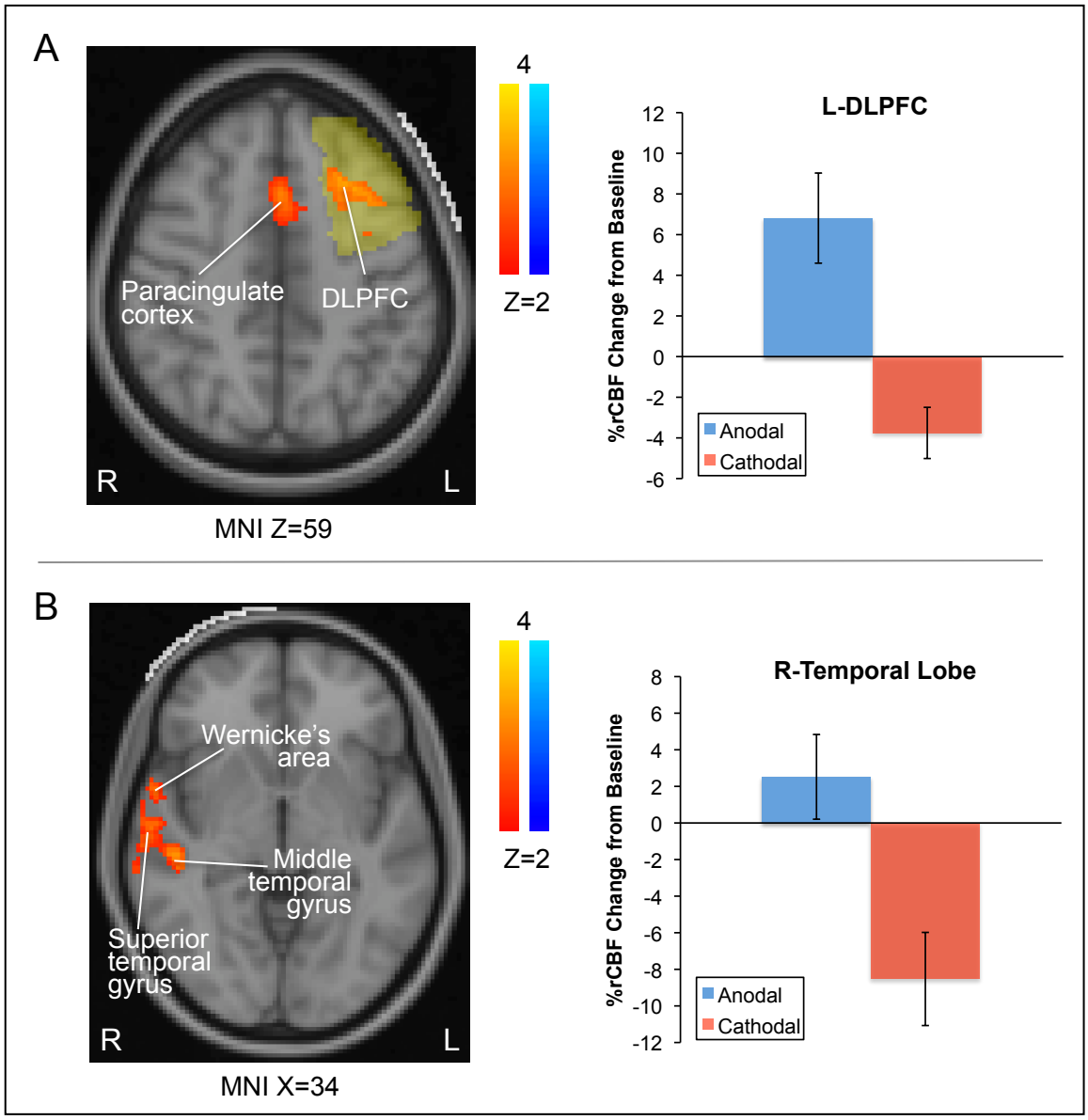


Figure 3.8. **A)** Perfusion activity map associated with $Anodal_{stimulation - baseline}$ – $Cathodal_{stimulation - baseline}$ (mixed effects; Z>2, cluster corrected at p<0.01). Only DLPFC (denoted by the yellow mask) and the paracingulate cortex showed higher rCBF during anodal tDCS than during cathodal tDCS. Within L-DLPFC, the %rCBF change of voxels with significant difference was plotted to show relative sizes between anodal and cathodal conditions. **B)** Perfusion activity map associated with $Anodal_{after-effect - baseline}$ – $Cathodal_{after-effect - baseline}$ (mixed effects; Z>2, cluster corrected at p<0.01). Differences in L-DLPFC rCBF did not survive statistical thresholds in the after-effect period. However, activity in the right temporal lobe, which included superior and middle temporal gyri and Wernicke's area, was lower after cathodal tDCS than after anodal tDCS. Within the right temporal lobe, the %rCBF change of voxels with significant difference was plotted to show relative sizes between anodal and cathodal conditions. White lines along the outside of the skull delineate the locations of the electrodes. Error bars denote the standard error means across subjects.

3.4 Discussion

This study found significant changes in brain perfusion and functional connectivity during and after L-DLPFC tDCS. The patterns were different between anodal and cathodal stimulations and between intra-stimulation and post-stimulation periods. This was also the first demonstration of concurrent ASL-tDCS in the lab.

3.4.1 Perfusion Activity of L-DLPFC During tDCS

Perfusion activity maps were used to determine the effect of tDCS on the targeted cortex of L-DLPFC. Anodal stimulation was associated with increased activity in L-DLPFC, while rCBF changes of the region did not survive statistical thresholds with cathodal stimulation. Previous attempts to find such cortical changes with fMRI-tDCS have been inconclusive (Antal et al., 2011), although these studies were restricted by the standard BOLD requirement of a high task frequency. Employing ASL fMRI, I could obtain a relative rCBF measurement of the neuromodulatory effect from tonic stimulus like tDCS, which appeared to be consistent with previous TMS (Speer et al., 2000) and physiological studies (Nitsche and Paulus, 2000; Nitsche et al., 2003a; Nitsche et al., 2005). However, a recent ASL-tDCS study by Zheng and colleagues found increased rCBF in the stimulated cortex (M1) with both anodal and cathodal tDCS, although the magnitude was larger for anodal stimulation (Zheng et al., 2011). In contrast, animal literature with laser Doppler flowmetry (LDF) has also suggested that anodal tDCS increased, while cathodal tDCS decreased, CBF through changes in neurovascular coupling (Wachter et al., 2011). For my data, I used the perfusion-subtracted time courses to calculate the relative rCBF changes of L-DLPFC from baseline and found higher rCBF during task-free anodal tDCS than during cathodal tDCS, a difference that was marginally significant. However, no significant differences were found between baseline and intra-stimulation L-DLPFC activities with this analysis approach. Contrast perfusion maps between $\text{Anodal}_{\text{stimulation – baseline}}$ and $\text{Cathodal}_{\text{stimulation – baseline}}$ also found

higher L-DLPFC activity in the former. Thus, while I cannot reach firm conclusions on the region's activity during cathodal tDCS, my data suggests that L-DLPFC rCBF during anodal tDCS increased from the baseline level and was higher than its stimulation counterpart.

3.4.2 Whole Brain rCBF Changes During tDCS

Besides changes in L-DLPFC activity, connected regions also appeared to be functionally affected. During anodal tDCS, the SI, MCC, and paracingulate cortex experienced increased rCBF from baseline levels. The connections between these regions and L-DLPFC are well established in both human and animal literature (Ruff et al., 2006; Wachter et al., 2011; Zheng et al., 2011). For example, patients with DLPFC damage generate abnormal electrophysiological activity from visual detection tasks (Barcelo et al., 2000). The lateralized pattern of activations suggests that the effects were directly associated with the anodal stimulation. The possibility that tDCS directly induced these rCBF changes could be excluded because other in-between structures were unaffected. In addition to these increases, higher activity was observed from the baseline in the right frontal pole, which is covered by the reference electrode. While the air sac beneath the supraorbital ridge should minimize the effect, these data suggest that the frontal pole is not completely unaffected by tDCS.

The perfusion activity map during cathodal tDCS showed a different activation pattern. In particular, I observed deactivation of the thalamus, which suggested that tDCS induced L-DLPFC to perform top-down suppression of the region. Previous literature on frontal-subcortical networks showed a strong top-down network between DLPFC and thalamus, possibly through the caudate nucleus and pallidum (Cummings, 1993). Thus, it is not surprising to observe rCBF decreases in subcortical structures during tDCS from baseline. While these changes were not observed on the perfusion map of anodal tDCS,

the contrast map between $Anodal_{stimulation - baseline}$ and $Cathodal_{stimulation - baseline}$ did not show significant differences. This suggests sub-threshold changes in thalamic activity during anodal tDCS.

In addition to the thalamus, rCBF decreases during cathodal tDCS were also associated with regions in the right superior temporal lobe, including middle and inferior temporal gyri and Wernicke's area. A previous fMRI study that applied inhibitory (low-frequency) TMS to L-DLPFC also found decreased activity in the temporal lobe, which highlights the distal effects of brain stimulation through default mode networks (DMN) (van der Werf et al., 2010). These rCBF decreases could also be attributed to the robust structural connectivity between right temporal lobe and right anterior DLPFC (Takahashi et al., 2007). Since the reference electrode readily covered the latter region due its large size, its stimulation (anodal) of R-DLPFC may have triggered the changes in the activity of the right temporal lobe. The changes in Wernicke's area, a key region in language processing, may explain why verbal ability is impaired through cathodal tDCS (Elmer et al., 2009).

3.4.3 L-DLPFC Functional Connectivity During tDCS

The changes in whole-brain perfusion activity strongly suggest that the effect of tDCS can spread beyond the targeted region. The rCBF of connected areas can also be significantly affected and altered, which underscores the value of a functional connectivity analysis. During anodal tDCS, prominent decreases were found in L-DLPFC functional connectivity to midbrain and bilateral thalami from baseline. A previous study by Lorenz *et* al. proposed a top-down model from L-DLPFC to the thalamus and the midbrain in the application of pain alleviation (Lorenz et al., 2003). With increased L-DLPFC rCBF during anodal stimulation, I observed severe interference in the communication between L-DLPFC, thalamus, and midbrain in the functional connectivity maps. Not only are these key regions within the pain matrix, changes to the

frontal-thalamic circuit would alter L-DLPFC's interaction with the rest of the body (Tekin and Cummings, 2002). These observations were separately verified with Pearson correlation tests. The trend suggests that the theory proposed by Lorenz and colleagues may indeed explain the clinical efficacy of brain interference techniques over L-DLPFC in past chronic pain studies (Fregni et al., 2006b; Boggio et al., 2008a; Borckardt et al., 2011). Not surprisingly, the same relationship to thalamus and midbrain was not observed during cathodal tDCS, where the average L-DLPFC activity was lower.

3.4.4 Immediate Whole Brain rCBF Changes After tDCS

In the after-effect period within 10 minutes after the stimulation ended, widespread rCBF decreases were observed across the whole brain. This phenomenon was not polarity-specific, and participants were given no indication of the termination of the stimulation. In addition, possible contributions from confounding factors, such as ASL-specific artefacts, were ruled out because the imaging method has been successfully used in functional scans with long stimulus blocks (Wang et al., 2003). Thus, while the long-term physiological after-effect of anodal and cathodal tDCS may be respectively facilitatory and inhibitory, the results of this study suggest that the rCBF decreases immediately post-stimulation (~10 minutes) may be a general outcome of tDCS on neuronal activity. This contrasts with previous data that suggested similar neurophysiological states during and after stimulation (Nitsche et al., 2005). Future tDCS users, especially those seeking to apply the technique within an fMRI setting, should be attentive to such differences. This may also explain why a recent concurrent BOLD-tDCS study (Antal et al., 2011), which applied short, interleaved blocks of stimulation, showed decreased activity in the targeted cortical region with anodal tDCS of the M1. The repeated acts of shutting off the stimulation may lead to an accumulation of brain deactivations that could confound the final results.

The L-DLPFC functional connectivity to thalamus and midbrain in the after-effect period of anodal tDCS did not significantly differ from the baseline. This connectivity rebound between L-DLPFC and thalamus after excitatory stimulation to baseline levels suggests that the main therapeutic effect should only occur during stimulation. The existing clinical literature appears to support this conclusion (Brighina et al., 2004). Besides the initial relief induced by the stimulation, patients reported neither improvement nor deterioration in the follow-up sessions. However, these results did differ from a previous study that investigated changes in functional connectivity before and after tDCS (Polania et al., 2010), though the authors stimulated the M1 instead and used graph theoretical analysis to derive the final correlation maps.

3.4.5 Future Directions and Conclusion

Future studies should include current modeling when investigating task-free effects of tDCS. While I successfully standardized the stimulation location with the EEG coordinate system, current distribution can still vary according to the subject's cranial geometry (Miranda et al., 2006). Since the first modeling work that used a generic spherical head model and a single stimulation montage (Miranda et al., 2006), the literature has now included current calculations with realistic head models (Sadleir et al., 2010; Parazzini et al., 2011), multiple montages (Wagner et al., 2007), and skulls with defects and plates (Datta et al., 2010). The relevance of these studies to the current project is limited because most focused on M1 stimulation. However, modeling work with DLPFC tDCS combined with the study's fMRI data could link current distribution to functional effects and is expected to be highly informative.

The explorations on L-DLPFC tDCS have provided suggestions on how the technique can induce pain alleviation. The following chapters will directly investigate these hypotheses with the inclusion of an ongoing pain model.

CHAPTER 4 – MODELS OF ONGOING PAIN

A robust ongoing pain model that best replicates aspects of chronic neuropathic pain is necessary for this investigation of pain modulation. This chapter will describe the efforts to establish such models using electrical, thermal, and chemical stimuli. It will also cover the effects of discrete and continuous reporting systems on subject ratings. Lastly, I will discuss the advantages and disadvantages of using a capsaicin-based approach for further studies.

4.1 Introduction

To study the modulatory effect of tDCS, I first needed to establish an ongoing pain model that best mimics the characteristics of chronic neuropathic pain. As illustrated in Section 1.4.3, such a model is more difficult to establish than standard, acute pain paradigms. One major component of neuropathic pain is hypersensitivity at both the site of pain and its surrounding region (Woolf and Salter, 2000). A model of neuropathic pain also needs to mimic the phenomena of allodynia and hyperalgesia. Allodynia occurs when normally harmless stimuli may elicit a painful response, while hyperalgesia is defined as noxious stimuli causing more intense and prolonged pain than normally expected. A model of neuropathic pain should also modulate the excitability of nociceptive synaptic transmission in the central pain pathways. In particular, it should introduce secondary hyperalgesia, a key sign of central sensitization and a significant component in neuropathic pain. Lastly, the model needs to provide subjects with a sustained pain experience at levels between medium and high intensity levels for an extended duration (Campbell and Meyer, 2006).

In addition, practical considerations of safety risks and tonic robustness need to be taken into account when designing a model of chronic pain. Temporal and spatial summations of noxious inputs can be hazardous for the participants and, depending on the model, can cause bruises, burns, frostbite, and/or peripheral nerve damage. These injuries may be exacerbated by habituation to the pain sensation, which can allow the stimuli to further

damage tissue integrity without immediate awareness of the subject. While circumventing these physical risks, the ongoing pain model simultaneously needs to impart a stable, long-lasting (~ 30 minutes) pain that does not drastically fluctuate over time. These factors all bring additional challenges to the task of developing an adequate model.

In the following sections, I will describe my attempts to setup such models with electrical, thermal, and chemical stimuli. These three stimulation types were candidates for developing a chronic pain model as has previously been suggested in the literature (Koltzenburg et al., 1994; Granot et al., 2006; Geber et al., 2007). Electrical and thermal stimuli have been used to achieve tonic pain experiences (>1 minute) with a rapid, phasic stimulation paradigm (Granot et al., 2006; Geber et al., 2007). Previous findings have also suggested that capsaicin may be a suitable candidate for inducing an ongoing pain experience (Koltzenburg et al., 1994). I characterized the elicited pain responses of the individual models to validate their stability and intensity over time. After identifying the ideal model, I could then incorporate it into studies in combination with fMRI and tDCS.

4.2 Electrical Stimuli

4.2.1 Methods

I recruited 3 healthy subjects (right handed; age: 18-45 years) for a pilot study to explore the intensity and duration of pain sensations from noxious electrical stimuli. Three stimulation parameters needed to be controlled: current intensity, current frequency, and stimulus frequency. The current intensity was controlled by a current generator (Constant Current Stimulator model D57A, Digitimer, Welwyn Garden City, United Kingdom), which was connected to a stimulus programmer (Train/Delay Generator model DG2A, Digitimer, Welwyn Garden City, United Kingdom) to modulate the current frequency (Figure 4.1A). Lastly, a frequency generator (TG230 - 2MHz Dial-set Function Generator, Thurlby Thandar Instruments Ltd., Huntingdon, United Kingdom) was added to this setup to adjust the stimulus frequency. The output from the current generator was connected to either an oscilloscope (Model 54610B, Agilent/HP, Santa Clara, CA, USA) for verifying the pulse properties or to an in-house electrode set (diameter = 3mm) for stimulation.

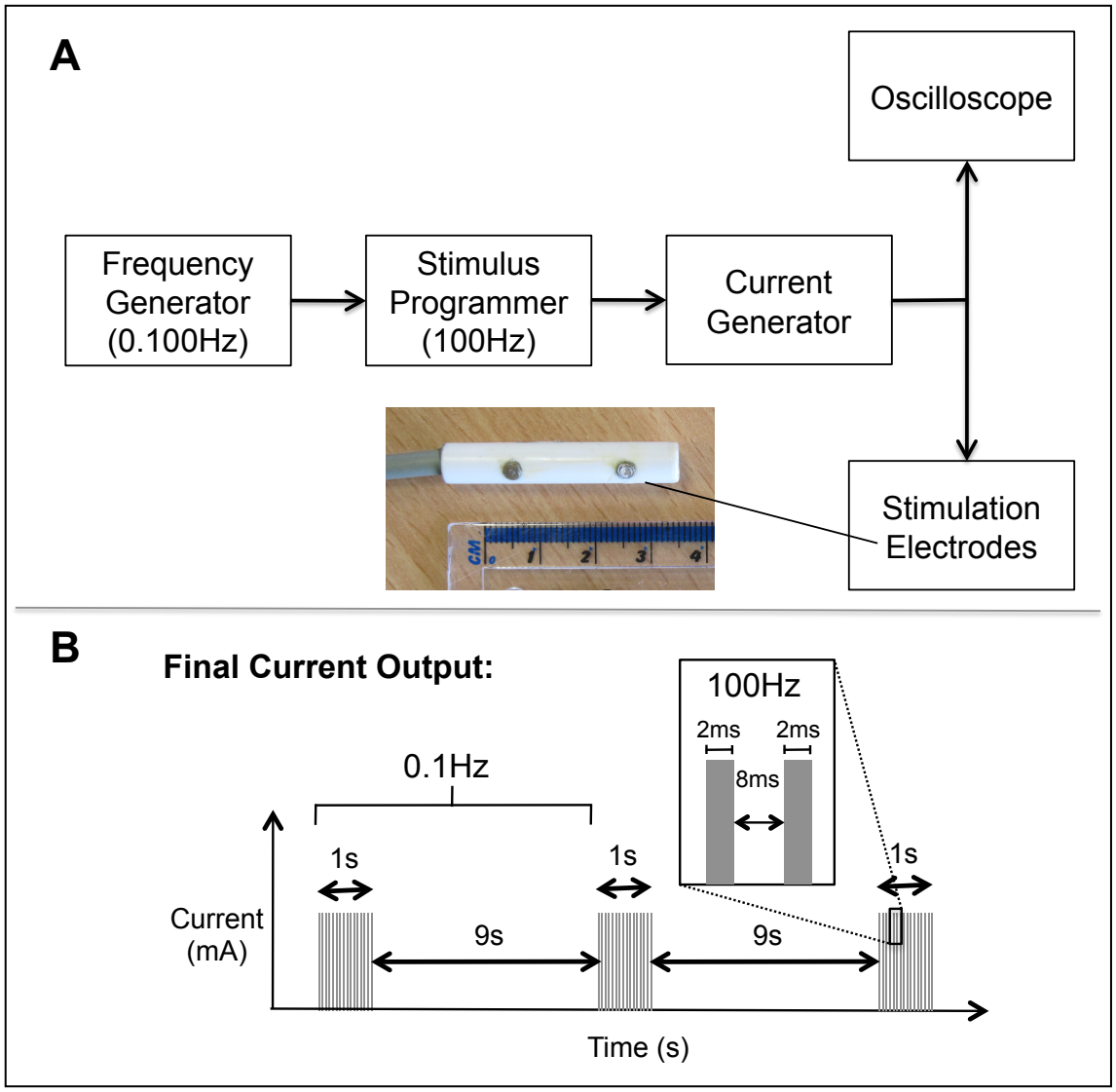


Figure 4.1. **A)** Setup of electrical stimuli generation. The frequency generator controls the duration and the inter-stimuli interval of the electrical pulses. At a frequency of 0.100Hz, each pulse train lasts for a second and stops for 9 seconds. The stimulus programmer controls the number of pulses in a single train. At a frequency of 100Hz, each train consists of 100 pulses per second. The current generator controls the intensity and duration of each pulse. The intensity was calibrated to the pain threshold of each subject, while the duration was set to 2ms. Before every experiment, the frequencies and intensity of the pulse train were first checked with an oscilloscope. The stimulation electrodes (diameter = 3mm) were then used to stimulate the right forearm. **B)** The diagram illustrates the frequencies and durations of the current output.

At the start of the experiment, each subject had the electrode set attached to the right forearm at 5cm distal to the antecubital fossa. Through stepwise increases of 0.1mA in the current intensity from 0mA, I used the current generator to measure the individual pain thresholds, which constituted a verbal rating of >0 on a 0 (no pain) to 10 (worst

imaginable) numerical scale. The determined threshold becomes the current intensity that was applied in the experiment. The stimulation pulses were delivered at a frequency of 0.1Hz (six 1-second pulse trains per minute) by the frequency generator, and the stimulus programmer was set at 100Hz to ensure the generation of a phasic pulse train (Figure 4.1B). The current generator controlled the duration of each 2ms pulse. The current frequencies and intensity were checked with the oscilloscope before every experiment. Each stimulation paradigm lasted ~5 minutes.

4.2.2 Results

While subjects continued to report pain sensations within 2 minutes after the experiment began, the response became inconsistent in the final 3 minutes. The subjects also experienced no pain during the inter-stimuli intervals, although the stimulated region did show redness, which indicated the occurrence of primary and possibly secondary hyperalgesia. In addition, the shock from the electrical stimulation caused a visible jerking motion of some subjects, which could pose problems for concurrent fMRI. Given the lack of ongoing pain experience and the association with potential motion artefacts, I excluded electrical stimuli as a possible model and explored thermal stimuli instead.

4.3 Thermal Stimuli

4.3.1 Methods

Four healthy subjects (right handed; age: 18-45 years) participated in the pilot study with noxious heat stimulation. For the stimulus source, I used an in-house thermal probe that has a fast rise time (over 35°C/s) and a self-calibration capability to ensure rapid and accurate delivery of the correct temperature (Brooks et al., 2005). The instrument was then controlled with Presentation software (Version 14.5, Neurobehavioral Systems, Albany, CA, USA). A highly phasic paradigm of thermal stimulation was attempted, but the slow cooling process limited the inter-stimuli interval to be at least 30 seconds (Figure 4.2). A thermode ($1x1cm^2$) was attached to the subject's right forearm at 5cm distal to the antecubital fossa after instrument setup. The stimulus temperature was then calibrated to be at the level where the individual pain intensity reached 5 on a numerical scale from 0 (none) to 10 (worst imaginable). During the experiment, fifteen 30-second heat stimulus blocks were applied with randomly determined inter-stimuli intervals of 30 to 60 seconds to minimize subject anticipation. Pain ratings were recorded at the end of each stimulus on the same numerical scale as above, and the subjects were instructed to use any number between 0 and 10 without feeling bounded by the integer marks.

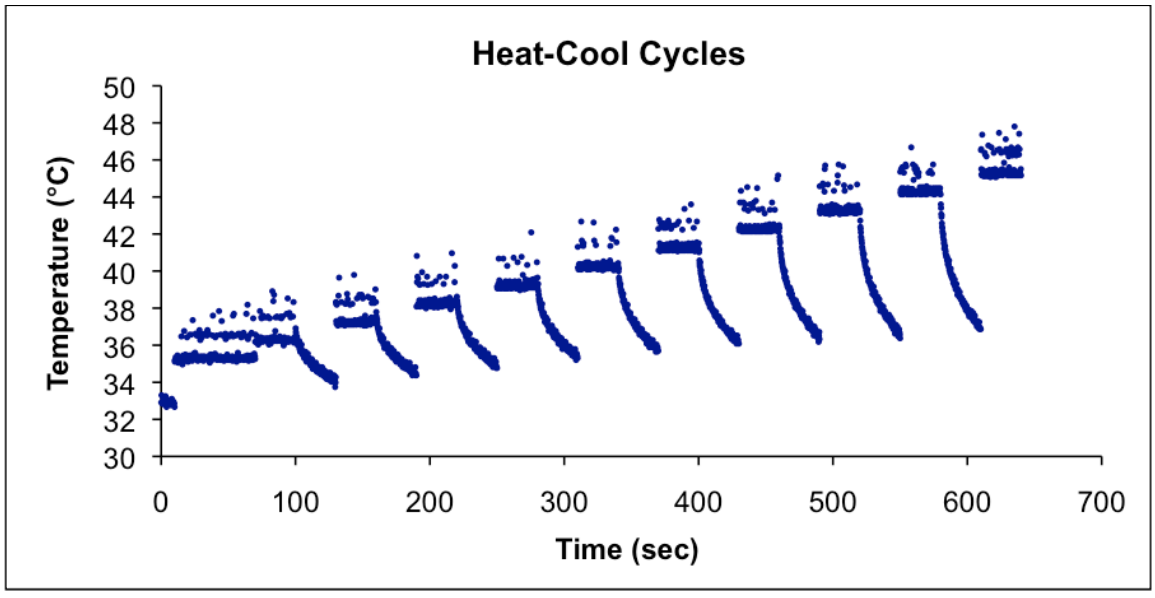


Figure 4.2. The temperature of the thermal probe during successive heat-cool cycles. These measurements were recorded during the thermal stimulation of the right forearm from a single subject. Each cycle started with 30 seconds of stimulation followed by 30 seconds of inter-stimuli gap. The stimulus temperature began at 36°C and increased by 1°C with every cycle. Regardless of the applied stimulus temperature, at least 30 seconds were required for the probe temperature to return to the baseline level. This demonstrates the rate limitation of both the resistor thermode and the skin to dissipate heat and limits the pursuit of a highly phasic stimulation paradigm.

4.3.2 Results

Subjects initially reported a pain rating of 5 after the first stimulus but ceased to feel intense pain afterward (Figure 4.3). In addition, the pain sensation did not linger in the inter-stimuli intervals, thus imparting a pulsed rather than ongoing pain paradigm. The repeated stimulations did leave a patch of primary hyperalgesia, but I did not detect any signs of secondary hyperalgesia. Given these observations, I excluded thermal stimuli as a possible model and explored the use of capsaicin instead.

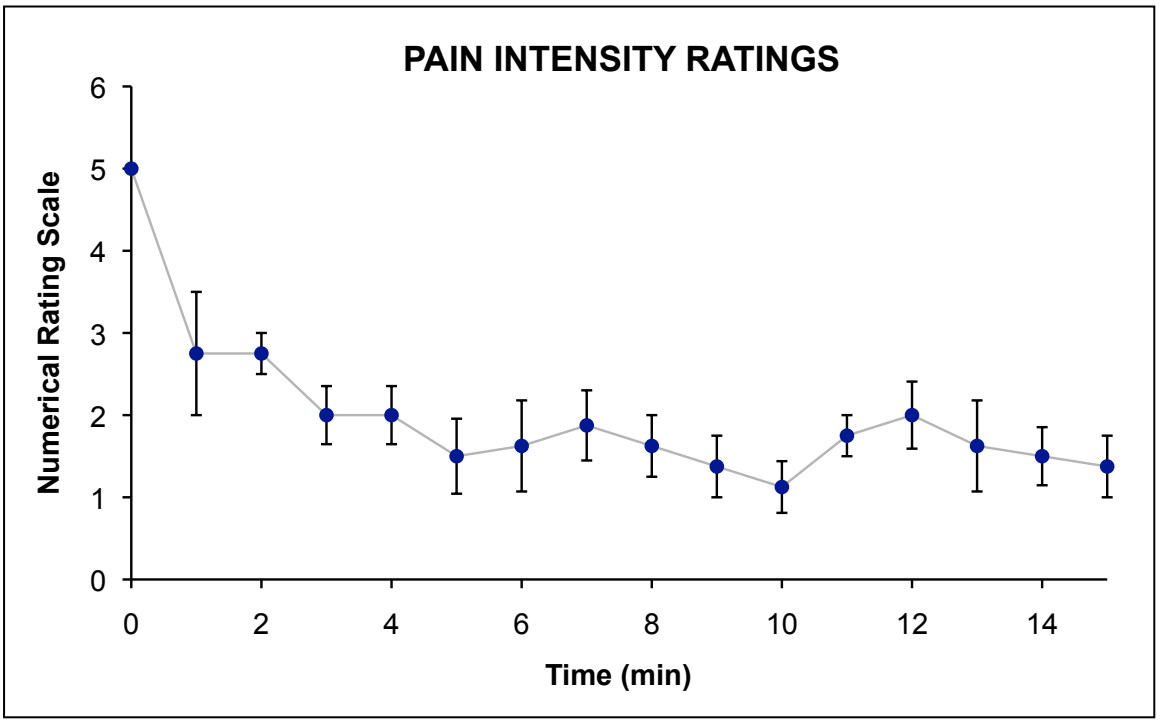


Figure 4.3. Pain intensity ratings were verbally recorded from healthy subjects during the thermal stimulus paradigm. After an initial pain of 5 on a 0-to-10 numerical rating scale, the subjects habituated to the sensation and experienced lower pain throughout the remainder of the experiment. In addition, the pain sensation did not linger into the inter-stimuli intervals. Error bars denote the standard error means across subjects.

4.4 Capsaicin Model (Part I)

4.4.1 Methods

The investigation of capsaicin application first involved establishing it as a possible ongoing pain model. I recruited 9 healthy subjects (right handed; age: 18-45 years) in the following pilot study to explore such effects. The subjects were not informed about the specific aims and were only told that the examination seeks to determine the pain intensity elicited by capsaicin.

All volunteers received a topical patch of capsaicin cream (1% w/w, Pharmasol Limited, Andover, UK) on the center of the inner side of their right calf. The volume used ranged between 5ml and 10ml (Density: 0.5ml/cm^2) depending on the subject's response. If a subject underwent multiple sessions of capsaicin screening to calibrate for the appropriate capsaicin volume, a minimum gap of one week was maintained between sessions to allow neuronal recovery and prevent tachyphylaxis after capsaicin desensitization. Previous literature has shown this rest period to be necessary to avoid damage to the peripheral nociceptors (Karrer and Bartoshuk, 1991).

For the pain rating, I used a 0-to-10 numerical scale that was anchored between "None" and "Worst Imaginable." I verbally asked the subjects for their pain rating every 30 seconds after they began to feel pain, in which they were instructed to provide any number between 0 and 10 without being restricted to integers. Each experiment session lasted between 1 and 2 hours depending on the individual response.

4.4.2 Results

Of the nine subjects, four sustained an ongoing pain intensity response between 5 and 7 on the numerical rating scale, although rough changes in the ratings over time underlined the low temporal resolution of the rating method (Figure 4.4). The remaining five subjects did not experience pain above a rating of 4.5. Red flare was visible in areas both

under and around the capsaicin patches of the four qualified capsaicin responders, which indicated robust signs of primary and secondary hyperalgesia. These observations suggested that capsaicin is a viable candidate for an ongoing pain model, but careful screening is required to identify the qualified responders.

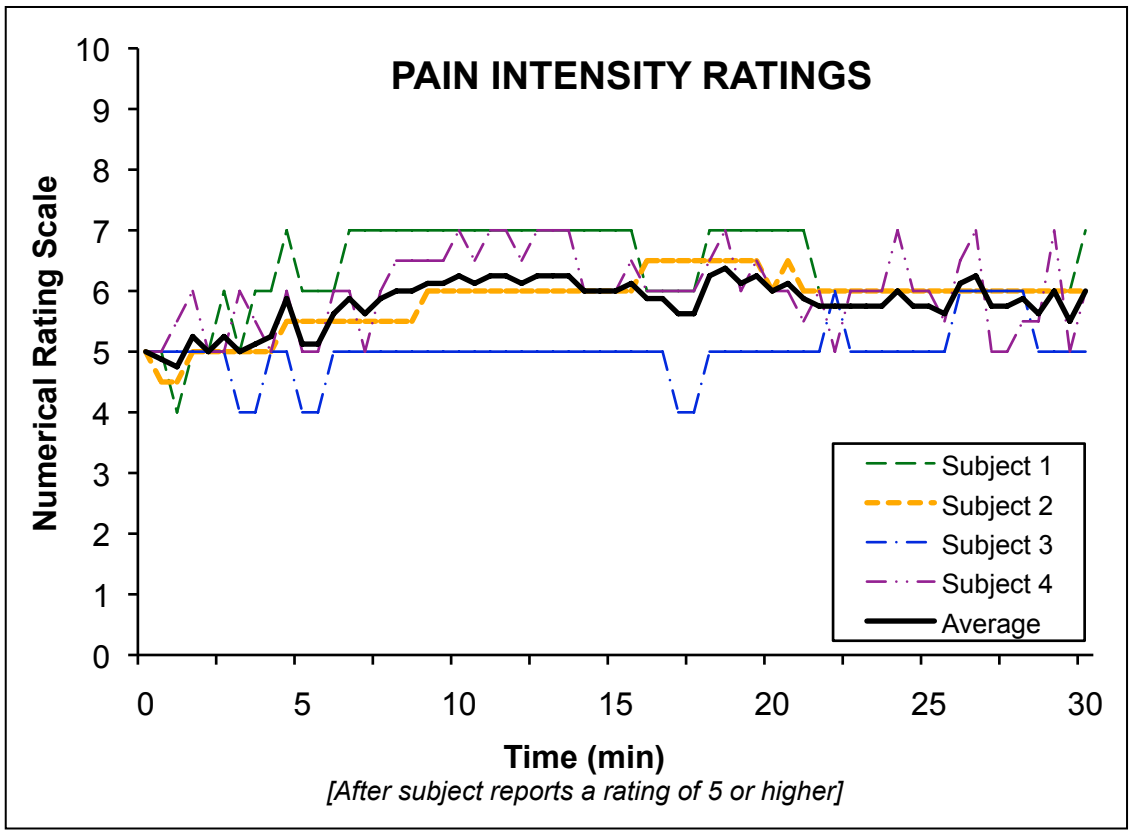


Figure 4.4. Pain intensity ratings from the four subjects with an ongoing pain response. After reaching a numerical rating of 5, they continued to experience a sustained pain that generally ranged between 5 and 7. The lack of temporal resolution was also notable as the rating was verbally recorded every 30 seconds. The data from the pilot study suggested that capsaicin could be used to establish an ongoing pain model, but careful screening will be needed.

4.5 Capsaicin Model (Part II)

Section 4.4 showed that capsaicin could be used to sustain an ongoing pain experience in healthy subjects, but not everyone was a responder. Thus, I screened for the eligible capsaicin responders and recruited them for later studies involving an ongoing pain model. While the overall protocol was identical to that of the previous section, I applied a continuous VAS instead of a discrete, numerical rating approach to gain better temporal resolution of the subjects' pain intensity ratings.

4.5.1 Methods

I recruited 51 healthy subjects (right handed; age: 18-45 years) to explore the effects of capsaicin in inducing an ongoing pain sensation. None of these volunteers were taking any prescriptions, antidepressants, and/or pain medications throughout their study participation, and all were fully informed of the techniques involved and the potential risks associated with capsaicin. However, they were not aware of the specific aims of the study and were only told that the examination seeks to determine the pain intensity elicited by capsaicin.

The protocol and safety considerations in the capsaicin application were identical to the ones in Section 4.4.1. For the pain intensity rating, I used a continuous VAS that was anchored between "None" and "Worst Imaginable." The rating scale was programmed with Presentation software (Version 14.5, Neurobehavioral Systems, Albany, CA, USA) and was placed beside the subject on a notebook computer. The participants were instructed to give a rating whenever they felt a change in pain, and they had full control of the scale throughout the experiment by moving it with the right or left arrow keys. This setup also minimizes the subjects' interactions with the experimenter and thus reduces any possible interference factors. Unknown to the subjects, their ratings were monitored on a separate screen to track their progress. Each experiment session lasted from 1 to 2 hours depending on the individual response. Subjects were included if they

maintained a consistent pain intensity rating between 5 and 7 (on the VAS of 0 to 10) for at least 30 minutes.

4.5.2 Results

Of the recruited subjects, nineteen reported a stable ongoing pain for at least 30 minutes that ranged between 5 and 7 on a 10-point VAS (Figure 4.5). Habituation did not occur with this paradigm, unlike with thermal and electrical stimuli. After I removed the cream, I clearly observed a patch of flare that was larger than the site of capsaicin application, which indicated the presence of primary and secondary hyperalgesia. After completing the study sessions, subjects reported no redness or uncomfortable sensations after one day of rest. These results suggest that capsaicin can provide a safe, robust ongoing pain model.

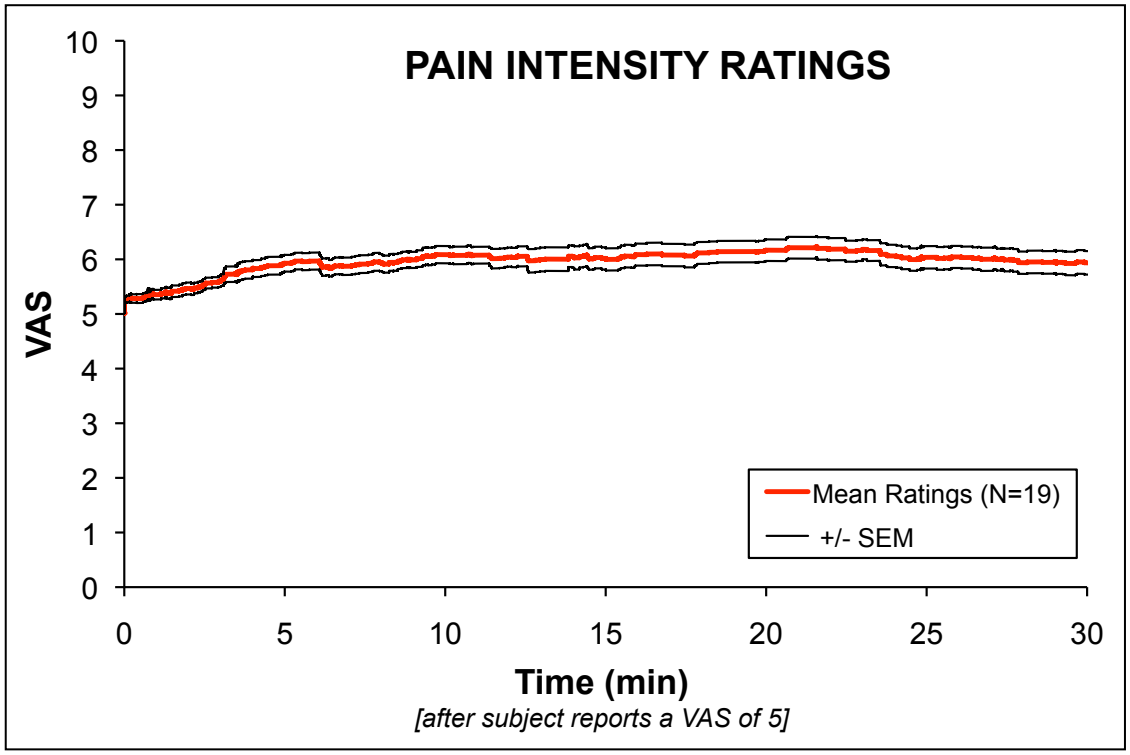


Figure 4.5. Mean pain intensity ratings of the nineteen responders with topical application of 1% capsaicin cream. Within the 30 minutes after subjects reached a rating of 5 on a 10-point continuous VAS, the pain scores stabilized between VAS of 5 and 7. The continuous pain intensity VAS was anchored on both extremes by "None" and "Worst Imaginable."

4.6 Discussion

The series of studies above demonstrated that capsaicin provided the most ideal candidate for an ongoing pain model after both electrical and thermal stimuli appeared to induce habituation in the subjects. It is important to note that the size of subject cohort was reduced in the latter studies after discouraging preliminary results, but the observations were consistent with the existing literature (Condes-Lara et al., 1981; Milne et al., 1991; Becerra et al., 1999; Geber et al., 2007). Previous studies seemed to circumvent the habituation in one-minute experiments through stepwise increases in the intensity of the noxious input (Granot et al., 2006; Geber et al., 2007). However, this was not attempted because the process could pose safety concerns for subjects in a 30-minute paradigm. Future studies could include more subjects in experiments involving electrical and thermal stimuli to increase the overall scientific rigor.

While capsaicin elicits a wider range of pain responses between subjects than thermal and electrical stimuli, capsaicin causes a persistent discharge of the slow-firing C fibers (Koltzenburg et al., 1994), which can recharge more quickly than Aδ fibers. Thus, topical application of capsaicin can lead to an ongoing pain experience in some healthy subjects without leading to irreversible tissue damage. Capsaicin can also induce effects similar to the traits of chronic neuropathic pain. In response to the stimulus, the skin develops hyperalgesia and allodynia through increased sensitivity of the nociceptive neurons (Lynn, 1990), a process mediated by ion channel proteins in the Transient Receptor Potential Vanilloid (TRPV) family (Caterina et al., 1997; Yao and Qin, 2009). In addition, the heightened sensitivity in regions around the capsaicin patch signified the occurrence of central sensitization, another key feature of neuropathic pain.

Lastly, I applied the capsaicin ongoing pain model to screen for the eligible responders in section 4.4. These subjects were then recruited to participate in further studies to investigate the effects of tDCS on pain modulation.

CHAPTER 5 – FUNCTIONAL IMAGING OF PAIN MODULATION BY TRANSCRANIAL DIRECT CURRENT STIMULATION

Previous chapters have explored the task-free effects of tDCS with perfusion fMRI and established an ongoing pain model based on capsaicin. Building upon this understanding, I could now proceed to investigate the neural changes during pain modulation by tDCS. In this study, I combined concurrent tDCS-fMRI with the pain model and applied this to healthy capsaicin responders, who were screened in Section 4.5. They underwent multiple scans with different tDCS and pain conditions, with pain ratings recorded in-between to track the magnitude of pain modulation.

5.1 Introduction

In Chapter 4, I showed how I could establish an ongoing pain model with topical application of capsaicin cream. In Chapter 3, I also demonstrated the technical feasibility of concurrent tDCS-fMRI and investigated the neural effects of L-DLPFC stimulation in Chapter 3. Specifically, L-DLPFC activity and functional correlations changed during and after anodal tDCS, which also affected connected regions such as the thalamus. These modulations may partially explain the efficacy of L-DLPFC tDCS as a pain alleviation tool. Section 1.7.2 described these tDCS applications in pain, including post-ERCP pain (Borckardt et al., 2011), fibromyalgia (Fregni et al., 2006b), and experimental pain (Boggio et al., 2008a; Boggio et al., 2009). However, the neuroscience that links tDCS with pain relief has never been directly examined. DLPFC and thalamus are regions with multiple roles, and their modulations by tDCS may affect functions unrelated to pain processing.

Building upon prior results presented in earlier chapters, I integrated the current understanding and techniques to investigate the neural state during pain modulation by tDCS. Subjects who had demonstrated an ongoing pain response from capsaicin in Section 4.5 were recruited to participate in experiments involving perfusion fMRI and tDCS. Each subject underwent two sessions, one with sham and the other with anodal

stimulation. The sessions included multiple scans with different pain and tDCS conditions, between which numerical pain ratings were verbally recorded. Thus, I collected both behavioral and fMRI data to allow for a fuller exploration of brain functions during pain modulation by non-invasive brain stimulation. In particular, the main question of interest was the immediate changes from tDCS on pain modulation. Further investigations into the relationship between structural connectivity, functional correlations, and behavioral changes in pain sensation are covered in Chapter 6.

5.2 Methods

5.2.1 Subject Recruitment

From the subjects tested in Section 4.5, I recruited the nineteen healthy capsaicin responders to participate in the experiment. All of these subjects reported ongoing (>30 minutes) pain intensity ratings between 5 and 7 on a 0 (none) to 10 (worst imaginable) scale after topical application of capsaicin cream. One volunteer eventually withdrew due to sensations of discomfort during her first fMRI session, which involved sham tDCS, and was hence excluded in the data analysis. The final subject cohort had a mean age of 24.5 years with a standard deviation of 5.4 years. In adherence to ethical regulations from the U.K. National Research Ethics Service, all research participants were fully informed of the techniques and the potential risks in the study. Besides observing MRI safety guidelines, I further screened for possible contradictions to capsaicin and tDCS (Nitsche et al., 2008).

5.2.2 Experiment Setup and Paradigm

The protocols on tDCS and capsaicin were identical to the ones used in Sections 3.2 and 4.5.2, respectively. The subject cohort received counterbalanced sessions of anodal and sham tDCS with capsaicin cream. The two experiments were spaced by an interval of at least one week for every subject. Prior to every session, I marked the area where capsaicin was to be applied on the subject's right calf.

The active electrode for tDCS was centered at the F3 position in EEG 10/20 system, the location for L-DLPFC used in previous tDCS-pain studies (Fregni et al., 2006b; Boggio et al., 2008b; Boggio et al., 2008a). I also placed an Omega-3 oil pill (Ultra-Pure Omega-3 Fish Oil, Purity Products, Plainview, NY, USA) above the electrode center in order to visualize the electrode's location in on MR images. The reference electrode was placed above the contralateral supraorbital ridge to complete the electrical circuit. To minimize

the contact resistance between the scalp and the electrodes, high-chloride EEG gel (Abralyt HiCl, EasyCap, Herrsching, Germany) was used as a conducting medium. Each subject received approximately 15 seconds of tDCS to familiarize himself with the sensation. tDCS of such short duration has been shown to exert no lasting effects (Nitsche et al., 2008).

The experimental paradigm is illustrated in Figure 5.1. I verbally asked for the subjects' baseline pain ratings (both intensity and unpleasantness) on a 0 (none) to 10 (worst imaginable) numerical scale while they were in the scanner before applying topical capsaicin cream (1% w/w, Pharmasol Limited, Andover, UK) on the center of the inner side of his or her right calf. The volume used ranged between 5ml and 10ml (Density: 0.5ml/cm^2) depending on the subject's response in Section 4.5. The subject was instructed to alert the researcher when his or her pain intensity rating reached 5 on the numerical rating scale.

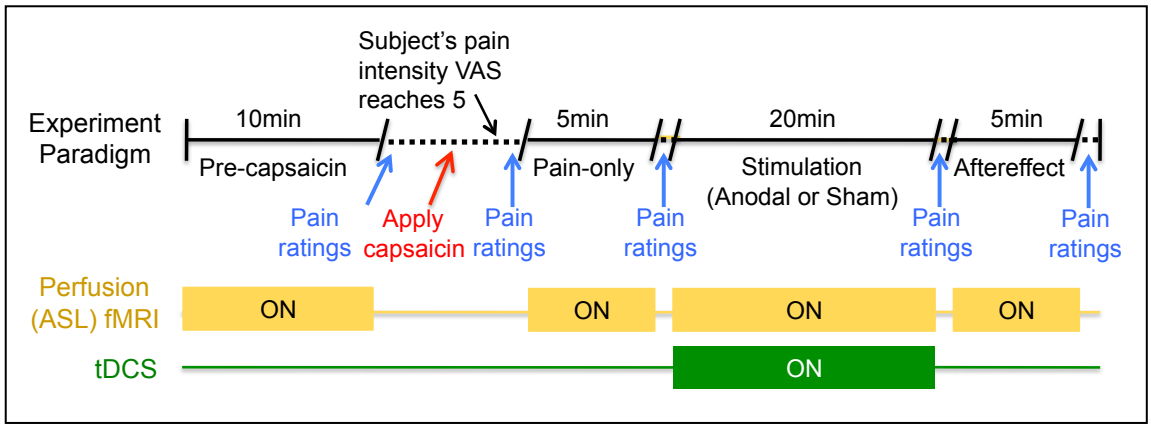


Figure 5.1. Electrodes were secured to the subjects, and they were familiarized with the stimulation sensation before they entered the scanner. After recording the baseline pain ratings, I applied 1% capsaicin cream on the subject's inner right calf. Once the subject's pain intensity rating reached a score of 5, which typically required 20 to 40 minutes, a 5-minute pain-only perfusion fMRI scan was performed. This was followed by a 20-minute scan with concurrent tDCS (anodal or sham) and pain sensation and a 5-minute after-effect scan without tDCS. Subjects' pain ratings were verbally recorded at all inter-scan intervals, which included intensity and unpleasantness levels on a numerical rating scale from 0 (none) to 10 (worst imaginable). When rating, the subjects were instructed to use any numbers or decimals necessary to best describe their sensation without being restricted to integers. For exploratory purposes, a 10-minute pre-capsaicin scan was conducted prior to capsaicin application for all sessions.

Once this rating was reached, I initiated a 5-minute pain-only perfusion fMRI scan without tDCS. A concurrent tDCS-fMRI was then performed for 20 minutes between two 10-second ramp-up and -down periods. For anodal tDCS sessions, subjects were given 1mA current throughout the entire 20 minutes. For sham tDCS sessions, subjects experienced 30 seconds of stimulation before the tDCS kit was turned off. The subjects were blinded to the polarity of their stimulation sessions, and there were no significant differences in the reported sensations of anodal and sham tDCS (Gandiga et al., 2006). After tDCS, the subjects were given a 5-minute perfusion fMRI scan to record any possible after-effects. To prevent the occurrence of adverse events, I used the first 15 seconds of the stimulation to make sure that the subjects were comfortable before I began scanning. However, I did not inform the subjects when the stimulation ended and continued scanning into the after-effect period without giving any such indications.

Subjects verbally reported their numerical pain ratings (both intensity and unpleasantness) at all inter-scan intervals throughout each session. They were also specifically instructed to give any number between 0 and 10 without being restricted to integers. Besides experiencing pain and providing their ratings, the subjects did not carry out any other tasks during the session and were asked to remain motionless and awake. For exploratory purposes, the perfusion maps prior to capsaicin application were also recorded in a 10-minute task-free fMRI pre-capsaicin scan.

After each session, the subjects were asked to fill out a questionnaire regarding possible tDCS sensations, which consisted of tingling, itching, burning, tiredness, nervousness, concentration, headache, and visual problems (Poreisz et al., 2007). If a question was answered “yes,” the subjects were then asked to rate the sensation intensity from 1 to 5 (1=mild, 2=moderate, 3=average, 4=severe, and 5=intolerable). In addition, they were asked whether they saw a flash from tDCS due to retinal stimulation from the reference

electrode. These ratings were then compared between anodal and sham tDCS conditions with a paired t-test to check for significant differences in stimulation sensations.

5.2.3 MRI Sequences

For the perfusion imaging, I used similar MRI sequences and setups as those detailed in Chapter 3. The only difference was the removal of parallel imaging to improve SNR, which modified the parameters for the gradient-echo EPI readout (TR=3.48s, TE=13ms, 6/8 k-space).

5.2.4 Data Analysis

Separate first-level analyses of pre-capsaicin, stimulation, and after-effect scans were carried out with FMRIB software library (FSL) version 4.1.7 (http://www.fmrib.ox.ac.uk/fsl) (Smith et al., 2004; Woolrich et al., 2009). For each scan, the functional data first underwent motion correction with a six-parameter affine algorithm (Jenkinson et al., 2002). Skull removal was then performed with the Brain Extraction Tool (BET) in the FSLtools (Smith, 2002) followed by manual extraction to ensure thoroughness and precision. I used non-linear high-pass temporal filtering (sigma of 200s) to remove scanner drifts and BOLD contaminations (Chuang et al., 2008) and applied spatial smoothing (full-width half-maximum of 8mm). The perfusion subtraction of the ASL data was modeled with a boxcar regressor by using the TR (3.48s) as the duration of each on or off period. Finally, functional data was registered to the respective high-resolution T1 structural scan, which was subsequently registered to Montreal Neurological Institute (MNI) standard brain.

The second-level analysis used paired t-tests to perform intra-subject comparisons between pre-capsaicin, pain-only, stimulation, and after-effect periods. These individual analyses were submitted to a third and final level of analysis for the averaged group

comparison of rCBF across periods (mixed effect; $Z>2.0$, cluster corrected at $p<0.01$). This sequence of analyses allowed for consideration of both the intra-scan (pre-capsaicin, pain-only, stimulation, and after-effect periods) and intra-subject (anodal and sham sessions) variances, thus minimizing the bias from any single session or participant.

5.2.5 Statistics

All statistical analyses of the behavioral measurements were performed with SPSS software (version 19, IBM, Armonk, NY, USA). Unless otherwise specified, paired t-tests (two-tailed) were used to determine statistical significance. Results with $p<0.05$ were considered significant, while those with $p<0.10$ were regarded to suggest a strong trend.

5.2.6 Investigation of rCBF Changes Pre- and Post-Waiting Period

While the main focus of the study was to examine pain neuromodulation by tDCS, the rCBF changes before and after the waiting period of ~20–40 minutes were also investigated for exploratory purposes. Two different topical applications were tested at the beginning of the waiting period, one with 1% capsaicin cream and the other with innocuous lotion. For the former, the protocol was integrated to the experimental paradigm detailed in Section 5.2.2. For the latter, 7 healthy subjects (2 females, all right-handed, mean ± SD age: 24.9 ± 4.7 years) were recruited and prepared in the same manner as described in Section 5.2.2. All participants were capsaicin responders.

The study paradigm is shown in Figure 5.2. Subjects first underwent a 10-minute resting scan after they were prepared for the scanner. Innocuous cream (10ml) was then placed on a 5cm-by-4cm patch at the center of the inner side of the right calf. A randomly determined waiting period between 20 and 40 minutes (mean ± SD minutes: 32.4 ± 6.5) ensued without giving the subjects any anticipation. This was followed by a 5-minute

scan, akin to the pain-only scan in Section 5.2.2. Analysis of the collected rCBF data was identical to the method detailed in Section 5.2.4.

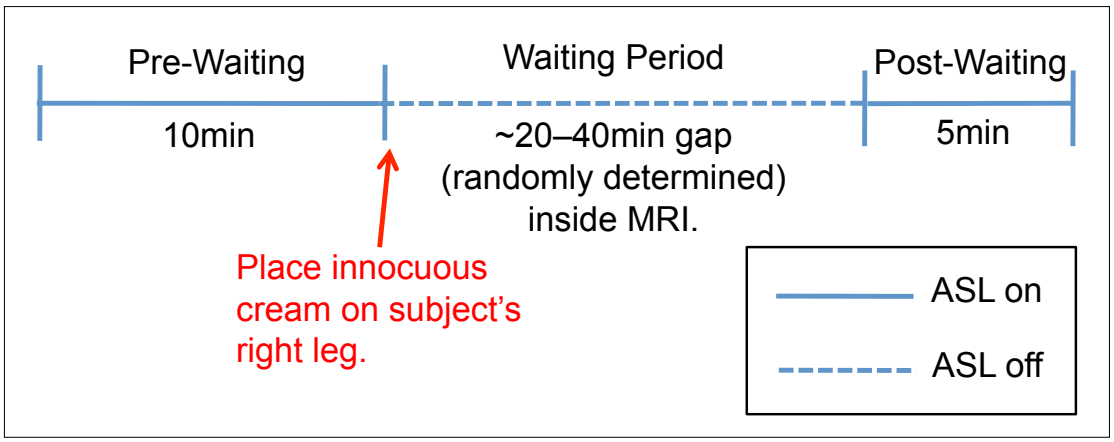


Figure 5.2. Experiment paradigm for the pilot investigation of rCBF changes before and after the waiting period. Subjects underwent a 10-minute resting ASL scan before innocuous cream (10ml) was placed on a 20cm^2-patch at the center of the inner side of the right calf. This was followed by a randomly determined ~20-40 min gap (mean ± SD minutes: 32.4 ± 6.5) in the scanner, for which the subjects were not given any anticipation. Like the 5-minute pain-only scan in Section 5.2.2, the subjects were then scanned for 5 minutes in the post-waiting period.

5.3 Results

5.3.1 Ongoing Pain Model with Capsaicin

To demonstrate the efficacy of capsaicin in inducing ongoing pain, I reported the pain intensity ratings of the eighteen remaining subjects (and excluded the one subject who withdrew) from Section 4.5 following topical application of capsaicin cream (Figure 5.3). The figure showed the average ratings after the subjects reached a score of 5 on a VAS from 0 ("None") to 10 ("Worst Imaginable"), in accordance with the experimental paradigm in this chapter. The pain intensity ratings of all subjects were mainly within 5 and 7 on the VAS. Besides small incline at the beginning and decline at the end, the mean pain intensity rating remained steady throughout the 30-minute interval. With this foundation, the discussion on pain modulation by tDCS could then be broached.

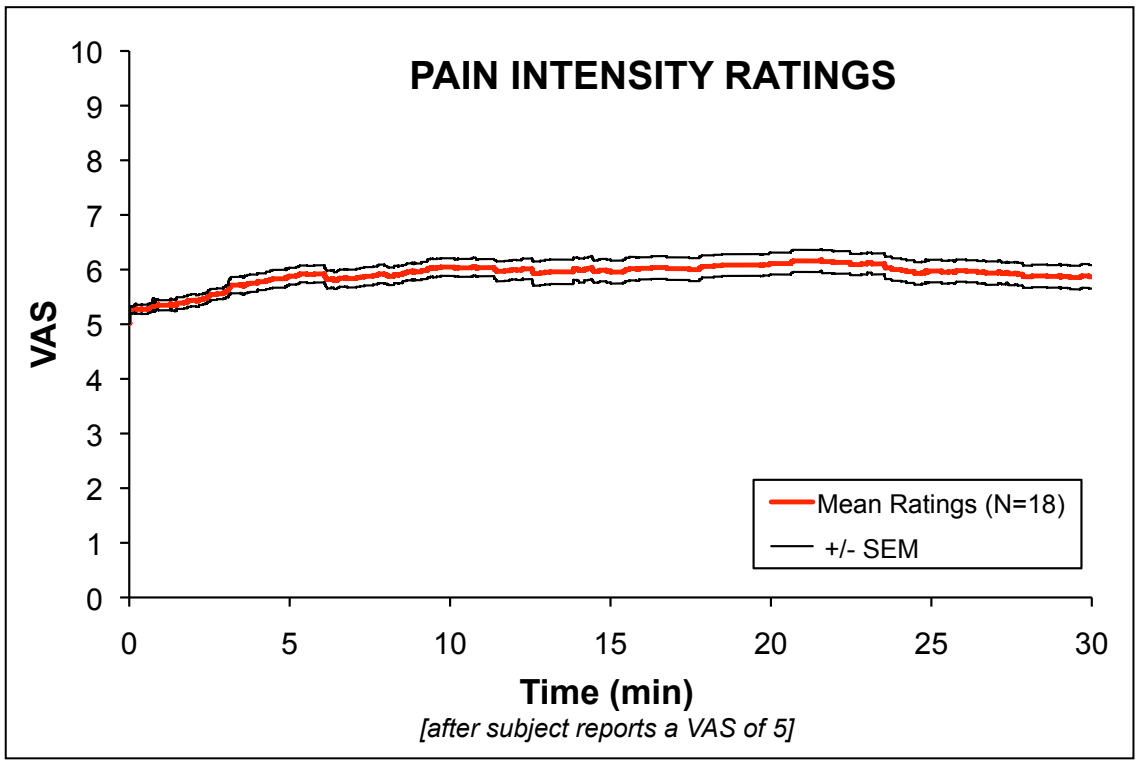


Figure 5.3. Mean pain intensity ratings of the eighteen remaining subjects with topical application of 1% capsaicin cream on the right calf. In the 30-minute interval after subjects reached a rating of 5 on a 10-point continuous VAS, the pain scores largely stabilized between scores of 5 and 7. The continuous pain intensity VAS was anchored between the extremes of "None" and "Worst Imaginable."

5.3.2 Pain Ratings During tDCS-fMRI Experiments

Between all of the scans in each session, the subject's pain intensity and unpleasantness ratings were verbally recorded. A numerical scale was used in lieu of VAS because high temporal resolution was not required. In addition, subjects were all instructed to rate with any number from 0 to 10 without being restricted to integers.

The baseline pain intensity and unpleasantness ratings for all sessions before capsaicin application were 0. The pain intensity measures were also investigated in other statistical tests. As expected, the pain-only ratings were 5 for both anodal and sham tDCS conditions because the pain-only scans did not start unless this score was reached. An ANOVA was performed on the groups for the pre-stimulation, post-stimulation, and after-effect ratings. The results had a significant dependence on time (ANOVA main effect $F(2,17) = 5.468$, $p<0.01$) and a strong trend of variation with polarity (ANOVA main effect $F(1,17) = 4.412$, $p=0.051$). No interaction effect was found (ANOVA interaction effect $F(2,17) = 2.397$, $p=0.11$).

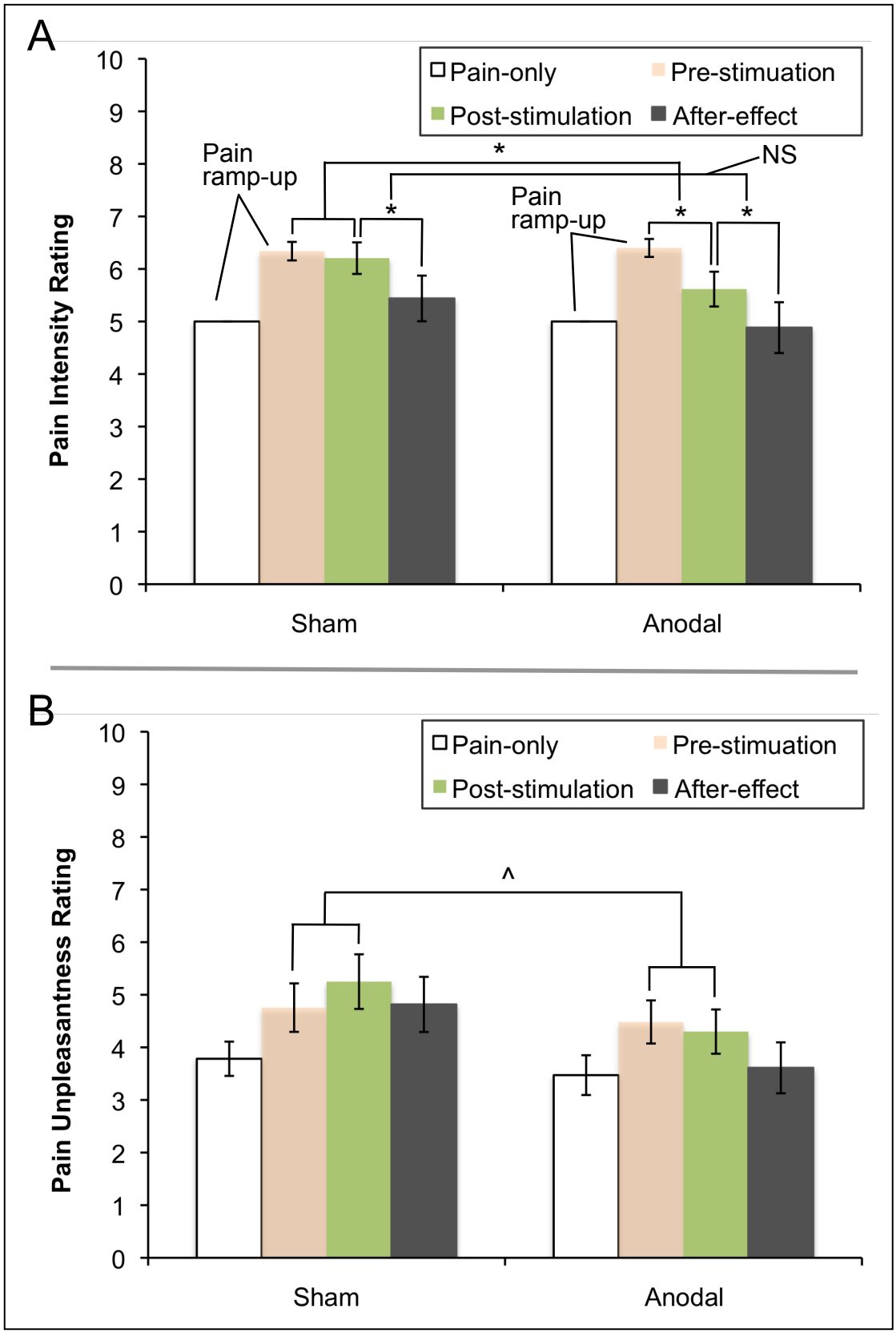


Figure 5.4. Pain ratings recorded during inter-scan intervals for both sham and anodal tDCS conditions. The numerical rating scale was anchored between the extremes of 0 ("None") and 10 ("Worst Imaginable"). Subjects were specifically instructed to rate with any number without being restricted to integers. **A)** For pain intensity, the pain-only ratings were 5 for all subjects of both anodal and sham tDCS. After pain ramp-up, the mean pre-stimulation, post-stimulation, and after-effect ratings for sham tDCS condition

were 6.34 ± 0.18, 6.21 ± 0.30, and 5.44 ± 0.43 (mean ± SEM), respectively. Of these ratings, only the post-stimulation and after-effect scores were significantly different from each other. For the anodal tDCS condition, the mean pre-stimulation, post-stimulation, and after-effect ratings were 6.40 ± 0.17, 5.62 ± 0.34, and 4.88 ± 0.48, respectively. Two pairs of pain intensity ratings, the pre- and post-stimulation score and the post-stimulation and after-effect scores, were significantly different. Between anodal and sham tDCS conditions, their pre-stimulation ratings were not significantly different ($p=0.64$). An ANOVA across pre-stimulation, post-stimulation, and after-effect ratings found a significant dependence on time and a strong trend of variation with polarity. No interaction effect was found. Further analysis was performed on the ratings between pre- and post-stimulation and between post-stimulation and after-effect. The differences between pre- and post-stimulation pain intensity ratings of the anodal tDCS condition (-0.78 ± 0.35) were significantly different from those of the sham tDCS condition (-0.13 ± 0.29). The differences between post-stimulation and after-effect pain intensity ratings of the anodal tDCS condition (-0.73 ± 0.33) were not significantly different from those of the sham tDCS condition (-0.77 ± 0.35). **B)** For pain unpleasantness, the pain-only ratings were 3.78 ± 0.33 for sham tDCS condition and 3.47 ± 0.38 for the anodal tDCS condition, which were not significantly different from each other. The mean pre-stimulation, post-stimulation, and after-effect ratings for the sham tDCS condition were 4.76 ± 0.46, 5.25 ± 0.52, and 4.82 ± 0.52, respectively. For the anodal tDCS condition, the mean pre-stimulation, post-stimulation, and after-effect ratings were 4.48 ± 0.41, 5.62 ± 0.33, and 4.92 ± 0.48, respectively. An ANOVA was performed on both groups for the pre-stimulation, post-stimulation, and after-effect ratings, which found significant dependence on polarity and not to time. A significant interaction effect was also present. A further ANOVA suggested that the differences between pre- and post-stimulation pain unpleasantness ratings of the anodal tDCS condition (-0.18 ± 0.39) showed a strong trend of being smaller than those of the sham tDCS condition (0.49 ± 0.31). All statistical tests were performed with two-tailed t-tests or an ANOVA. Error bars denote the standard error means across subjects. (* – statistical significance with $p<0.05$; ^ – strong statistical trend with $p<0.10$; NS – not statistically significant)

Given my *a priori* interest in the intra-stimulation effect of tDCS, further analysis was done between pre- and post-stimulation ratings. The differences between pre- and post-stimulation pain intensity ratings of the anodal tDCS condition (-0.78 ± 0.35; Post-stimulation – Pre-stimulation; mean ± SEM) were significantly different from those of the sham tDCS condition (-0.13 ± 0.29) (ANOVA interaction effect $F(1,17) = 4.460$, $p<0.05$; post-hoc t-test $p<0.05$) (Figure 5.4A). The results did not have a significant dependence on time (ANOVA main effect $F(1,17) = 2.646$, $p=0.12$) or tDCS polarity (ANOVA main effect $F(1,17) = 3.879$, $p=0.07$).

The pain intensity measures were also investigated in other statistical tests. The differences between post-stimulation and after-effect pain intensity ratings of the anodal tDCS condition (-0.73 ± 0.33; After-effect – Post-stimulation) were not significantly different from those of the sham tDCS condition (-0.77 ± 0.35) (ANOVA interaction effect $F(1,17) = 0.011$, $p=0.92$; post-hoc t-test $p=0.92$). These behavioral measurements had significant dependence on time (ANOVA main effect $F(1,17) = 6.239$, $p=0.02$) and tDCS polarity (ANOVA main effect $F(1,17) = 4.911$, $p=0.04$). The mean pre-stimulation pain intensity rating was 6.34 ± 0.18 for the sham tDCS condition and 6.40 ± 0.17 for the anodal tDCS condition, which were not significantly different from each other ($p=0.64$). The mean post-stimulation pain intensity rating was 6.21 ± 0.30 for the sham tDCS condition and 5.62 ± 0.33 for anodal tDCS condition. These values were significantly different from the pre-stimulation ratings for the anodal tDCS condition ($p=0.04$) but not for the sham tDCS condition ($p=0.65$). The mean after-effect pain intensity rating was 5.44 ± 0.43 for the sham tDCS condition and 4.88 ± 0.48 for the anodal tDCS condition. These values were significantly different from post-stimulation ratings for both anodal ($p=0.04$) and sham tDCS conditions ($p=0.04$).

For pain unpleasantness, the mean rating was 4.76 ± 0.46 for the sham tDCS condition and 4.48 ± 0.41 for the anodal tDCS condition, which were not significantly different from each other ($p=0.18$). An ANOVA was performed on both groups for the pre-stimulation, post-stimulation, and after-effect ratings. The results suggested a significant dependence on polarity (ANOVA main effect $F(1,17) = 7.036$, $p=0.02$) and not to time (ANOVA main effect $F(2,17) = 1.078$, $p=0.352$). A significant interaction effect was found (ANOVA interaction effect $F(2,17) = 4.105$, $p=0.03$).

Similar to the analysis of the pain intensity ratings, the pain unpleasantness ratings were further investigated for the stimulation period. The differences between pre- and post-

stimulation pain unpleasantness ratings of the anodal tDCS condition (-0.18 ± 0.39) showed a strong trend of being smaller than those of the sham tDCS condition (0.49 ± 0.31) (ANOVA interaction effect $F(1,17) = 3.062$, $p<0.10$; post-hoc t-test $p<0.10$). The effect had a significant dependence on tDCS polarity (ANOVA main effect $F(1,17) = 4.569$, $p<0.05$) but not to time (ANOVA main effect $F(1,17) = 0.275$, $p=0.607$).

For other statistical tests, the differences between post-stimulation and after-effect pain unpleasantness ratings of the anodal tDCS condition (-0.69 ± 0.36) were not significantly different from those of the sham tDCS condition (-0.43 ± 0.39) (ANOVA interaction effect $F(1,17) = 0.769$, $p=0.39$; post-hoc t-test $p=0.38$). This effect had significant dependence on tDCS polarity (ANOVA main effect $F(1,17) = 8.009$, $p=0.01$) but not on time (ANOVA main effect $F(1,17) = 2.675$, $p=0.12$). The mean pre-stimulation unpleasantness rating was 4.76 ± 0.46 for the sham tDCS condition and 4.48 ± 0.41 for the anodal tDCS condition, which were not significantly different from each other ($p=0.24$). The mean post-stimulation pain unpleasantness rating was 5.25 ± 0.52 for the sham tDCS condition and 4.31 ± 0.42 for the anodal tDCS condition. These values were not significantly different from the pre-stimulation ratings for both anodal ($p=0.65$) and sham tDCS condition ($p=0.13$). The mean after-effect pain unpleasantness rating was 4.82 ± 0.52 for the sham tDCS condition and 3.61 ± 0.48 for the anodal tDCS condition.

5.3.3 Questionnaire Results Between Anodal and Sham tDCS conditions

Subjects were given an exit questionnaire after each session to determine whether they experienced different sensations between anodal and sham tDCS. No significant differences were found with paired t-tests in the questions, which included tingling ($p=0.83$), itching ($p=0.47$), burning ($p=0.79$), tiredness ($p=0.39$), nervousness ($p=0.67$), concentration ($p=0.71$), headache ($p=0.55$), visual problems ($p=0.33$), and visible flash ($p=0.33$) (Figure 5.5). This suggests that sham tDCS was not physically discernible from

anodal tDCS for the subjects. To be more certain, future studies could include forced-choice questions or add a temporal dimension on the sensation questionnaire for the participants.

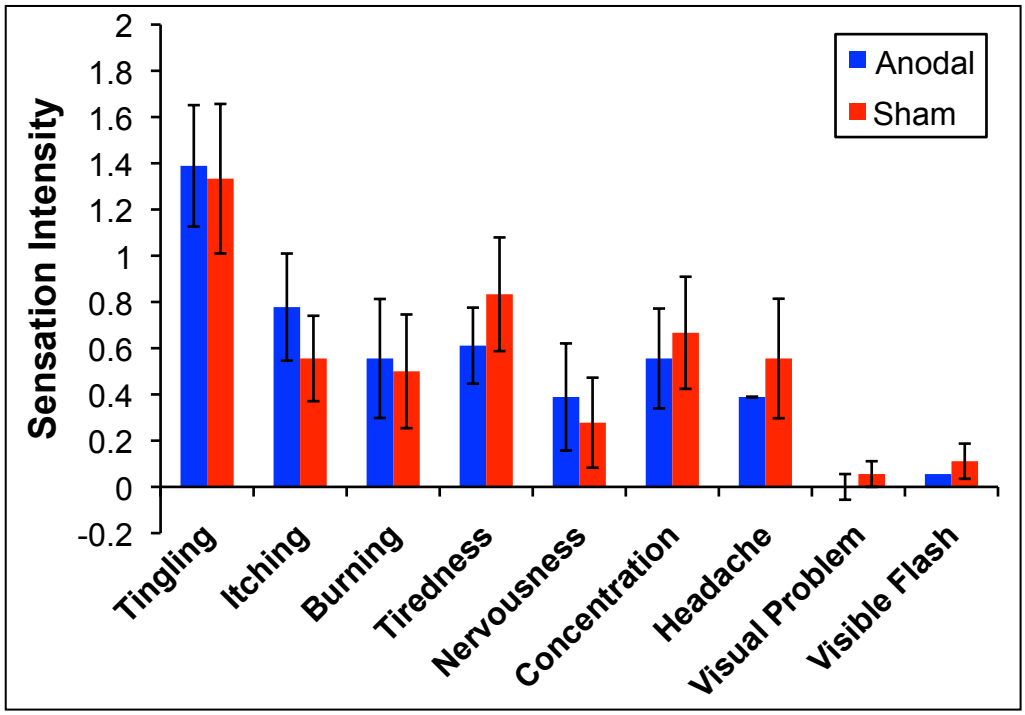


Figure 5.5. Questionnaire results on stimulation sensations after anodal and sham tDCS sessions. No significant differences were observed in all surveyed categories, which consisted of tingling, itching, burning, tiredness, nervousness, concentration, headache, visual problems, and visible flash. Presence of visual flash was determined with a binary yes/no question, while the others were rated from 1 to 5 (1=mild, 2=moderate, 3=average, 4=severe, and 5=intolerable). If subjects did not experience a particular sensation during stimulation, their rating in that category was marked 0. These results suggested that successful blinding was achieved with sham tDCS. All statistical tests were performed with two-tailed t-tests. Error bars denote the standard error means across subjects.

5.3.4 Perfusion Activity During tDCS

Collected across the cohort of 18 healthy subjects, the perfusion fMRI data was used to generate the perfusion maps to infer changes in gray matter activity across the whole brain. During modulation of pain by L-DLPFC tDCS, there was an increased rCBF in L-DLPFC, M1, SI, and the visual cortex compared to the pain-only period (Figure 5.6). No significant rCBF decreases were observed, and the effect on the frontal cortex appeared lateralized to the stimulated hemisphere.

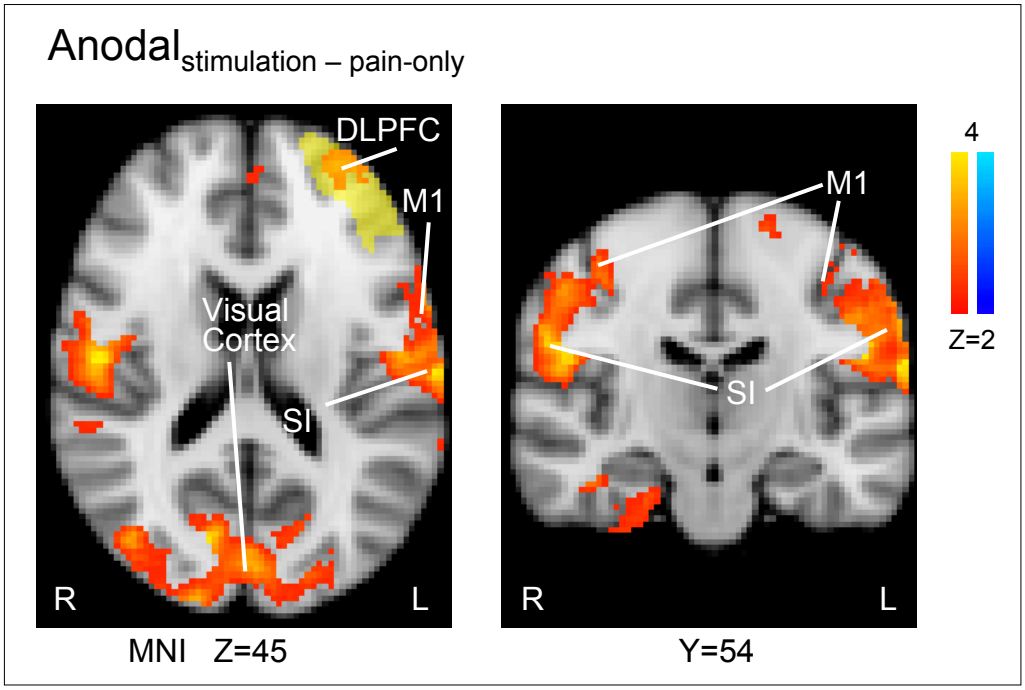


Figure 5.6. Perfusion activity map of gray matter associated with $Anodal_{stimulation - pain\text{-}only}$ (mixed effects; Z>2, cluster corrected at p<0.01). L-DLPFC (denoted by the yellow mask), M1, SI, and the visual cortex showed increased rCBF during stimulation from pain-only period. (DLPFC = dorsolateral prefrontal cortex; M1 = primary motor cortex; SI = primary somatosensory cortex)

In comparison, neuromodulation by sham tDCS was associated with fewer regions of significant rCBF changes (Figure 5.7). Increases were observed in the visual cortex and SI from the pain-only period, while decreases were associated with the right middle temporal gyrus.

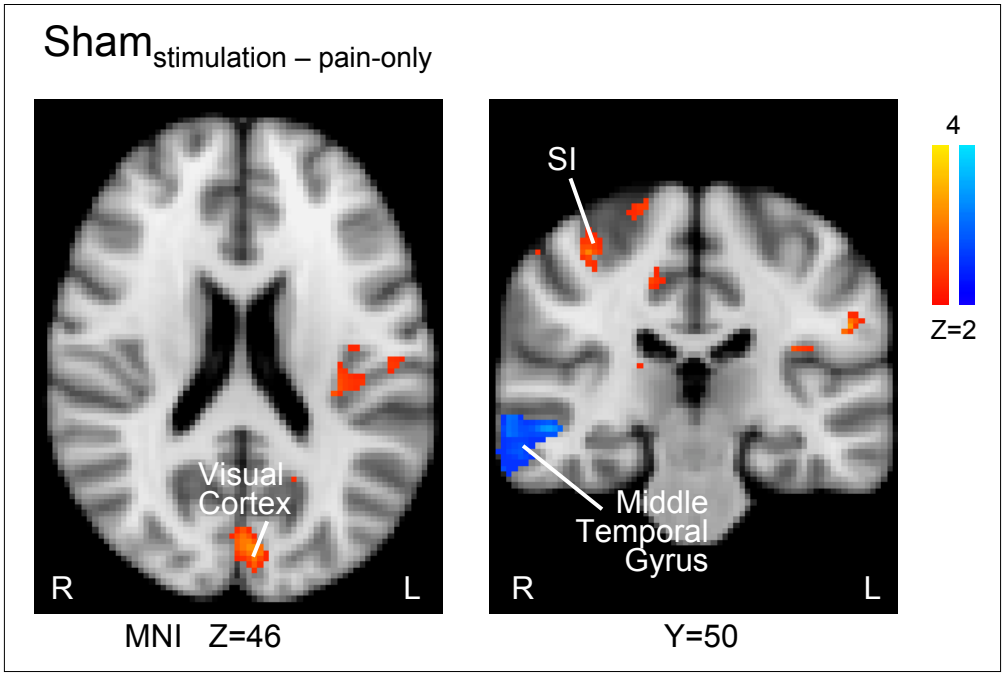


Figure 5.7. Perfusion activity map of gray matter associated with $Sham_{stimulation - pain\text{-}only}$ (mixed effects; Z>2, cluster corrected at p<0.01). SI and visual cortex were associated with increased rCBF during stimulation from the pain-only period, while decreases were observed with the right middle temporal gyrus. (SI = primary somatosensory cortex)

In addition, the % rCBF changes of L-DLPFC as a whole were calculated because tDCS modulates cortical activity through large electrodes. The mean perfusion signals were extracted across the pain-only and stimulation periods for both anodal and sham tDCS conditions. The data showed higher perfusion in L-DLPFC during anodal tDCS (1.11 ± 1.26%; mean ± SEM) than during sham tDCS (-0.86 ± 1.88%), though the difference was not significant (p=0.34). There were also no significant differences between stimulation and pain-only periods for both anodal (p=0.37) and sham (p=0.64) tDCS groups in the whole L-DLPFC.

To dissociate possible placebo influences from direct neuromodulatory effect, the difference in rCBF maps between $Sham_{stimulation - pain\text{-}only}$ and $Anodal_{stimulation - pain\text{-}only}$ was computed (Figure 5.8A). The observed changes were lateralized to the stimulated hemisphere. While the anodal condition was associated with greater rCBF in the left M1 than the sham condition, the sham condition showed higher blood flow to the left

posterior insula and left thalamus. Since the activity of the posterior insula has been shown to indicate pain (Owen et al., 2010), the time series of activated voxels in the left posterior insula were extracted across the pain-only, stimulation, and after-effect periods to show any temporal changes (Figure 5.8B). With the exception of an outlier in the sham condition that led to a large, sudden rCBF decrease in the stimulation period, the perfusion to left posterior insula was consistently higher for the sham condition than for the anodal condition after the pain-only period. Changes in the rCBF of left M1 and thalamus also occurred in the directions suggested by the perfusion map (Figure 5.8C), which may be a result of L-DLPFC modulation by anodal tDCS. The same thalamic voxels also showed sub-threshold changes in the functional connectivity map of Figure 3.5 in Chapter 3.

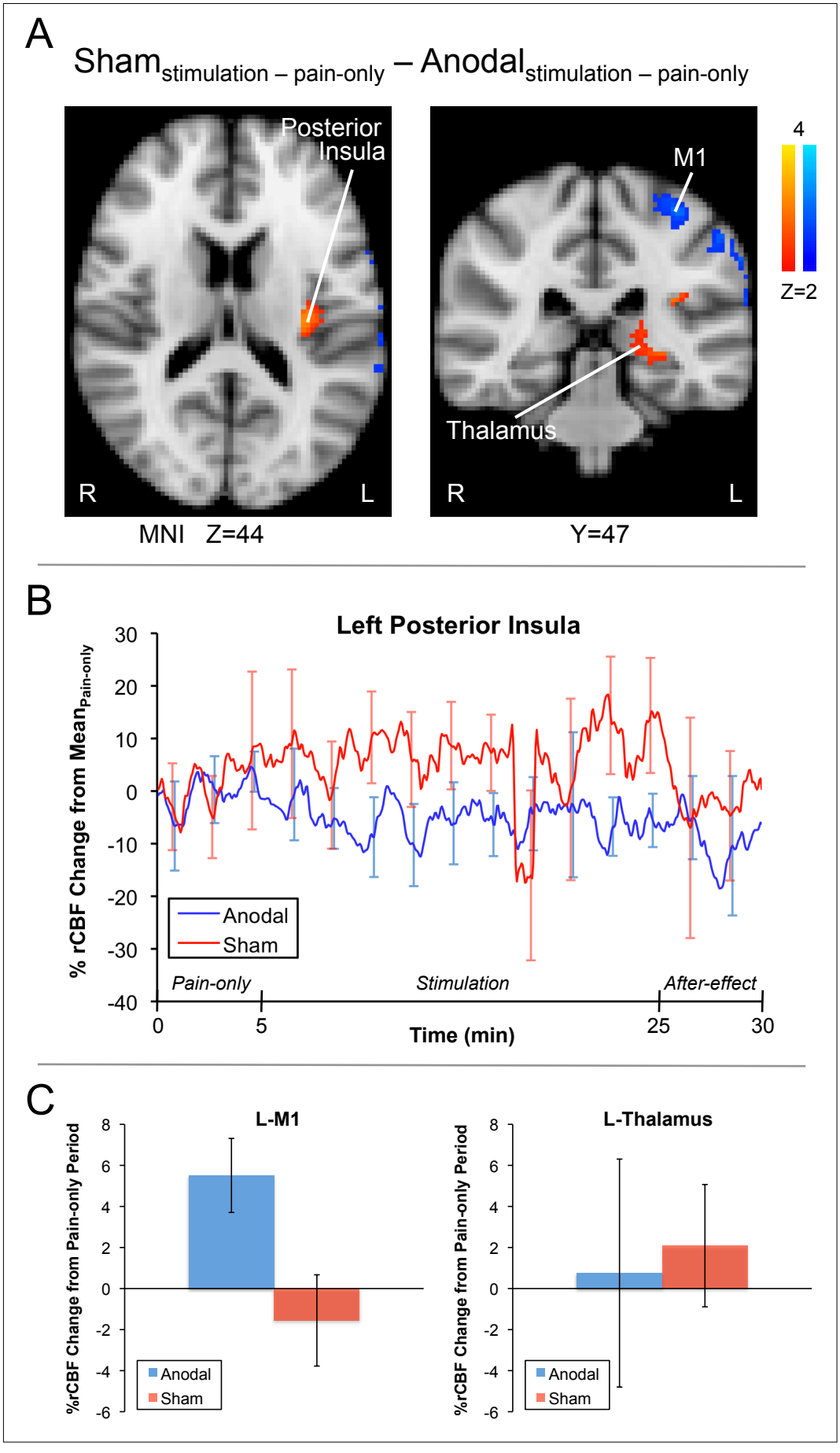

A
Sham stimulation – pain-only – Anodal stimulation – pain-only
Posterior Insula
M1
Thalamus
R
L
R
L
4
Z=2
MNI Z=44
Y=47
B
Left Posterior Insula
% rCBF Change from Mean Pain-only
30
20
10
0
-10
-20
-30
-40
Anodal
Sham
Pain-only
Stimulation
After-effect
0
5
25
30
Time (min)
C
L-M1
L-Thalamus
%rCBF Change from Pain-only Period
8
6
4
2
0
-2
-4
-6
Anodal
Sham

Figure 5.8. **A)** Perfusion activity map of gray matter associated with $Anodal_{stimulation - pain\text{-}only} - Sham_{stimulation - pain\text{-}only}$ (mixed effects; $Z>2$, cluster corrected at $p<0.01$). The sham condition showed higher rCBF to left posterior insula and left thalamus and lower rCBF to the left M1 than the anodal condition. The lateralized differences suggest that the changes were caused by anodal tDCS modulation. **B)** Due to the indication of pain with posterior insula activity (Owen et al., 2010), the perfusion time course of the activated voxels in the left posterior insula was extracted for illustrative purposes. Despite temporal variations across the three periods, the rCBF of posterior insula was consistently higher for the sham condition than for the anodal condition after the pain-only period. The only exception of a large, sudden rCBF decrease in the stimulation period of the sham session was driven by a set of outlier values from a single subject (Grubb's test; $p<10^{-10}$). All perfusion percentages were compared to the mean time course value of the pain-only period in the respective stimulation session. The data points were smoothed with a moving average filter (period = 1min). **C)** Of the voxels in left M1 and thalamus that showed significant perfusion difference in part **A**, their relative rCBF in the stimulation period (from the pain-only period) was plotted for both anodal and sham tDCS conditions. As expected, anodal tDCS condition was associated with higher left M1 and lower left thalamic activities than sham tDCS condition. The difference in rCBF of left thalamus between anodal and sham tDCS conditions appeared small, but the perfusion average of the latter was affected by a set of large, negative outliers (Grubb's test; $p<10^{-10}$) that, if removed, would raise the group mean by ~3%. These outliers were located in the same volumes of the same subject as the set described in part **B**. Error bars denote the standard error means across subjects.

5.3.5 Perfusion Activity After tDCS

For the anodal tDCS condition, the perfusion activity decreased after the stimulation ended (Figure 5.9). Structures that showed higher rCBF in the stimulation period from the after-effect period included L-DLPFC, M1, SI, and visual cortex, while no regions were associated with lower blood flow.

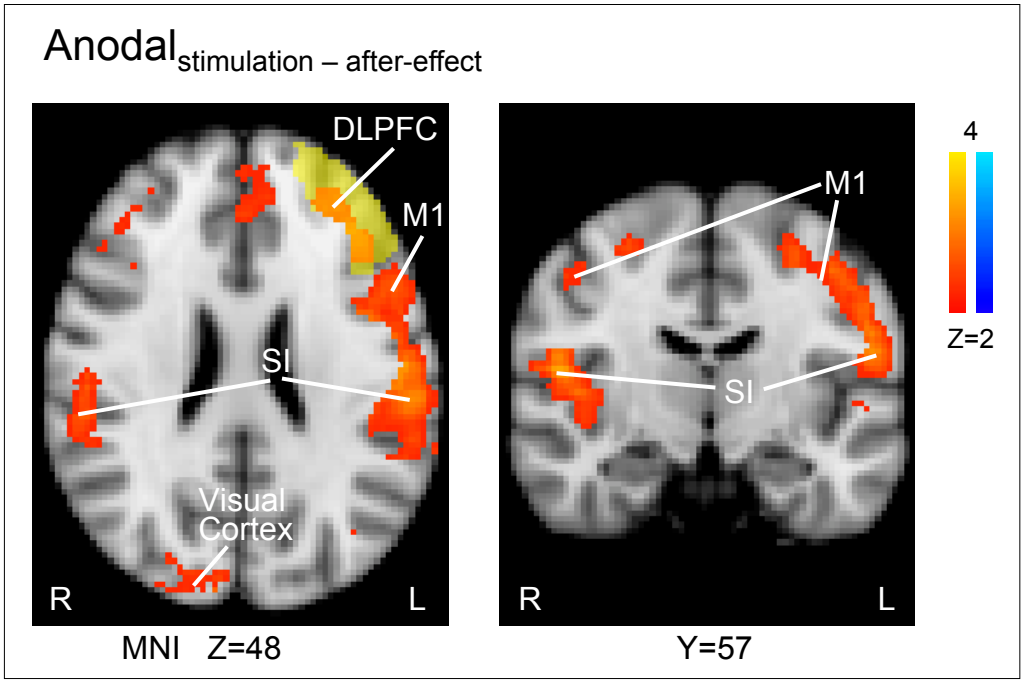


Figure 5.9. Perfusion activity map associated with $Anodal_{stimulation - after\text{-}effect}$ (mixed effects; Z>2, cluster corrected at p<0.01). L-DLPFC (denoted by the yellow mask), M1, SI, and the visual cortex showed higher rCBF during stimulation than in the after-effect period, while no regions showed lower blood flow. (DLPFC = dorsolateral prefrontal cortex; M1 = primary motor cortex; SI = primary somatosensory cortex)

For the sham tDCS condition, no significant differences were observed between the perfusion maps of the stimulation period and after-effect period. A direct comparison between $Anodal_{stimulation - after\text{-}effect}$ and $Sham_{stimulation - after\text{-}effect}$ also found no regions with significant rCBF differences.

5.3.6 Perfusion Activity Between Pre- and Post-Waiting Periods

For exploratory purposes, the rCBF changes before and after the waiting period were also investigated. In the perfusion maps, global rCBF decreases were observed regardless of whether capsaicin or innocuous cream was used (Figure 5.10). The affected regions were located across the whole brain in frontal, temporal, parietal, and occipital lobes. A direct comparison between the two perfusion maps did not find any differences in the cortical regions.

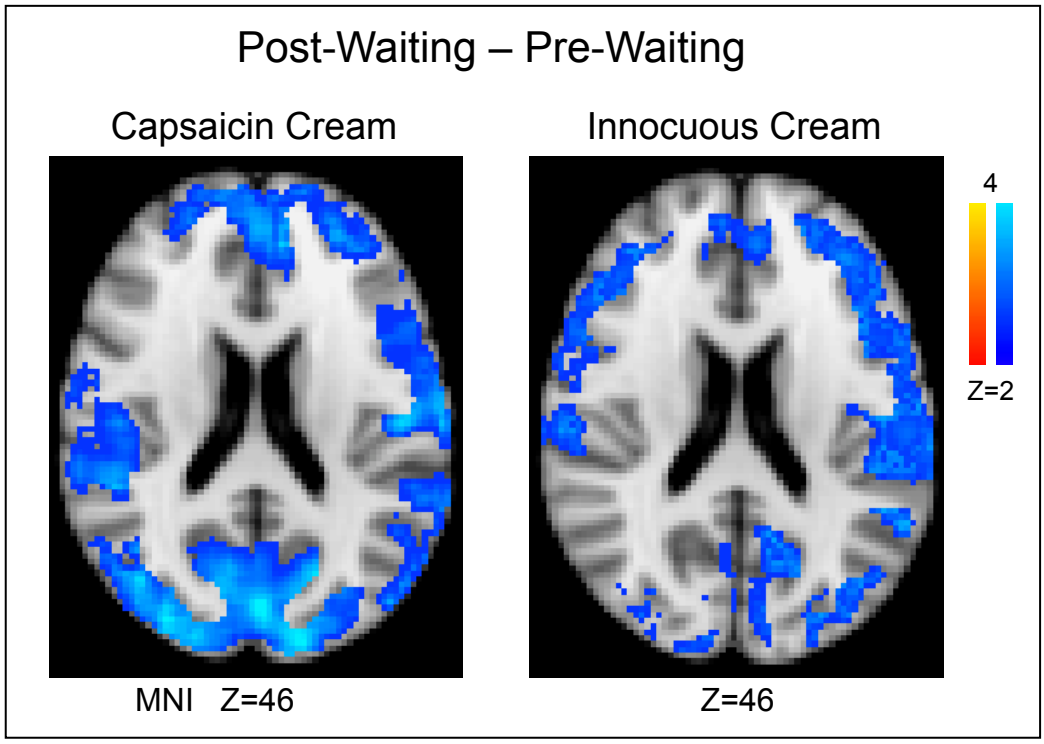


Figure 5.10. Perfusion activity maps associated with Post-Waiting – Pre-Waiting with topical application of either capsaicin or innocuous cream (mixed effects; Z>2, cluster corrected at p<0.01). Global rCBF decreases in gray matter were observed for both conditions. No significant differences were observed between the cortical regions of the two perfusion maps.

5.4 Discussion

In this chapter, the modulation of pain by tDCS was directly investigated with perfusion fMRI. Besides observations of mild behavioral changes, whole rCBF changes were also associated with the use of tDCS.

5.4.1 Behavioral Changes in Pain Sensation

The anodal tDCS condition found a modest but significant reduction in pain intensity after tDCS. This magnitude was significantly greater than that of the sham tDCS condition, which noted a smaller, non-significant decrease in pain intensity. In both tDCS groups, an increase in pain intensity from pain-only to pre-stimulation ratings and a decrease from post-stimulation to after-effect were observed and expected. The capsaicin-based pain model induced stable pain sensation, which ranged between 5 and 7 in pain intensity on a 0-to-10 rating scale. However, small ramp-up and ramp-down were still present in the first and last 5-minute blocks, respectively, of the 30-minute capsaicin screening session outside the scanner (Figure 5.3). These changes were consequently reflected in the pain intensity ratings between scans.

While the overall tDCS-related effect on pain intensity was only marginally significant, this could be contributed by the large decrease in the after-effect ratings from the post-stimulation ratings for both tDCS groups. The significant interaction effect between both groups for the pre- and post-stimulation ratings suggests that anodal tDCS was significantly more effective in pain reduction than sham treatment. The mild (on the order of ~10%) magnitude of pain modulation is consistent with previous findings (Boggio et al., 2008a). While a “minimally clinically important difference” has been defined as a >15% decrease (O'Connell et al., 2010), multiple stimulation sessions have generally been used in literature (Fregni et al., 2006a; Arul-Anandam et al., 2009) to form a treatment regimen and elicit greater pain reduction. Thus, the cumulative effect over time could reach the necessary clinical threshold. Similar to these studies, the

present study also supported the observation that pain reduction occurred during rather than after anodal tDCS.

For pain unpleasantness, a significant tDCS-specific decrease was found in the anodal tDCS condition over the sham tDCS condition for the overall effect. Between pre- and post-stimulation ratings, a strong trend of pain unpleasantness reduction was also observed for the anodal tDCS condition over the sham tDCS condition. Previous literature has suggested the involvement of DLPFC in affective pain processing (Price, 2000; Lorenz et al., 2003), e.g. anticipation (Wager et al., 2004) and anxiety (Bishop et al., 2004). The modulation during tDCS did not reach statistical significance, possibly because the ongoing pain unpleasantness was not as well controlled in the capsaicin screening session as pain intensity. However, the trend does support the suggestion that L-DLPFC tDCS can modulate affective processing. Future studies could include a psychology questionnaire to allow for better control of inter-subject and intra-subject (between anodal and sham sessions) mood differences.

5.4.2 Perfusion Changes Associated With tDCS

For both anodal and sham tDCS sessions, careful attention was paid to ensuring that the subjects could not discern one stimulation modality from the other. The post-experiment questionnaires did not find any significant differences in the physical sensations of the stimulation between the two groups. This result is consistent with previous findings that sham tDCS can serve as a valid placebo for active tDCS (Gandiga et al., 2006).

The contrast perfusion map between anodal and sham tDCS conditions was calculated by using the latter as a control. As expected, only regions with the same lateralization (left) as the active stimulation electrode showed significantly different rCBF. The left M1 was more active during anodal tDCS than during sham tDCS, which supports earlier

explanations that this region might be elicited by a stimulated L-DLPFC for somatosensory processing. The left posterior insula, which was contralateral to the capsaicin site, was found to have a lower rCBF for the anodal tDCS condition than for the sham tDCS condition. The contralateral posterior insula has been shown to reflect pain intensity in ongoing pain paradigms (Owen et al., 2010). Its rCBF change in this study might have been induced by L-DLPFC tDCS or could simply serve to indicate the lower pain intensity ratings. However, the perfusion time course of the activated voxels in the left posterior insula does corroborate the behavioral data. In the pain-only and after-effect periods, the perfusion activity of both anodal and sham tDCS conditions followed similar ramp-up and ramp-down patterns, respectively. The main noticeable difference was in the rCBF changes during stimulation, which suggested higher pain intensity for the sham tDCS condition over the anodal tDCS condition.

The contrast perfusion map also helped to shed light on the mechanism of pain modulation. While L-DLPFC might recruit the assistance of M1, it still needed a conduit to exert top-down influences. Perfusion changes in the thalamus supported the hypothesis that the subcortical structure was involved in the pain modulatory process during L-DLPFC tDCS. Robust structural connections link L-DLPFC and thalamus via a fronto-subcortical circuit (Cummings, 1993; Tekin and Cummings, 2002). In addition, the joint involvement of L-DLPFC and thalamus in the descending pain modulatory system has been well established in past studies (Lorenz et al., 2003; Valet et al., 2004). As the main relay center between brain and body, the thalamus is well positioned to dampen nociceptive transmission from lower structures. Its modulation by L-DLPFC tDCS can thus alter one's pain sensation. For example, high L-DLPFC activity has been shown to change midbrain-thalamic coupling that resulted in pain relief (Lorenz et al., 2003). Also, the white matter connection between PAG, a region with extensive antinociceptive roles

(Bittar et al., 2005), and L-DLPFC might well pass through the thalamus (Hadjipavlou et al., 2006).

For the anodal tDCS condition, the perfusion map associated with the stimulation period showed higher rCBF in multiple structures than the maps of pain-only and after-effect periods. The modulated regions included DLPFC, M1, SI, and visual cortex. Previous studies have shown that brain stimulation can increase the rCBF of the stimulated area (Wachter et al., 2011; Zheng et al., 2011) and affect the activity of connecting regions. During rTMS of the frontal cortex, concurrent fMRI found top-down modulation of visual cortical activity through the frontal eye-field (Ruff et al., 2006).

M1 and SI also maintain strong functional (Owen et al., 1996; Tracey et al., 2000; Lu et al., 2007) and structural (Lu et al., 1994; Takada et al., 2004) connections with L-DLPFC. Information from DLPFC often transmits to motor-related regions when coordinating somatosensory processing and response (Wang et al., 2001; Takada et al., 2004). In an ongoing pain state, anodal tDCS might assist L-DLPFC in recruiting M1 and SI to provide pain relief. This idea is corroborated by past tDCS studies that successfully used anodal tDCS of the left M1 to treat chronic pain patients (Fregni et al., 2006a; Fenton et al., 2009).

Fewer voxels showed significant rCBF changes between pain-only and stimulation periods for the sham tDCS condition, in which regions such as SI and visual cortex observed higher rCBF. No significant differences were found between the perfusion maps of stimulation and after-effect periods. A physiological study has demonstrated that short-duration (<1min) tDCS, which was used as a sham substitute, does not have lasting effects on cortical activity (Nitsche and Paulus, 2000). These findings were supported by the rCBF data from this study.

Besides the impact of L-DLPFC tDCS on pain-related rCBF changes, the reverse effect could be discussed by accounting for the results in Chapter 3. Activations of L-DLPFC, cingulate cortex, SI, and other DLPFC-connected regions were associated with anodal tDCS in the absence of any tasks. While significant L-DLPFC activity was observed in the $\text{Anodal}_{\text{stimulation – pain-only}}$ contrast map, rCBF changes were not significantly present in cingulate structures. Further control with the sham condition showed even smaller DLPFC activity but larger rCBF changes in the left posterior insula and thalamus. Thus, the perfusion map associated with both tDCS and pain was not a simple sum of its parts, and an interaction component needed to be included in the consideration. This observation is not unusual in concurrent tDCS-fMRI studies. For instance, earlier works found no significant M1 activation during task-free, M1, anodal tDCS (Lang et al., 2005; Antal et al., 2011). However, the addition of a motor task, such as finger-tapping, led to a significant difference in BOLD signal when compared to the baseline or tDCS-free condition (Lang et al., 2005; Stagg et al., 2009a; Dechent et al., 2010).

5.4.3 Possibility of Cognitive-Behavioral Treatment

Besides its involvement in the descending pain modulatory system, L-DLPFC is highly involved in a person's cognitive functions (MacDonald et al., 2000), which raises the possibility of using anodal tDCS coupled to a cognitive behavioral treatment (CBT) for pain. Traditionally, CBTs seek to target the psychological processes that underlie pain (Eccleston et al., 2009). The efficacy of various CBTs in chronic pain patients has been demonstrated in previous works (Keefe and Caldwell, 1997; Morley et al., 1999) and requires the activation of cognition-related brain regions. Past fMRI experiments that simultaneously engaged healthy subjects in both cognitive tasks and pain stimuli found higher activity in such areas and lower pain ratings than those of volunteers in pain-only conditions (Peyron et al., 1999; Seminowicz et al., 2004). In this study, the perfusion

activity of L-DLPFC, a region involved in attention (Valet et al., 2004) and anticipation (Watson et al., 2009), was altered during anodal tDCS. It is thus conceivable that L-DLPFC stimulation may elicit a comparable effect to that of a cognitive load by artificially inducing a similar brain activation pattern. The findings present a promising first step towards the establishment of coupling tDCS with pain-related CBT to produce possibly synergistic effects and greater outcomes, although further work is needed.

5.4.4 Investigation of rCBF Changes Before and After Waiting Period

Lastly, the rCBF changes before and after the waiting period were studied in an exploratory exercise. Both maps showed whole brain rCBF decreases from pre-waiting to post-waiting period, but the contrast map between capsaicin and innocuous cream conditions did not show any significant results. This was especially surprising given the presence of pain (0 to 5 on a 0-10 scale) in the capsaicin condition, suggesting that a strong background effect had compensated for the pain-related rCBF changes. This also ruled out any contributions by capsaicin-specific effects and turned my attention to the long experimental paradigm.

An exhaustive literature search did not find any studies that investigated the effect of long-term rest in a scanner in the absence of stimulus input, including the noise of scanner operation. The widespread manner of the perfusion decrease may indicate general physiological changes, such as the slowing of heart rate after 20 to 40 minutes of uninterrupted rest inside the scanner. To investigate this effect, future experiments may incorporate physiological monitoring both during and between scans to correlate recorded measures with rCBF changes. In addition, the exact waiting times between scans may be controlled to test for time-dependent perfusion fluctuations.

This activation pattern between pre- and post-waiting periods also has implications for Chapter 3, which did not include a task during experiment. The overall paradigm in Chapter 3 (~40min) was considerably shorter than that in Chapter 5 (~70-100min), so it should be less susceptible to this problem. However, this data underlines the need for a sham condition in ASL-tDCS experiments, especially those involving a prolonged period of rest. This will allow for the control of any unexpected rCBF decreases across the cortex.

5.4.5 Conclusion

In this chapter, the neuromodulation of pain was directly investigated with concurrent perfusion fMRI. Significant reductions in pain intensity were found during anodal rather than sham tDCS of L-DLPFC, which were supported by changes in functional data. In addition, the involvement of the thalamus during stimulation continued to underline the importance of L-DLPFC–thalamic connections in pain modulation with tDCS. To extend the investigation of this hypothesis, diffusion tensor imaging was used in the following chapter in an attempt to find possible relationships between structural integrity and the behavioral changes induced following tDCS.

CHAPTER 6 – CORRELATION OF STRUCTURAL CONNECTIVITY AND PAIN MODULATION USING DIFFUSION TENSOR IMAGING

The previous chapter detailed the behavioral and rCBF changes during pain modulation by tDCS. However, the mechanisms behind this process remain unclear, thus posing new questions such as why this technique works better for some subjects than others. To identify the possible determinants of its efficacy, I explored the correlations of between subjects' structural measures and their pain intensity rating changes induced by tDCS. Diffusion tensor imaging and furthere analysis techniques, such as probability tractography, were extensively used for this investigation.

6.1 Introduction

The previous chapter showed that pain modulation occurs with L-DLPFC tDCS, as confirmed by both behavioral and rCBF data. However, the underlying mechanisms behind this process still require elucidation. Previous literature has suggested that top-down regulation occurs with the involvement of L-DLPFC to alter the activity of other regions in the pain matrix (Petrovic et al., 2002; Wager et al., 2004; Wager et al., 2007). Among the possible candidates, the thalamus is ideally positioned to be a key target due to its functional roles in pain processing (Bingel et al., 2003). The region also has robust structural connections to L-DLPFC (Cummings, 1993; Tekin and Cummings, 2002), which projects to the thalamus through cortico-thalamic tracts (Goldman, 1979; Selemon and Goldman-Rakic, 1988; Carretta et al., 1996; Negyessy et al., 1998). While tDCS does not change a brain's structural connectivity (Nitsche et al., 2004b), I have demonstrated in Chapter 3 that anodal tDCS of L-DLPFC can alter the functional connections between L-DLPFC and thalamus. The white matter connection between L-DLPFC to PAG, a key antinociceptive region, might also be routed through the thalamus (Hadjipavlou et al., 2006). In addition, clinical literature has reported joint gray matter loss in the L-DLPFC and thalamus of chronic pain patients (Apkarian et al., 2004). More recently, the atrophy was shown to recover with improvement in the pain condition

(Gwilym et al., 2010). Thus, as the key cortical relay center to the body, the thalamus is likely to be involved in any pain modulations from L-DLPFC tDCS.

Given this supporting evidence, I hypothesized that the strength of structural connections between L-DLPFC and thalamus will correlate with the efficacy of pain modulation by tDCS. This investigation requires diffusion tensor imaging (DTI), a technique which has proven to be ideal for evaluating white matter connectivity (Behrens et al., 2007; Johansen-Berg et al., 2007). The tool is based on the concept that random, passive movements of water molecules, or Brownian motion, within tissue structures will be larger than MRI voxel dimensions within a second-order frame (Le Bihan et al., 2001). The typical diffusion speed in the brain is ~0.2mm every second, during which water molecules collide and interact with surrounding cell membranes and macromolecules (Le Bihan et al., 2001). Physical barriers, such as blood vessels, can restrict water mobility in certain directions and lead to anisotropic diffusion patterns. With sufficiently long TRs, such displacement distribution of water molecules may be observed and used for estimating the three-dimensional geometry of nearby tissues. The latter is achieved by MRI's utilization of gradient pulses to determine the diffusion magnitude along the respective direction. At the same time, typical MRI resolution is on the order of millimeters while the size of neurons is on the order of micrometers (Mori and van Zijl, 2002). This technical limitation suggests that DTI can only allow the robust detection of large axonal and neuroglial bundles.

To quantify diffusion directionality in tissues, a measure called fractional anisotropy is often used (Figure 6.1). For neuronal axons, diffusion occurs easily along the longitudinal direction but meets restrictions, such as myelin sheaths, when it pursues a perpendicular course from the fibers. Thus, white matter has a higher FA than gray matter, which contains few myelinated tracts, even though both have similar mean

diffusivity properties. FA values have consequently been used as indicators of connectivity strength because strong structural links should require anisotropic diffusion to maintain robust neuronal communication (Beaulieu, 2002). Previous studies have applied this idea to explore relationships between structural differences and behavioral measurements such as bimanual coordination skills (Johansen-Berg et al., 2007) and age-related cognitive declines (Charlton et al., 2006).

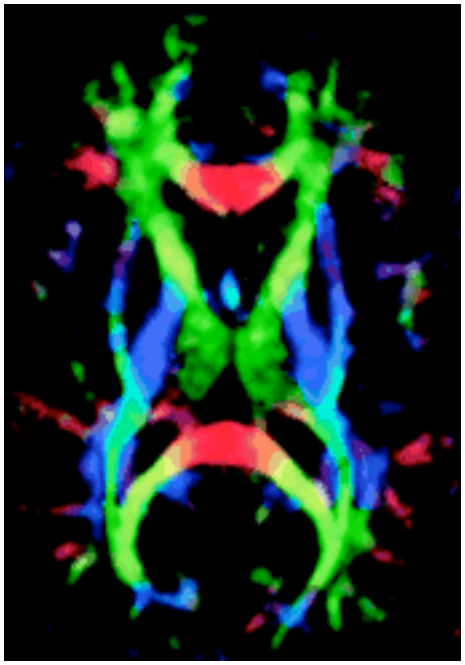


Figure 6.1. [Adapted from Jellison *et* al.] An axial slice (in MNI space) of a fractional anisotropy map taken from a single subject. The map was generated by using DTI orientation information to extract the locations of white matter tracts. The fibers were also overlaid with color codes to indicate their directionality. (Red = right–left; Green = interior–superior; Blue = anterior–posterior) (Jellison et al., 2004)

FA can be further divided into individual components. λ_1 typically represents the axis with the greatest magnitude (or eigenvalue), while λ_2 and λ_3 denote the two minor axes and average to become the radial diffusivity (RD) (Beaulieu, 2002). For its application, RD has sometimes been used to indicate the amount of myelination in white matter tracts (Le Bihan et al., 2001). FA can also be related to mean diffusivity (MD) through these variables. While FA varies with the ratio of λ_1 and RD to provide a measure of diffusion directionality, MD is the average of λ_1, λ_2, and λ_3 and denotes the water mobility in any

particular voxels. MD is typically useful for comparison between healthy and diseased cohorts to demonstrate changes in the overall diffusion property (Heise et al., 2011).

To explore the involvement of fronto-thalamic connection in pain modulation, I recruited the same subject cohort from Chapter 5 to participate in an additional DTI experiment. From these scans, I explored the correlations of the subjects' fractional anisotropy (FA) values between L-DLPFC and thalamus to their reported pain intensity rating changes. In addition, I investigated the possible pain-altering influences of variations in gray matter density. I hypothesized that subjects with stronger structural connection from L-DLPFC to thalamus would experience greater pain modulation during L-DLPFC tDCS.

6.2 Methods

6.2.1 Subject Recruitment

I recruited the same subject cohort as in Chapter 5, which included 18 healthy subjects (6 females, all right-handed, mean ± SD age: 24.8 ± 5.4 years) after excluding the one subject who withdrew. The exclusion criteria were identical to those imposed in Sections 4.5.1 and 5.2.1.

6.2.2 Image Acquisition

All scans were collected with a 3T MRI scanner (3-T Trio, Siemens, Germany) using a 12-channel head coil. The subjects underwent two high-resolution (1x1x1mm^3 voxels) T1-weighted structural scans (TR=2.04s, TE=4.7ms, FOV=192mm, and acquisition time = 6min/scan) and two EPI diffusion-weighted (2x2x2mm^3 voxels) scans (TR=9.30s, TE=94ms, FOV=192mm, and acquisition time = 10min/scan) that applied 60 isotropically-distributed gradient directions and a *b*-value of 1000 s/mm^2. These sequences have been successfully used in previous literature (Heise et al., 2011). Each set of scans contained two repetitions to allow averaging during image analysis, which can improve the overall signal-to-noise ratio.

6.2.3 Image Analysis

All data analyses were performed with tools from FSL version 4.1.7 (Smith et al., 2004). Skull removal was first performed with the Brain Extraction Tool (BET) in the FSLtools (Smith, 2002) on the two structural images, which were then registered with FMRIB's Linear Image Registration Tool (FLIRT) and averaged for use in further analyses.

DTI Preprocessing. Eddy current correction was used on the two sets of raw DTI images to remove motion artefacts and distortions associated with the applied gradient directions. Similar to the processing of the structural images, the two DTI volumes were

then registered with FMRIB's Linear Image Registration Tool (FLIRT) and averaged. Deriving the magnitude and directionality of diffusion in tissues, the DTIFit tool in the FMRIB's Diffusion Toolbox (FDT) was applied to model the diffusion tensor of each voxel as an ellipsoid symmetrical across its three axes (Behrens et al., 2003a). This allowed the generation of FA and RD maps for further analyses with probability tractography and tract-based spatial statistics.

Probability Tractography. In this study, the *a priori* hypothesis is that the pain modulatory effects of tDCS will be related to the strength of the structural connectivity between L-DLPFC and thalamus. The L-DLPFC–thalamic tract was first determined with probabilistic tractography, a built-in tool of the FDT (Behrens et al., 2003a). Seed masks of L-DLPFC and left thalamus were drawn in MNI space (2x2x2mm^3 voxels) by using the same anatomical demarcations as in Chapters 3, but they were further thresholded to be more conservative to avoid overlap with any nearby structures or white matter. For the L-DLPFC mask, any voxels with a sub-50% probability of being gray matter, as determined by the MNI152 gray matter probabilistic mask, were excluded. The thalamus mask was derived from the Harvard-Oxford probabilistic atlas at a high 75% threshold due to the close proximity of basal ganglia structures. The two ROI masks were then manually examined to ensure their validity.

The technical methods of probabilistic tractography have been described and applied in previous literature (Behrens et al., 2003a; Behrens et al., 2007; Johansen-Berg et al., 2007). The individual FA maps were first warped into MNI space (2x2x2mm^3 voxels) with an optimized FMRIB's Non-linear Image Registration Tool (FNIRT) and fitted to a multi-fiber model. This allowed the tracing of the incoming tract at each voxel through complex fiber crossings by estimating the probability distributions of the 60 sampled fiber directions.

Probability tractography traced the connection from L-DLPFC to thalamus and vice versa for each subject and reported on the mean tractography map. Bound by a limiting curvature of 0.2 (equivalent to ~±80°), the analysis sampled the voxel-wise distribution of principle diffusion directions to compute a streamline that linked seed to target. This process was repeated 5000 times for each seed voxel to approximate the overall distribution of connection paths. For each direction, the analysis recorded the waytotal, or the total number of generated tracts that successfully linked L-DLPFC and thalamus. I subsequently calculated the average waytotal for each subject and used 2% of this value as a threshold to remove spurious connections. Only the mean FA of the surviving tracts, which served as a binary mask, was derived in order to acquire a quantitative measure of the structural connectivity. These values were then correlated with the pain intensity ratings of the respective subjects to investigate the relationship between the two variables. Functional correlations between L-DLPFC and thalamus, which were determined by the Pearson coefficient between the mean time series of the two regions, were also correlated with the mean FA to explore possible associations between structural and functional connectivities.

For visualization, the individual probability tractography maps were prepared by the same methods described above and averaged across the subject cohort. Voxels were colored according to the number of individual probability tractography maps that they corresponded to. Lastly, the tracts were overlaid on MNI152 standard space ($2x2x2mm^3$ voxels). Since the maps were already thresholded on a subject level with an average waytotal, the mean tractography map was not thresholded further in the final visualization.

Tract-based Spatial Statistics (TBSS). TBSS (version 1.2) is an FSL tool for performing voxelwise analysis of whole brain DTI data without an *a priori* hypothesis (Rueckert et al., 1999; Smith, 2002; Smith et al., 2004; Smith et al., 2006). The technique is unique because it uses specialized nonlinear registration to project individual FA maps to a tract skeleton. By restricting the analysis to this representation, TBSS can minimize biases from registration misalignment and arbitrary spatial smoothing to improve overall objectivity.

TBSS analysis served two purposes in this study. First, it may affirm or dispute the conclusions reached by the probability tractography analysis described above. Second, it can determine whether the FA of white matter voxels outside of fronto-thalamic tracts correlated with pain intensity changes. The FA maps generated from DTIFit were first slightly eroded to remove likely outliers and aligned to FMRIB58_FA standard space ($1x1x1mm^3$ voxels) with FMRIB's Non-linear Image Registration Tool (FNIRT) and averaged. An FA skeleton was then generated from this mean FA image to identify the common set of white matter tracts in the cohort.

After the standardized FA maps were projected onto the group skeleton, the individual FA skeletons were transformed into MNI152 space and thresholded by 0.2 to remove spurious voxels. They were submitted for voxelwise cross-subject statistics with general linear modeling against demeaned pain intensity ratings. Correlated voxels were determined by permutation-based nonparametric tests (5000 permutations) with threshold-free cluster enhancement (TFCE) to avoid biases from arbitrary cluster thresholds (Smith and Nichols, 2009) and statistically thresholded at $p<0.05$ (corrected). This calculation was conducted with the randomise function (version 2.1) in FSL (Nichols and Holmes, 2002; Hayasaka and Nichols, 2003), a permutation program that performs statistical modeling using the same GLM application as in FEAT. Analogous

TBSS analysis was also performed on skeletonized RD maps to explore possible contributions from other diffusion variables.

Gray Matter Voxel-based Morphology. Besides correlations with white matter FA, I explored possible contributions from inter-subject differences in gray matter volume. Whole brain voxel-based morphometry analyses were performed with FSL-VBM (version 1.1) (Ashburner and Friston, 2000; Good et al., 2001; Smith et al., 2004). This tool differs from standard VBM approaches in its use of an optimized nonlinear registration algorithm with limited degrees of freedom. This is critical because voxel-wise comparison across subjects requires registration into standard space. Insufficient registration will lead to incomparable data, while excessive registration will remove any inherent inter-subject differences. Besides this tradeoff, FSL-VBM does not require *a priori* information about the location of gray matter differences. However, it is not unaffected by some of the usual limitations in gray matter VBM, such as possible biases from different gyrification patterns.

Brain images, previously extracted with BET, underwent tissue-type segmentation with FMRIB's Automated Segmentation Tool (FAST), version 4.1 (Zhang et al., 2001). Partial image volumes of gray matter were registered to MNI152 standard space ($2x2x2mm^3$ voxels) with FNIRT and averaged across subjects to generate a template specific to the study cohort. The original partial gray matter volumes were then non-linearly aligned to this template and corrected for abnormal local distortions from the registration process, followed by spatial smoothing with an isotropic Gaussian kernel (4.6mm).

The final statistical analysis steps were identical to those applied in TBSS. Using the randomise function (version 2.1) in FSL (Hayasaka and Nichols, 2003), the processed

gray matter volumes were submitted for voxelwise cross-subject statistics with general linear modeling against the pain intensity ratings. To identify the gray matter voxels with significant correlation, a permutation-based nonparametric testing (5000 permutations) was applied with threshold-free cluster enhancement (TFCE) to avoid biases from arbitrary cluster thresholds (Smith and Nichols, 2009) and statistically thresholded at $p<0.05$ (corrected).

6.3 Results

6.3.1 Probability Tractography Between L-DLPFC and Thalamus

The tracts between L-DLPFC and thalamus were traced through probability tractography. The calculated tracts were thresholded at 2% of the average waytotal on a subject level to remove spurious links and preserve only the robust connections. For visualization purposes, the thresholded tractography maps were averaged across the subject cohort (Figure 6.2A). The main white matter structures involved were left corpus callosum and left anterior thalamic radiation.

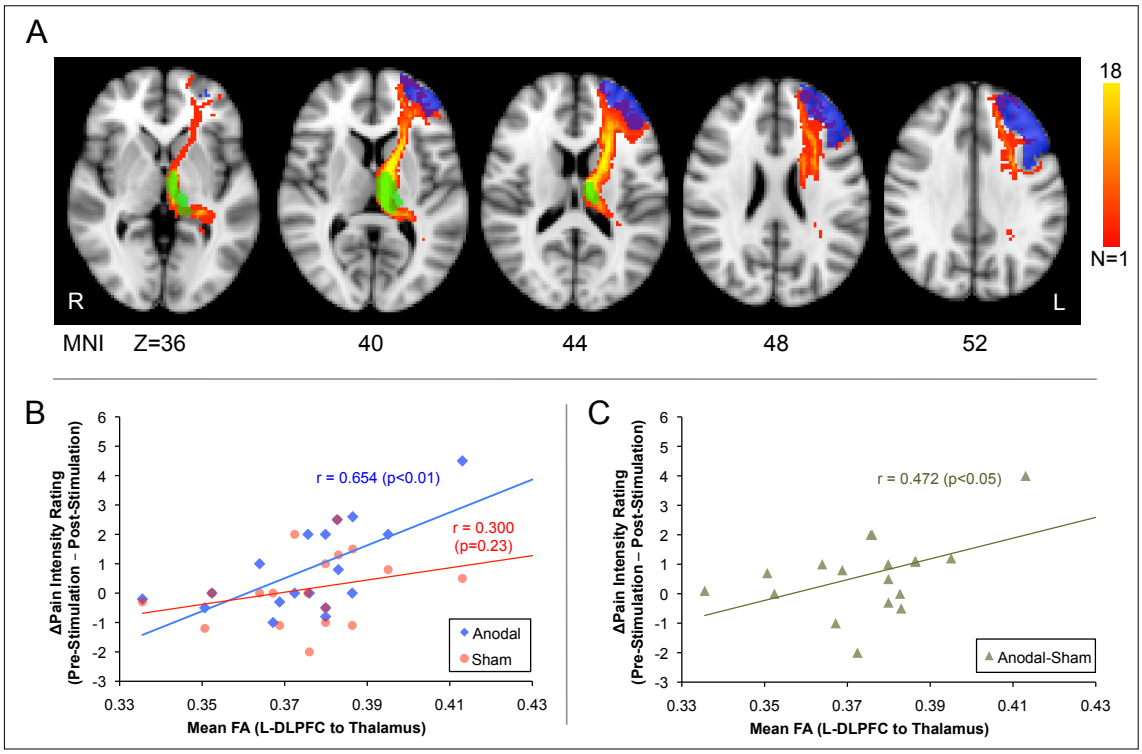


Figure 6.2. **A)** For visualization purposes, axial slices from the mean probability tractography map between L-DLPFC (in blue) and left thalamus (in green) were shown. The map was also used as a binary mask to derive the mean FA of the L-DLPFC–thalamic tract. The prominent white matter structures that were involved in the connection included the corpus callosum and anterior thalamic radiation. **B)** The correlation test between pain intensity rating (Pre-stimulation – Post-stimulation) and mean FA was significant for the anodal tDCS condition but not for the sham tDCS condition. The correlations were not significantly different (p=0.20), which may be attributed to the significant covariance in the ratings of anodal and sham tDCS conditions (r=0.553, p<0.01). **C)** Thus, the rating difference between groups ($Anodal_{pre\text{-}stimulation\ –\ post\text{-}stimulation}$ – $Sham_{pre\text{-}stimulation\ –\ post\text{-}stimulation}$) was correlated against the mean FA, and a significant correlation was found. No statistically significant outliers were observed in the data points with Grubb's test.

The thresholded probability tractography maps were also used to determine the strength of the L-DLPFC–thalamic connection for each subject. The derived paths were then applied as a binary mask to extract the individual FA. Relationships between the FA values and pain intensity changes from Section 5.3 were tested with Pearson correlation tests. The rating difference from pre- to post-stimulation (Pre-stimulation – Post-stimulation) was used as the behavioral covariant. A significant correlation was found with the anodal tDCS condition ($r=0.654$, $p<0.01$) but not with the sham tDCS condition ($r=0.300$, $p=0.23$) (Figure 6.2B). The difference in correlations was not significant ($p=0.20$), which may be due to the significant correlation between the behavioral results of anodal and sham tDCS conditions ($r=0.553$, $p<0.01$). Thus, an additional correlation test of their difference ($Anodal_{\text{pre-stimulation – post-stimulation}} - Sham_{\text{pre-stimulation – post-stimulation}}$) was performed against the mean FA, which produced a significant result ($r=0.472$, $p<0.05$) (Figure 6.2C). The same test did not find any significant correlation with pain unpleasantness measurements.

In addition, the relationship between structural and functional connectivity was explored. The functional correlation between L-DLPFC and thalamus, as measured by the Pearson correlation coefficient of their respective time courses, was covaried against the mean FA. The correlation for the anodal tDCS condition was statistically significant ($r=0.529$, $p=0.02$), but that of the sham tDCS condition was not ($r=-0.083$, $p=0.74$) (Figure 6.3A). A strong trend of difference was found between the two groups ($p=0.065$). The contrast perfusion map between anodal and sham tDCS conditions ($Anodal_{\text{stimulation – pain-only}} - Sham_{\text{stimulation – pain-only}}$; Figure 5.8A) also showed rCBF changes in thalamic voxels that overlapped with the path traced by probability tractography (Figure 6.3B). Across subjects, the average functional connectivity between L-DLPFC and thalamus did not vary from pain-only to simulation periods.

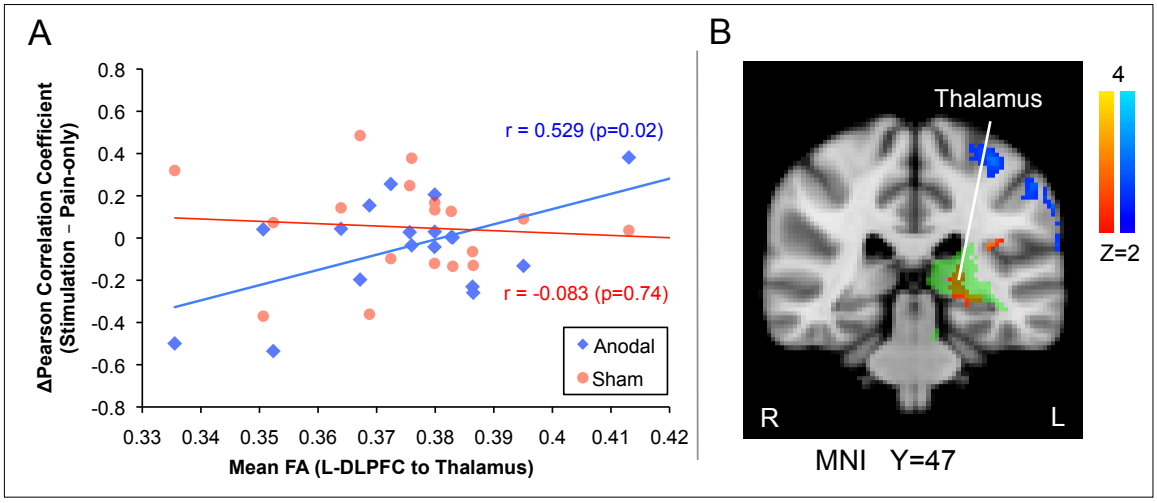


Figure 6.2. **A)** The relationship between structural integrity and functional correlation of L-DLPFC and thalamus during tDCS was investigated. The former was represented by mean FA, while the latter was measured by the Pearson correlation coefficient between the time courses of L-DLFPC and thalamus. The correlation between these two variables was significant for the anodal tDCS condition but not for the sham tDCS. The former showed a strong trend for greater correlation over the latter (p=0.065). No data points were found to be outliers by Grubb's test. **B)** The coronal slice of the perfusion map between anodal and sham tDCS conditions ($Anodal_{stimulation - pain\text{-}only} - Sham_{stimulation - pain\text{-}only}$) from Figure 5.8A was overlaid with the path traced by probability tractography (in green). An overlap could be observed between the thresholded tracts and left thalamic voxels with rCBF changes.

6.3.2 Tract-Based Spatial Statistics

TBSS was performed both to explore possible correlations from other white matter voxels and to substantiate the above probability tractography analysis. Since the key behavioral result was the difference between the pain intensity ratings of anodal and sham tDCS conditions ($Anodal_{pre\text{-}stimulation - post\text{-}stimulation} - Sham_{pre\text{-}stimulation - post\text{-}stimulation}$), these values were submitted for TBSS analysis against the individual FA skeletons. Through nonparametric tests across whole brain, the only voxels that showed significant correlation ($p<0.05$, TFCE-corrected) were located in the left anterior thalamic radiation and left callosal body (Figure 6.3A), which matched the tract traced by probability tractography (Figure 6.3B). No other voxels showed statistical significance. Additional TBSS analysis of RD was performed to investigate contributions by a key component of FA, which showed white matter voxels with a significant inverse correlation against pain

intensity changes (Figure 6.4). TBSS analyses of pain unpleasantness ratings against FA and RD did not yield any significant results.

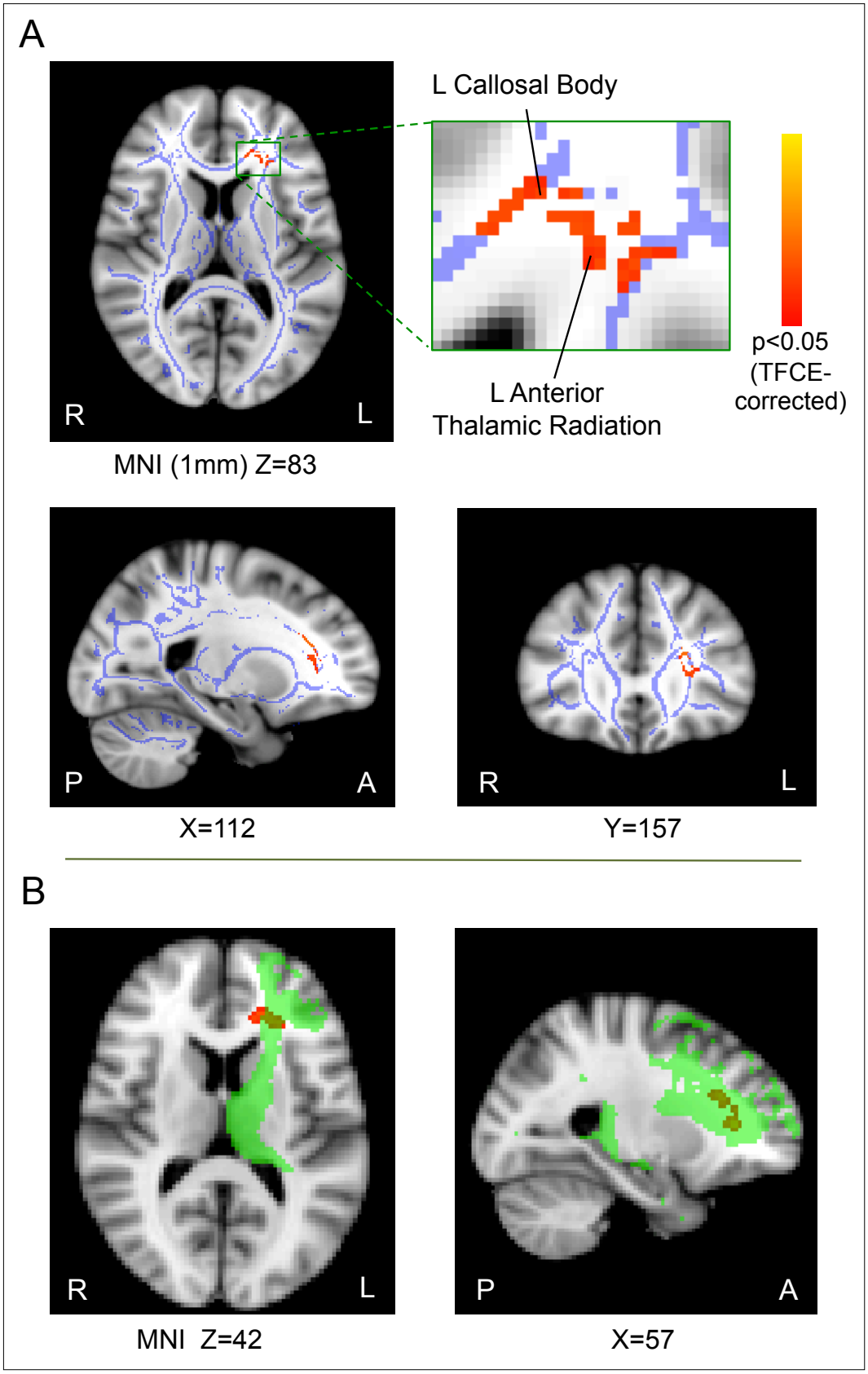


Figure 6.3. **A)** TBSS analysis of whole brain FA skeleton (in blue) against pain intensity rating ($Anodal_{pre\text{-}stimulation\ –\ post\text{-}stimulation} – Sham_{pre\text{-}stimulation\ –\ post\text{-}stimulation}$) ($p<0.05$, TFCE-corrected). Besides significant correlation with voxels in left callosal body and left anterior thalamic radiation, no other voxels showed a significant result. This suggests that the significant correlations were localized to the L-DLPFC–thalamic tract. The results were overlaid on MNI 1x1x1mm^3 space since this was the resolution in which the TBSS analysis was run. **B)** TBSS result (smoothed by a Gaussian kernel of 1.5mm) was overlaid with the tract traced by probability tractography (in green). An overlap could be observed between the two analyses.

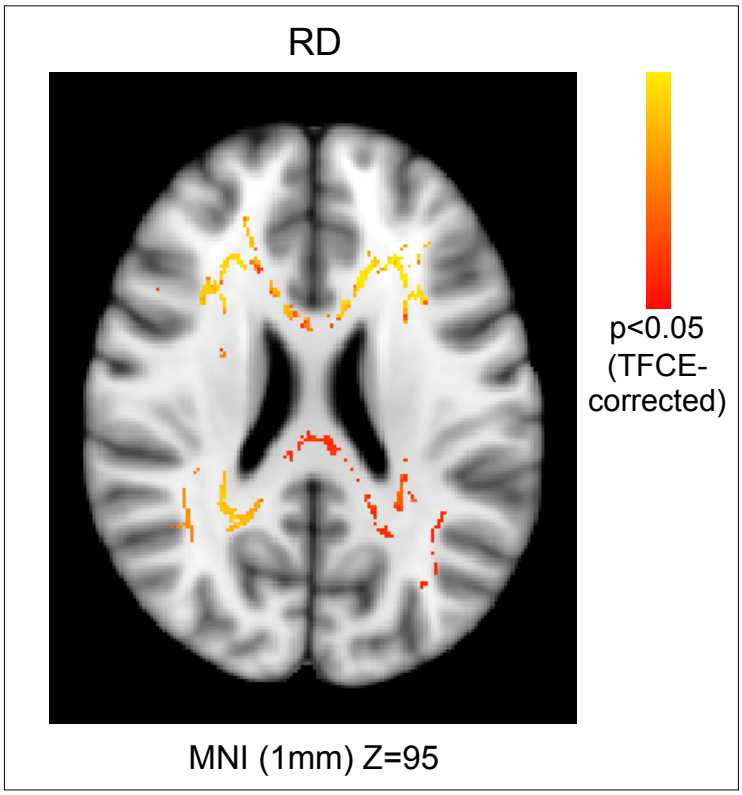


Figure 6.4. TBSS analysis of whole brain RD skeleton found significant inverse relationship against pain intensity rating ($Anodal_{pre\text{-}stimulation\ –\ post\text{-}stimulation} – Sham_{pre\text{-}stimulation\ –\ post\text{-}stimulation}$) ($p<0.05$, TFCE-corrected).

6.3.3 Gray Matter Voxel-Based Morphometry.

To control for possible contributions by gray matter difference, VBM analysis was performed against pain intensity ratings ($Anodal_{pre\text{-}stimulation\ –\ post\text{-}stimulation} – Sham_{pre\text{-}stimulation\ –\ post\text{-}stimulation}$). No significant correlations were found across the whole brain ($p<0.05$, TFCE-corrected).

6.4 Discussion

This chapter presents the first study to integrate DTI into an investigation of pain modulation by brain stimulation. In both probability tractography and TBSS analyses, a significant correlation between pain intensity changes ($Anodal_{pre\text{-}stimulation - post\text{-}stimulation} - Sham_{pre\text{-}stimulation - post\text{-}stimulation}$) and mean FA of L-DLPFC–thalamic tract was found. This relationship was not present with other white matter voxels. Correlation analyses against pain intensity changes with gray matter VBM did not yield significant results.

6.4.1 Probability Tractography and TBSS

Given my *a priori* hypothesis that L-DLPFC tDCS modulates the thalamus to induce pain relief, probability tractography was seeded at the two regions to identify the interconnecting white matter tracts that included anterior thalamic radiation and corpus callosum. Their mean FA, which was extracted by using the tracts as a binary mask, correlated with changes in pain intensity measurements of the anodal tDCS condition ($Anodal_{pre\text{-}stimulation - post\text{-}stimulation}$). However, the changes in pain intensity between anodal and sham tDCS conditions significantly covaried, possibly assisted by the small magnitude of behavioral modulation. To remove statistical confounds, the mean FA was correlated against the difference in their behavioral effects, which again produced significant results.

TBSS analysis, which did not rely on any *a priori* hypothesis, separately verified this conclusion. On the whole brain FA skeleton, the white matter voxels that covaried with the pain intensity measurement ($Anodal_{pre\text{-}stimulation - post\text{-}stimulation} - Sham_{pre\text{-}stimulation - post\text{-}stimulation}$) were only found in the left callosal body and left anterior thalamic radiation. A plot of the mean FA of these voxels against behavioral measures indicated that outliers did not drive the correlation. Also, no other clusters showed significant correlation, which suggested that the relationship was specific to the L-DLPFC–thalamic tract.

6.4.2 L-DLPFC–Thalamic Tract and Pain Modulation

The DTI results suggest that white matter integrity between L-DLPFC and thalamus is an important factor in the anodal tDCS modulation of L-DLPFC to reduce pain intensity. A wealth of pain literature supports the importance of DLPFC, thalamus, and their connection. L-DLPFC has been shown to modulate pain sensation in placebo analgesia studies (Petrovic et al., 2002; Wager et al., 2004; Wager et al., 2007; Watson et al., 2009), possible by changing thalamic coupling to midbrain (Lorenz et al., 2003). Clinical literature with chronic pain patients has also found decreased FA in the left callosal fibers compared to age-matched controls (Geha et al., 2008). For fibromyalgia patients, right thalamus FA has been reported to be lower than that of controls (Sundgren et al., 2007). This is supported by later studies that found lower FA in bilateral thalami and thalamic-cortical tracts for fibromyalgia and migraine patients than for controls (DaSilva et al., 2007; Lutz et al., 2008). Lastly, pain patients from spinal cord injuries have been shown to have a lower mean diffusivity in DLPFC than both matched control subjects and matched, non-pain spinal cord patients (Gustin et al., 2010).

Past VBM studies have also found L-DLPFC and thalamic gray matter density to be lower in chronic pain patients than in matched healthy controls (Apkarian et al., 2004; Gwilym et al., 2010). For this chapter, only healthy, young subjects (average age of 24.8) were recruited, which could minimize the inherent gray matter variability. This may explain the lack of significant correlation in the gray matter VBM analysis. While the study could not confirm nor dispute the role of gray matter, the data suggest that the white matter tract between L-DLPFC and thalamus is also important for pain and its modulation.

6.4.3 Conclusion

In this chapter, the integrity of L-DLPFC–thalamic tracts was found to correlate with pain intensity ratings. Previous literature has underlined the importance of the regions and their structural connection for antinociceptive modulation (Lorenz et al., 2003; Hadjipavlou et al., 2006). Building upon this foundation, the data suggest that this connection may affect the efficacy of L-DLPFC tDCS as a therapeutic tool. As such, it would be interesting to speculate whether FA integrity between these regions could be used to pre-select patients. Alterations in FA with repeated sessions of CBT and tDCS may also be produced to improve the efficacy of these treatments.

CHAPTER 7 – CONCLUSION

This chapter provides a summary of the studies performed in this thesis. Drawing on their conclusions, the chapter will discuss future directions for investigation to offer areas for improvement. Lastly, the final ending will elaborate on the role of tDCS as a viable treatment tool for chronic pain patients.

7.1 Overview of Thesis

This thesis meets at the intersection of pain, fMRI, and brain stimulation to examine the neural basis of tDCS as a possible pain treatment tool. While previous brain stimulation studies have associated pain relief with anodal tDCS of L-DLPFC (Fregni et al., 2006b; Boggio et al., 2008a; Arul-Anandam et al., 2009; Borckardt et al., 2011), the underlying mechanisms have never been directly investigated. The existing pain literature has proposed that L-DLPFC may facilitate alleviation through its connections with the thalamus (Lorenz et al., 2003; Apkarian et al., 2004; Valet et al., 2004; Hadjipavlou et al., 2006; Geha et al., 2008). Thus, the two regions were hypothesized to be the key factors behind the application of L-DLPFC tDCS as a pain treatment tool.

Chapter 3 began the investigation by studying the task-free effects of L-DLPFC tDCS. An initial feasibility test was conducted to check for possible tDCS-related artefacts before the functional experiments were performed with ASL. In the lab, this was the first technical demonstration of concurrent ASL-tDCS as well as the first establishment of an analysis pipeline for ASL data. The perfusion fMRI data suggested that anodal tDCS of L-DLPFC could significantly modulate the activity of L-DLPFC and its connected regions, such as SI and thalamus. It was unlikely that tDCS directly caused perfusion changes in non-frontal regions because the activity of the intervening regions were unaffected, which suggested the involvement of inherent neuronal networks. For cathodal tDCS, rCBF decreases were associated with bilateral thalami and right temporal lobe. Contrast perfusion maps between the polarities demonstrated higher rCBF in L-DLPFC

and SI for the anodal tDCS condition. Seeded at L-DLPFC, further correlation analyses of the anodal tDCS condition found modulations of functional connectivity to the thalamus and midbrain, both of which constitute key regions for nociceptive processing. This pattern was not observed with cathodal tDCS.

To extend the investigation of pain neuromodulation, a robust ongoing pain model that best imitates neuropathic pain was required to examine the effects of tDCS. Healthy subjects were used in lieu of a patient cohort because chronic pain patients are a heterogeneous group with varying conditions. Thus, multiple pain-inducing techniques were tested on healthy volunteers in Chapter 4. Both thermal and electrical stimuli, which were applied in phasic paradigms, did not induce an ongoing pain sensation. Over time, the subjects habituated to the pain stimuli and felt the pain intensity reduced despite receiving same stimulus inputs. An ongoing pain sensation was attained with topical application of capsaicin cream, which activates slow-firing C-fibers rather than the Aδ fibers. Not all subjects were sensitive to the chemical, so additional screening sessions were performed to separate the responders from the remaining subject cohort.

Chapter 5 combined the understanding from Chapters 3 and 4 to investigate rCBF changes during pain modulation by tDCS. Only capsaicin responders were invited to participate in this study, which included both pain and tDCS components. Undergoing both anodal and sham tDCS of L-DLPFC, the subject cohort experienced significantly greater pain relief with the former. The concurrent application of perfusion fMRI helped measure the rCBF changes of the pain neuromodulation and its post-tDCS effects. Compared to the pain-only scans, the perfusion map associated with anodal tDCS showed increased rCBF in L-DLPFC, SI, M1, and visual cortex. For sham tDCS, fewer voxels showed perfusion changes, which included SI and visual cortex. A direct contrast between both polarities showed higher rCBF for posterior insula with sham tDCS and

higher rCBF for thalamus and M1 with anodal tDCS. The changes in posterior insula activity, which could be a good indicator for ongoing pain intensity (Owen et al., 2010), supported the behavioral measurements. Recruitment of M1 by DLPFC to assist with somatosensory pain processing may explain the higher M1 activity in the anodal tDCS condition compared to the sham tDCS condition. Indeed, past tDCS literature has also reported pain reduction with anodal tDCS of L-M1 (Fregni et al., 2006a; Fregni et al., 2006b). The change in thalamic activity appeared to support the hypothesis that pain modulation with L-DLPFC involved thalamic contributions. Thus, the activation of L-DLPFC with anodal tDCS may allow the region to provide pain reduction through the L-DLPFC–thalamic connection.

Discrepancy between results from Chapters 3 and 5 may have two explanations. First, the absence of a sham control in Chapter 3 could preclude an accurate comparison. While sham tDCS does not induce a discernible physiological effect (Nitsche and Paulus, 2000; Nitsche et al., 2003b; Nitsche et al., 2005), no studies have purely examined its associated rCBF changes. Second, the use of tDCS during a task (i.e. pain) may have an interaction factor that cannot be easily accounted for. If an activation pattern were specific to each set of conditions, this may allow for unexpected rCBF differences when comparing between the two chapters.

Chapter 6 used structural imaging tools on the subject cohort from Chapter 5 to investigate the relationship between L-DLPFC–thalamic connections and integrity with behavioral changes in pain intensity. After collection of DTI data, probability tractography was performed to trace the connection paths and to calculate their mean FA values. These values significantly correlated with behavioral measurements, an outcome that was verified with TBSS analysis. The key white matter structures involved consisted of corpus callosum and anterior thalamic radiations. No other voxels in the FA skeleton

were found to correlate in the TBSS analysis. In addition, since higher FA indicates a greater integrity of connection, this likely allows L-DLPFC to better influence thalamic activity. Indeed, Pearson coefficients between the mean time courses of the regions showed a positive trend with the mean FA. This result suggests L-DLPFC tDCS modulates the thalamus to induce pain relief.

Strong structural and functional connections have been known to exist between L-DLPFC and bilateral thalami (Goldman, 1979; Selemon and Goldman-Rakic, 1988; Cummings, 1993; Carretta et al., 1996; Negyessy et al., 1998; Tekin and Cummings, 2002). In addition, their link has been surmised to facilitate antinociceptive modulation. This may be induced by a variety of mechanisms, such as midbrain-thalamic decoupling (Lorenz et al., 2003) and modulation of PAG activity (Hadjipavlou et al., 2006). The contrast perfusion map between anodal and sham tDCS conditions also noted changes in thalamic activity, which overlapped with the tract calculated by probability tractography.

7.2 Future Directions

To follow up the findings from this thesis, several studies could be pursued in further investigations. After weighing the varying degrees of relevance, I will describe the three most pressing areas in the following section.

7.2.1. Clinical Tests

The thesis investigated the underlying mechanism of L-DLPFC tDCS to explain any resulting pain relief. While healthy subjects provided a clean platform for these studies, a demonstration of clinical relevance requires actual clinical applications that will determine whether tDCS can overcome the heterogeneity of chronic pain conditions. Multiple sessions should be used to amplify the modest treatment efficacy, which could then be correlated with structural and/or functional measures of the patients' L-DLPFC–thalamic connections. The clinical results could offer the final verification for the findings from this thesis.

7.2.2. Roles of L-DLPFC and Thalamic Subdivisions

Both L-DLPFC and thalamus are large regions with multiple roles (Behrens et al., 2003b; Wiech et al., 2008a), which may be shared among the anatomical subdivisions. The need for better resolution on the functions of individual partitions is less relevant with tDCS because large electrodes are used. However, recent M1 tDCS modeling studies have suggested that some areas receive more stimulation than others (Sadleir et al., 2010). If the same phenomenon were to be observed with L-DLPFC tDCS, a clearer understanding of L-DLPFC subdivisions would be useful, though little information is available on their pain-related functions.

7.2.3. Mechanism of M1 tDCS in Pain Modulation

Besides L-DLPFC tDCS, previous studies have found pain relief with M1 tDCS as well (Fregni et al., 2006a; Soler et al., 2010). However, the mechanism is not well understood. A common hypothesis is the facilitation of somatosensory pain processing by anodal tDCS (Boggio et al., 2008a), but this has never been directly tested. In addition, the involvement of connected regions, both functional and structurally, may affect the treatment efficacy. Thalamus is a possible candidate because of its link to brainstem, but contributions from other areas, such as posterior insula and SI, cannot be excluded without functional evidence. An experimental design similar to the one outlined in this thesis should be suitable for this investigation.

7.2.4. Current Modeling

The effect of tDCS depends on the path traveled by the electric current. With this in mind, numerous current modeling studies have been published in the tDCS literature (Miranda et al., 2006; Wagner et al., 2007; Datta et al., 2010; Sadleir et al., 2010), though only one explored the current distribution with L-DLPFC tDCS (Wagner et al., 2007). Further studies are needed to investigate how the current affects cortical regions in L-DLPFC tDCS. If these current models could be used in combination with functional imaging data, a relationship may be found to allow for predictions on the individual effect of the stimulation.

7.3 Final Conclusion

Chronic pain is a significant health problem that brings tremendous financial, emotional, and physical costs to its victims. However, only 60% of patients find some success in managing their illness with the current therapeutic options, which include expensive pharmacological treatments (Breivik et al., 2006). Thus, an immense need exists for novel, effective approaches to pain relief.

Harnessing the brain's inherent ability to modulate pain, tDCS can facilitate L-DLPFC activity to serve as an alternative pain treatment tool. To explore the underlying mechanism for its clinical efficacy, this thesis has suggested that the approach works by modulating thalamic activity through the L-DLPFC–thalamic connection. In addition, subjects with a stronger structural link between the two regions appeared to benefit from greater pain reduction. These findings may serve as a foundation for advancing tDCS treatments into clinical pain management settings.

REFERENCES

Almeida OP, Burton EJ, Ferrier N, McKeith IG, O'Brien JT (2003) Depression with late onset is associated with right frontal lobe atrophy. Psychol Med 33:675-681.

Almeida TF, Roizenblatt S, Tufik S (2004) Afferent pain pathways: a neuroanatomical review. Brain Res 1000:40-56.

Andersen E (1986) Periaqueductal gray and cerebral cortex modulate responses of medial thalamic neurons to noxious stimulation. Brain Res 375:30-36.

Antal A, Polania R, Schmidt-Samoa C, Dechent P, Paulus W (2011) Transcranial direct current stimulation over the primary motor cortex during fMRI. NeuroImage 55:590-596.

Antal A, Brepohl N, Poreisz C, Boros K, Csifcsak G, Paulus W (2008) Transcranial direct current stimulation over somatosensory cortex decreases experimentally induced acute pain perception. Clin J Pain 24:56-63.

Apkarian AV, Bushnell MC, Treede RD, Zubieta JK (2005) Human brain mechanisms of pain perception and regulation in health and disease. Eur J Pain 9:463-484.

Apkarian AV, Sosa Y, Sonty S, Levy RM, Harden RN, Parrish TB, Gitelman DR (2004) Chronic back pain is associated with decreased prefrontal and thalamic gray matter density. J Neurosci 24:10410-10415.

Ardolino G, Bossi B, Barbieri S, Priori A (2005) Non-synaptic mechanisms underlie the after-effects of cathodal transcutaneous direct current stimulation of the human brain. J Physiol 568:653-663.

Arul-Anandam AP, Loo C, Martin D, Mitchell PB (2009) Chronic neuropathic pain alleviation after transcranial direct current stimulation to the dorsolateral prefrontal cortex. Brain Stimul 2:149-151.

Ashburner J, Friston KJ (2000) Voxel-based morphometry--the methods. Neuroimage 11:805-821.

Bantick SJ, Wise RG, Ploghaus A, Clare S, Smith SM, Tracey I (2002) Imaging how attention modulates pain in humans using functional MRI. Brain 125:310-319.

Barcelo F, Suwazono S, Knight RT (2000) Prefrontal modulation of visual processing in humans. Nat Neurosci 3:399-403.

Barker AT, Jalinous R, Freeston IL (1985) Non-invasive magnetic stimulation of human motor cortex. Lancet 1:1106-1107.

Basbaum AI, Clanton CH, Fields HL (1976) Opiate and stimulus-produced analgesia: functional anatomy of a medullospinal pathway. Proc Natl Acad Sci U S A 73:4685-4688.

Baudewig J, Nitsche MA, Paulus W, Frahm J (2001) Regional modulation of BOLD MRI responses to human sensorimotor activation by transcranial direct current stimulation. Magn Reson Med 45:196-201.

Baumgartner U, Iannetti GD, Zambreanu L, Stoeter P, Treede RD, Tracey I (2010) Multiple somatotopic representations of heat and mechanical pain in the operculo-insular cortex: a high-resolution fMRI study. J Neurophysiol 104:2863-2872.

Beaulieu C (2002) The basis of anisotropic water diffusion in the nervous system - a technical review. NMR Biomed 15:435-455.

Becerra LR, Breiter HC, Stojanovic M, Fishman S, Edwards A, Comite AR, Gonzalez RG, Borsook D (1999) Human brain activation under controlled thermal stimulation and habituation to noxious heat: an fMRI study. Magn Reson Med 41:1044-1057.

Behrens TE, Berg HJ, Jbabdi S, Rushworth MF, Woolrich MW (2007) Probabilistic diffusion tractography with multiple fibre orientations: What can we gain? Neuroimage 34:144-155.

Behrens TE, Woolrich MW, Jenkinson M, Johansen-Berg H, Nunes RG, Clare S, Matthews PM, Brady JM, Smith SM (2003a) Characterization and propagation of uncertainty in diffusion-weighted MR imaging. Magn Reson Med 50:1077-1088.

Behrens TE, Johansen-Berg H, Woolrich MW, Smith SM, Wheeler-Kingshott CA, Boulby PA, Barker GJ, Sillery EL, Sheehan K, Ciccarelli O, Thompson AJ, Brady JM, Matthews PM (2003b) Non-invasive mapping of connections between human thalamus and cortex using diffusion imaging. Nat Neurosci 6:750-757.

Bell-McGinty S, Butters MA, Meltzer CC, Greer PJ, Reynolds CF, 3rd, Becker JT (2002) Brain morphometric abnormalities in geriatric depression: long-term neurobiological effects of illness duration. Am J Psychiatry 159:1424-1427.

Bingel U, Tracey I (2008) Imaging CNS modulation of pain in humans. Physiology 23:371-380.

Bingel U, Quante M, Knab R, Bromm B, Weiller C, Buchel C (2003) Single trial fMRI reveals significant contralateral bias in responses to laser pain within thalamus and somatosensory cortices. Neuroimage 18:740-748.

Bishop S, Duncan J, Brett M, Lawrence AD (2004) Prefrontal cortical function and anxiety: controlling attention to threat-related stimuli. Nat Neurosci 7:184-188.

Bittar RG, Kar-Purkayastha I, Owen SL, Bear RE, Green A, Wang S, Aziz TZ (2005) Deep brain stimulation for pain relief: a meta-analysis. J Clin Neurosci 12:515-519.

Boggio PS, Zaghi S, Fregni F (2009) Modulation of emotions associated with images of human pain using anodal transcranial direct current stimulation (tDCS). Neuropsychologia 47:212-217.

Boggio PS, Zaghi S, Lopes M, Fregni F (2008a) Modulatory effects of anodal transcranial direct current stimulation on perception and pain thresholds in healthy volunteers. Eur J Neurol 15:1124-1130.

Boggio PS, Rigonatti SP, Ribeiro RB, Myczkowski ML, Nitsche MA, Pascual-Leone A, Fregni F (2008b) A randomized, double-blind clinical trial on the efficacy of cortical direct current stimulation for the treatment of major depression. Int J Neuropsychopharmacol 11:249-254.

Borckardt JJ, Romagnuolo J, Reeves ST, Madan A, Frohman H, Beam W, George MS (2011) Feasibility, safety, and effectiveness of transcranial direct current stimulation for decreasing post-ERCP pain: a randomized, sham-controlled, pilot study. Gastrointest Endosc 73:1158-1164.

Breivik H, Collett B, Ventafridda V, Cohen R, Gallacher D (2006) Survey of chronic pain in Europe: prevalence, impact on daily life, and treatment. Eur J Pain 10:287-333.

Bridge H, Hicks SL, Xie J, Okell TW, Mannan S, Alexander I, Cowey A, Kennard C (2010) Visual activation of extra-striate cortex in the absence of V1 activation. Neuropsychologia 48:4148-4154.

Brighina F, Piazza A, Vitello G, Aloisio A, Palermo A, Daniele O, Fierro B (2004) rTMS of the prefrontal cortex in the treatment of chronic migraine: a pilot study. Journal of the neurological sciences 227:67-71.

Brooks J, Tracey I (2005) From nociception to pain perception: imaging the spinal and supraspinal pathways. J Anat 207:19-33.

Brooks JC, Zambreanu L, Godinez A, Craig AD, Tracey I (2005) Somatotopic organisation of the human insula to painful heat studied with high resolution functional imaging. NeuroImage 27:201-209.

Bushnell MC, Duncan GH, Hofbauer RK, Ha B, Chen JI, Carrier B (1999) Pain perception: is there a role for primary somatosensory cortex? Proc Natl Acad Sci U S A 96:7705-7709.

Campbell JN, Meyer RA (2006) Mechanisms of neuropathic pain. Neuron 52:77-92.

Carretta D, Sbriccoli A, Santarelli M, Pinto F, Granato A, Minciacchi D (1996) Crossed thalamo-cortical and cortico-thalamic projections in adult mice. Neurosci Lett 204:69-72.

Casey KL (1999) Forebrain mechanisms of nociception and pain: analysis through imaging. Proc Natl Acad Sci U S A 96:7668-7674.

Caterina MJ, Rosen TA, Tominaga M, Brake AJ, Julius D (1999) A capsaicin-receptor homologue with a high threshold for noxious heat. Nature 398:436-441.

Caterina MJ, Schumacher MA, Tominaga M, Rosen TA, Levine JD, Julius D (1997) The capsaicin receptor: a heat-activated ion channel in the pain pathway. Nature 389:816-824.

Charlton RA, Barrick TR, McIntyre DJ, Shen Y, O'Sullivan M, Howe FA, Clark CA, Morris RG, Markus HS (2006) White matter damage on diffusion tensor imaging correlates with age-related cognitive decline. Neurology 66:217-222.

Chen AC, Dworkin SF, Haug J, Gehrig J (1989) Human pain responsivity in a tonic pain model: psychological determinants. Pain 37:143-160.

Chi RP, Fregni F, Snyder AW (2010) Visual memory improved by non-invasive brain stimulation. Brain Res 1353:168-175.

Chuang KH, van Gelderen P, Merkle H, Bodurka J, Ikonomidou VN, Koretsky AP, Duyn JH, Talagala SL (2008) Mapping resting-state functional connectivity using perfusion MRI. NeuroImage 40:1595-1605.

Coghill RC, Talbot JD, Evans AC, Meyer E, Gjedde A, Bushnell MC, Duncan GH (1994) Distributed processing of pain and vibration by the human brain. J Neurosci 14:4095-4108.

Condes-Lara M, Calvo JM, Fernandez-Guardiola A (1981) Habituation to bearable experimental pain elicited by tooth pulp electrical stimulation. Pain 11:185-200.

Condes-Lara M, Omana Zapata I, Leon-Olea M, Sanchez-Alvarez M (1989) Dorsal raphe and nociceptive stimulations evoke convergent responses on the thalamic centralis lateralis and medial prefrontal cortex neurons. Brain Res 499:145-152.

Conte A, Barbanti P, Frasca V, Iacovelli E, Gabriele M, Giacomelli E, Aurilia C, Pichiorri F, Gilio F, Inghilleri M (2009) Differences in short-term primary motor cortex synaptic potentiation as assessed by repetitive transcranial magnetic stimulation in migraine patients with and without aura. Pain.

Costigan M, Scholz J, Woolf CJ (2009) Neuropathic pain: a maladaptive response of the nervous system to damage. Annu Rev Neurosci 32:1-32.

Craggs JG, Price DD, Verne GN, Perlstein WM, Robinson MM (2007) Functional brain interactions that serve cognitive-affective processing during pain and placebo analgesia. Neuroimage 38:720-729.

Craig AD, Reiman EM, Evans A, Bushnell MC (1996) Functional imaging of an illusion of pain. Nature 384:258-260.

Creutzfeldt OD, Fromm GH, Kapp H (1962) Influence of transcortical d-c currents on cortical neuronal activity. Exp Neurol 5:436-452.

Crown ED, Gwak YS, Ye Z, Johnson KM, Hulsebosch CE (2008) Activation of p38 MAP kinase is involved in central neuropathic pain following spinal cord injury. Exp Neurol 213:257-267.

Croxson PL, Johansen-Berg H, Behrens TE, Robson MD, Pinsk MA, Gross CG, Richter W, Richter MC, Kastner S, Rushworth MF (2005) Quantitative investigation of connections of the prefrontal cortex in the human and macaque using probabilistic diffusion tractography. J Neurosci 25:8854-8866.

Cummings JL (1993) Frontal-subcortical circuits and human behavior. Arch Neurol 50:873-880.

DaSilva AF, Granziera C, Tuch DS, Snyder J, Vincent M, Hadjikhani N (2007) Interictal alterations of the trigeminal somatosensory pathway and periaqueductal gray matter in migraine. Neuroreport 18:301-305.

Datta A, Bikson M, Fregni F (2010) Transcranial direct current stimulation in patients with skull defects and skull plates: high-resolution computational FEM study of factors altering cortical current flow. Neuroimage 52:1268-1278.

Davis KD, Taylor SJ, Crawley AP, Wood ML, Mikulis DJ (1997) Functional MRI of pain- and attention-related activations in the human cingulate cortex. J Neurophysiol 77:3370-3380.

Dechent P, Polania R, Schmidt-Samoa C, Paulus W, Antal A (2010) Concurrent transcranial direct current stimulation (tDCS) and functional MRI reveals modulatory effects on brain activation during a simple motor task. In: 16th Annual Meeting of the Organization for Human Brain Mapping. Barcelona, Spain.

Derbyshire SW, Jones AK (1998) Cerebral responses to a continual tonic pain stimulus measured using positron emission tomography. Pain 76:127-135.

Derbyshire SW, Jones AK, Devani P, Friston KJ, Feinmann C, Harris M, Pearce S, Watson JD, Frackowiak RS (1994) Cerebral responses to pain in patients with atypical facial pain measured by positron emission tomography. J Neurol Neurosurg Psychiatry 57:1166-1172.

Detre JA, Zhang W, Roberts DA, Silva AC, Williams DS, Grandis DJ, Koretsky AP, Leigh JS (1994) Tissue specific perfusion imaging using arterial spin labeling. NMR Biomed 7:75-82.

Devinsky O, Morrell MJ, Vogt BA (1995) Contributions of anterior cingulate cortex to behaviour. Brain 118 (Pt 1):279-306.

Eccleston C, Williams AC, Morley S (2009) Psychological therapies for the management of chronic pain (excluding headache) in adults. Cochrane Database Syst Rev:CD007407.

Edelman RR, Siewert B, Darby DG, Thangaraj V, Nobre AC, Mesulam MM, Warach S (1994) Qualitative mapping of cerebral blood flow and functional localization with echo-planar MR imaging and signal targeting with alternating radio frequency. Radiology 192:513-520.

Edelmuth RC, Nitsche MA, Battistella L, Fregni F (2010) Why do some promising brain-stimulation devices fail the next steps of clinical development? Expert Rev Med Devices 7:67-97.

Eippert F, Bingel U, Schoell ED, Yacubian J, Klinger R, Lorenz J, Buchel C (2009) Activation of the opioidergic descending pain control system underlies placebo analgesia. Neuron 63:533-543.

Eisenberg E, McNicol ED, Carr DB (2005) Efficacy and safety of opioid agonists in the treatment of neuropathic pain of nonmalignant origin: systematic review and meta-analysis of randomized controlled trials. JAMA 293:3043-3052.

Elmer S, Burkard M, Renz B, Meyer M, Jancke L (2009) Direct current induced short-term modulation of the left dorsolateral prefrontal cortex while learning auditory presented nouns. Behav Brain Funct 5:29.

Fenton BW, Palmieri PA, Boggio P, Fanning J, Fregni F (2009) A preliminary study of transcranial direct current stimulation for the treatment of refractory chronic pelvic pain. Brain Stimul 2:103-107.

Finnerup NB, Otto M, McQuay HJ, Jensen TS, Sindrup SH (2005) Algorithm for neuropathic pain treatment: an evidence based proposal. Pain 118:289-305.

Fregni F, Freedman S, Pascual-Leone A (2007) Recent advances in the treatment of chronic pain with non-invasive brain stimulation techniques. Lancet neurology 6:188-191.

Fregni F, Liguori P, Fecteau S, Nitsche MA, Pascual-Leone A, Boggio PS (2008) Cortical stimulation of the prefrontal cortex with transcranial direct current

stimulation reduces cue-provoked smoking craving: a randomized, sham-controlled study. The Journal of clinical psychiatry 69:32-40.

Fregni F, DaSilva D, Potvin K, Ramos-Estebanez C, Cohen D, Pascual-Leone A, Freedman SD (2005a) Treatment of chronic visceral pain with brain stimulation. Annals of neurology 58:971-972.

Fregni F, Boggio PS, Nitsche M, Bermpohl F, Antal A, Feredoes E, Marcolin MA, Rigonatti SP, Silva MT, Paulus W, Pascual-Leone A (2005b) Anodal transcranial direct current stimulation of prefrontal cortex enhances working memory. Experimental brain research Experimentelle Hirnforschung 166:23-30.

Fregni F, Boggio PS, Lima MC, Ferreira MJ, Wagner T, Rigonatti SP, Castro AW, Souza DR, Riberto M, Freedman SD, Nitsche MA, Pascual-Leone A (2006a) A sham-controlled, phase II trial of transcranial direct current stimulation for the treatment of central pain in traumatic spinal cord injury. Pain 122:197-209.

Fregni F, Gimenes R, Valle AC, Ferreira MJ, Rocha RR, Natalle L, Bravo R, Rigonatti SP, Freedman SD, Nitsche MA, Pascual-Leone A, Boggio PS (2006b) A randomized, sham-controlled, proof of principle study of transcranial direct current stimulation for the treatment of pain in fibromyalgia. Arthritis and rheumatism 54:3988-3998.

Gagnon B, Almahrezi A, Schreier G (2003) Methadone in the treatment of neuropathic pain. Pain Res Manag 8:149-154.

Gandiga PC, Hummel FC, Cohen LG (2006) Transcranial DC stimulation (tDCS): a tool for double-blind sham-controlled clinical studies in brain stimulation. Clin Neurophysiol 117:845-850.

Garcia-Larrea L, Peyron R, Mertens P, Gregoire MC, Lavenne F, Le Bars D, Convers P, Mauguiere F, Sindou M, Laurent B (1999) Electrical stimulation of motor cortex for pain control: a combined PET-scan and electrophysiological study. Pain 83:259-273.

Geber C, Fondel R, Kramer HH, Rolke R, Treede RD, Sommer C, Birklein F (2007) Psychophysics, flare, and neurosecretory function in human pain models: capsaicin versus electrically evoked pain. J Pain 8:503-514.

Geha PY, Baliki MN, Harden RN, Bauer WR, Parrish TB, Apkarian AV (2008) The brain in chronic CRPS pain: abnormal gray-white matter interactions in emotional and autonomic regions. Neuron 60:570-581.

Golay X, Hendrikse J, Lim TC (2004) Perfusion imaging using arterial spin labeling. Top Magn Reson Imaging 15:10-27.

Golay X, Stuber M, Pruessmann KP, Meier D, Boesiger P (1999) Transfer insensitive labeling technique (TILT): application to multislice functional perfusion imaging. J Magn Reson Imaging 9:454-461.

Goldman PS (1979) Contralateral projections to the dorsal thalamus from frontal association cortex in the rhesus monkey. Brain Res 166:166-171.

Goldstein DJ, Lu Y, Detke MJ, Lee TC, Iyengar S (2005) Duloxetine vs. placebo in patients with painful diabetic neuropathy. Pain 116:109-118.

Good CD, Johnsrude IS, Ashburner J, Henson RN, Friston KJ, Frackowiak RS (2001) A voxel-based morphometric study of ageing in 465 normal adult human brains. Neuroimage 14:21-36.

Granot M, Granovsky Y, Sprecher E, Nir RR, Yarnitsky D (2006) Contact heat-evoked temporal summation: tonic versus repetitive-phasic stimulation. Pain 122:295-305.

Graven-Nielsen T, Arendt-Nielsen L, Svensson P, Jensen TS (1997) Quantification of local and referred muscle pain in humans after sequential i.m. injections of hypertonic saline. Pain 69:111-117.

Griffin R, Woolf C (2007) Pharmacology of analgesia. In: Principles of Pharmacology: The Pathophysiological Basis of Drug Therapy, 2nd Edition (Golan D, Tashjian A, Armstrong E, Armstrong A, eds), pp 263-282. Baltimore, MD: Lippincott, Williams, and Wilkins.

Gustin SM, Wrigley PJ, Siddall PJ, Henderson LA (2010) Brain anatomy changes associated with persistent neuropathic pain following spinal cord injury. Cereb Cortex 20:1409-1419.

Gwilym SE, Filippini N, Douaud G, Carr AJ, Tracey I (2010) Thalamic atrophy associated with painful osteoarthritis of the hip is reversible after arthroplasty: a longitudinal voxel-based morphometric study. Arthritis and rheumatism 62:2930-2940.

Hadjipavlou G, Dunckley P, Behrens TE, Tracey I (2006) Determining anatomical connectivities between cortical and brainstem pain processing regions in humans: a diffusion tensor imaging study in healthy controls. Pain 123:169-178.

Hallett M (2000) Transcranial magnetic stimulation and the human brain. Nature 406:147-150.

Hallett M (2007) Transcranial magnetic stimulation: a primer. Neuron 55:187-199.

Hardy SG, Haigler HJ (1985) Prefrontal influences upon the midbrain: a possible route for pain modulation. Brain Res 339:285-293.

Hay JL, White JM, Bochner F, Somogyi AA, Semple TJ, Rounsefell B (2009) Hyperalgesia in opioid-managed chronic pain and opioid-dependent patients. J Pain 10:316-322.

Hayasaka S, Nichols TE (2003) Validating cluster size inference: random field and permutation methods. Neuroimage 20:2343-2356.

Heise V, Filippini N, Ebmeier KP, Mackay CE (2011) The APOE varepsilon4 allele modulates brain white matter integrity in healthy adults. Mol Psychiatry 16:908-916.

Henderson LA, Rubin TK, Macefield VG (2011) Within-limb somatotopic representation of acute muscle pain in the human contralateral dorsal posterior insula. Hum Brain Mapp 32:1592-1601.

Hosobuchi Y (1993) Motor cortical stimulation for control of central deafferentation pain. Adv Neurol 63:215-217.

Howard MA, Krause K, Khawaja N, Massat N, Zelaya F, Schumann G, Huggins JP, Vennart W, Williams SC, Renton TF (2011) Beyond patient reported pain: perfusion magnetic resonance imaging demonstrates reproducible cerebral representation of ongoing post-surgical pain. PLoS One 6:e17096.

Hsieh JC, Stahle-Backdahl M, Hagermark O, Stone-Elander S, Rosenquist G, Ingvar M (1996) Traumatic nociceptive pain activates the hypothalamus and the periaqueductal gray: a positron emission tomography study. Pain 64:303-314.

Hummel F, Celnik P, Giraux P, Floel A, Wu WH, Gerloff C, Cohen LG (2005) Effects of non-invasive cortical stimulation on skilled motor function in chronic stroke. Brain 128:490-499.

Iannetti GD, Hughes NP, Lee MC, Mouraux A (2008) Determinants of laser-evoked EEG responses: pain perception or stimulus saliency? J Neurophysiol 100:815-828.

Jellison BJ, Field AS, Medow J, Lazar M, Salamat MS, Alexander AL (2004) Diffusion tensor imaging of cerebral white matter: a pictorial review of physics, fiber tract anatomy, and tumor imaging patterns. AJNR Am J Neuroradiol 25:356-369.

Jenkinson M, Bannister P, Brady M, Smith S (2002) Improved optimization for the robust and accurate linear registration and motion correction of brain images. Neuroimage 17:825-841.

Ji RR, Kohno T, Moore KA, Woolf CJ (2003) Central sensitization and LTP: do pain and memory share similar mechanisms? Trends Neurosci 26:696-705.

Johansen-Berg H, Della-Maggiore V, Behrens TE, Smith SM, Paus T (2007) Integrity of white matter in the corpus callosum correlates with bimanual co-ordination skills. Neuroimage 36 Suppl 2:T16-21.

Jones VM, Moore KA, Peterson DM (2011) Capsaicin 8% topical patch (Qutenza)--a review of the evidence. J Pain Palliat Care Pharmacother 25:32-41.

Karrer T, Bartoshuk L (1991) Capsaicin desensitization and recovery on the human tongue. Physiol Behav 49:757-764.

Keefe FJ, Caldwell DS (1997) Cognitive behavioral control of arthritis pain. Med Clin North Am 81:277-290.

Keeser D, Padberg F, Reisinger E, Pogarell O, Kirsch V, Palm U, Karch S, Moller HJ, Nitsche MA, Mulert C (2011) Prefrontal direct current stimulation modulates resting EEG and event-related potentials in healthy subjects: a standardized low resolution tomography (sLORETA) study. NeuroImage 55:644-657.

Kelly DJ, Ahmad M, Brull SJ (2001) Preemptive analgesia I: physiological pathways and pharmacological modalities. Can J Anaesth 48:1000-1010.

Kety SS, Schmidt CF (1948) The nitrous oxide method for the quantitative determination of cerebral blood flow in man: theory, procedure and normal values. J Clin Invest 27:476-483.

Khedr EM, Ahmed MA, Fathy N, Rothwell JC (2005a) Therapeutic trial of repetitive transcranial magnetic stimulation after acute ischemic stroke. Neurology 65:466-468.

Khedr EM, Kotb H, Kamel NF, Ahmed MA, Sadek R, Rothwell JC (2005b) Longlasting antalgic effects of daily sessions of repetitive transcranial magnetic stimulation in central and peripheral neuropathic pain. Journal of neurology, neurosurgery, and psychiatry 76:833-838.

Kingery WS (1997) A critical review of controlled clinical trials for peripheral neuropathic pain and complex regional pain syndromes. Pain 73:123-139.

Klein T, Magerl W, Treede RD (2006) Perceptual correlate of nociceptive long-term potentiation (LTP) in humans shares the time course of early-LTP. Journal of neurophysiology 96:3551-3555.

Klein T, Magerl W, Hopf HC, Sandkuhler J, Treede RD (2004) Perceptual correlates of nociceptive long-term potentiation and long-term depression in humans. J Neurosci 24:964-971.

Knoch D, Treyer V, Regard M, Muri RM, Buck A, Weber B (2006) Lateralized and frequency-dependent effects of prefrontal rTMS on regional cerebral blood flow. Neuroimage 31:641-648.

Koltzenburg M, Lundberg LE, Torebjork HE (1992) Dynamic and static components of mechanical hyperalgesia in human hairy skin. Pain 51:207-219.

Koltzenburg M, Torebjork HE, Wahren LK (1994) Nociceptor modulated central sensitization causes mechanical hyperalgesia in acute chemogenic and chronic neuropathic pain. Brain 117 (Pt 3):579-591.

Koyama T, McHaffie JG, Laurienti PJ, Coghill RC (2005) The subjective experience of pain: where expectations become reality. Proc Natl Acad Sci U S A 102:12950-12955.

Krienen FM, Buckner RL (2009) Segregated fronto-cerebellar circuits revealed by intrinsic functional connectivity. Cereb Cortex 19:2485-2497.

Kujirai T, Caramia MD, Rothwell JC, Day BL, Thompson PD, Ferbert A, Wroe S, Asselman P, Marsden CD (1993) Corticocortical inhibition in human motor cortex. J Physiol 471:501-519.

Kupfermann I (1965) Effects of cortical polarization on visual discriminations. Experimental Neurology 12:179–189.

Kwan CL, Crawley AP, Mikulis DJ, Davis KD (2000) An fMRI study of the anterior cingulate cortex and surrounding medial wall activations evoked by noxious cutaneous heat and cold stimuli. Pain 85:359-374.

Kwon YH, Ko MH, Ahn SH, Kim YH, Song JC, Lee CH, Chang MC, Jang SH (2008) Primary motor cortex activation by transcranial direct current stimulation in the human brain. Neurosci Lett 435:56-59.

Kwong KK, Chesler DA, Weisskoff RM, Donahue KM, Davis TL, Ostergaard L, Campbell TA, Rosen BR (1995) MR perfusion studies with T1-weighted echo planar imaging. Magn Reson Med 34:878-887.

Lang N, Siebner HR, Ward NS, Lee L, Nitsche MA, Paulus W, Rothwell JC, Lemon RN, Frackowiak RS (2005) How does transcranial DC stimulation of the primary motor cortex alter regional neuronal activity in the human brain? The European journal of neuroscience 22:495-504.

Le Bihan D, Mangin JF, Poupon C, Clark CA, Pappata S, Molko N, Chabriat H (2001) Diffusion tensor imaging: concepts and applications. J Magn Reson Imaging 13:534-546.

Lee MC, Zambreanu L, Menon DK, Tracey I (2008) Identifying brain activity specifically related to the maintenance and perceptual consequence of central sensitization in humans. J Neurosci 28:11642-11649.

Lefaucheur JP, Drouot X, Nguyen JP (2001a) Interventional neurophysiology for pain control: duration of pain relief following repetitive transcranial magnetic stimulation of the motor cortex. Neurophysiologie clinique = Clinical neurophysiology 31:247-252.

Lefaucheur JP, Drouot X, Keravel Y, Nguyen JP (2001b) Pain relief induced by repetitive transcranial magnetic stimulation of precentral cortex. Neuroreport 12:2963-2965.

Legrain V, Iannetti GD, Plaghki L, Mouraux A (2011) The pain matrix reloaded: a salience detection system for the body. Prog Neurobiol 93:111-124.

Lenz FA, Gracely RH, Rowland LH, Dougherty PM (1994) A population of cells in the human thalamic principal sensory nucleus respond to painful mechanical stimuli. Neurosci Lett 180:46-50.

Leung A, Donohue M, Xu R, Lee R, Lefaucheur JP, Khedr EM, Saitoh Y, Andre-Obadia N, Rollnik J, Wallace M, Chen R (2009) rTMS for suppressing neuropathic pain: a meta-analysis. J Pain 10:1205-1216.

Loeser JD, Treede RD (2008) The Kyoto protocol of IASP Basic Pain Terminology. Pain 137:473-477.

Loo CK, Sachdev PS, Haindl W, Wen W, Mitchell PB, Croker VM, Malhi GS (2003) High (15 Hz) and low (1 Hz) frequency transcranial magnetic stimulation have different acute effects on regional cerebral blood flow in depressed patients. Psychol Med 33:997-1006.

Lorenz J, Minoshima S, Casey KL (2003) Keeping pain out of mind: the role of the dorsolateral prefrontal cortex in pain modulation. Brain 126:1079-1091.

Lu H, Zuo Y, Gu H, Waltz JA, Zhan W, Scholl CA, Rea W, Yang Y, Stein EA (2007) Synchronized delta oscillations correlate with the resting-state functional MRI signal. Proc Natl Acad Sci U S A 104:18265-18269.

Lu MT, Preston JB, Strick PL (1994) Interconnections between the prefrontal cortex and the premotor areas in the frontal lobe. J Comp Neurol 341:375-392.

Lutz J, Jager L, de Quervain D, Krauseneck T, Padberg F, Wichnalek M, Beyer A, Stahl R, Zirngibl B, Morhard D, Reiser M, Schelling G (2008) White and gray matter abnormalities in the brain of patients with fibromyalgia: a diffusion-tensor and volumetric imaging study. Arthritis Rheum 58:3960-3969.

Lynn B (1990) Capsaicin: actions on nociceptive C-fibres and therapeutic potential. Pain 41:61-69.

MacDonald AW, 3rd, Cohen JD, Stenger VA, Carter CS (2000) Dissociating the role of the dorsolateral prefrontal and anterior cingulate cortex in cognitive control. Science 288:1835-1838.

Magerl W, Fuchs PN, Meyer RA, Treede RD (2001) Roles of capsaicin-insensitive nociceptors in cutaneous pain and secondary hyperalgesia. Brain 124:1754-1764.

Mai VM, Bankier AA, Prasad PV, Li W, Storey P, Edelman RR, Chen Q (2001) MR ventilation-perfusion imaging of human lung using oxygen-enhanced and arterial spin labeling techniques. J Magn Reson Imaging 14:574-579.

Matharu MS, Good CD, May A, Bahra A, Goadsby PJ (2003) No change in the structure of the brain in migraine: a voxel-based morphometric study. Eur J Neurol 10:53-57.

McQuay HJ, Tramer M, Nye BA, Carroll D, Wiffen PJ, Moore RA (1996) A systematic review of antidepressants in neuropathic pain. Pain 68:217-227.

Mease PJ (2009) Further strategies for treating fibromyalgia: the role of serotonin and norepinephrine reuptake inhibitors. Am J Med 122:S44-55.

Merskey H, Bogduk N (1994) Classification of Chronic Pain: Descriptions of Chronic Pain Syndromes and Definitions of Pain Terms, 2 Edition: International Association for the Study of Pain.

Merzagora AC, Foffani G, Panyavin I, Mordillo-Mateos L, Aguilar J, Onaral B, Oliviero A (2010) Prefrontal hemodynamic changes produced by anodal direct current stimulation. NeuroImage 49:2304-2310.

Meyerson BA, Lindblom U, Linderoth B, Lind G, Herregodts P (1993) Motor cortex stimulation as treatment of trigeminal neuropathic pain. Acta Neurochir Suppl (Wien) 58:150-153.

Millan MJ (1999) The induction of pain: an integrative review. Prog Neurobiol 57:1-164.

Milne RJ, Kay NE, Irwin RJ (1991) Habituation to repeated painful and non-painful cutaneous stimuli: a quantitative psychophysical study. Experimental brain research Experimentelle Hirnforschung 87:438-444.

Miranda PC, Lomarev M, Hallett M (2006) Modeling the current distribution during transcranial direct current stimulation. Clin Neurophysiol 117:1623-1629.

Mori S, van Zijl PC (2002) Fiber tracking: principles and strategies - a technical review. NMR Biomed 15:468-480.

Morley JS, Bridson J, Nash TP, Miles JB, White S, Makin MK (2003) Low-dose methadone has an analgesic effect in neuropathic pain: a double-blind randomized controlled crossover trial. Palliat Med 17:576-587.

Morley S, Eccleston C, Williams A (1999) Systematic review and meta-analysis of randomized controlled trials of cognitive behaviour therapy and behaviour therapy for chronic pain in adults, excluding headache. Pain 80:1-13.

Moulin DE et al. (2007) Pharmacological management of chronic neuropathic pain - consensus statement and guidelines from the Canadian Pain Society. Pain Res Manag 12:13-21.

Nakamura H, Kitagawa H, Kawaguchi Y, Tsuji H (1997) Intracortical facilitation and inhibition after transcranial magnetic stimulation in conscious humans. J Physiol 498 (Pt 3):817-823.

Negyessy L, Hamori J, Bentivoglio M (1998) Contralateral cortical projection to the mediodorsal thalamic nucleus: origin and synaptic organization in the rat. Neuroscience 84:741-753.

Neugebauer V, Li W, Bird GC, Han JS (2004) The amygdala and persistent pain. Neuroscientist 10:221-234.

Nichols TE, Holmes AP (2002) Nonparametric permutation tests for functional neuroimaging: a primer with examples. Hum Brain Mapp 15:1-25.

Nicholson B (2006) Differential diagnosis: nociceptive and neuropathic pain. Am J Manag Care 12:S256-262.

Nitsche MA, Paulus W (2000) Excitability changes induced in the human motor cortex by weak transcranial direct current stimulation. The Journal of physiology 527 Pt 3:633-639.

Nitsche MA, Nitsche MS, Klein CC, Tergau F, Rothwell JC, Paulus W (2003a) Level of action of cathodal DC polarisation induced inhibition of the human motor cortex. Clin Neurophysiol 114:600-604.

Nitsche MA, Jaussi W, Liebetanz D, Lang N, Tergau F, Paulus W (2004a) Consolidation of human motor cortical neuroplasticity by D-cycloserine. Neuropsychopharmacology 29:1573-1578.

Nitsche MA, Schauenburg A, Lang N, Liebetanz D, Exner C, Paulus W, Tergau F (2003b) Facilitation of implicit motor learning by weak transcranial direct current stimulation of the primary motor cortex in the human. J Cogn Neurosci 15:619-626.

Nitsche MA, Niehaus L, Hoffmann KT, Hengst S, Liebetanz D, Paulus W, Meyer BU (2004b) MRI study of human brain exposed to weak direct current stimulation of the frontal cortex. Clin Neurophysiol 115:2419-2423.

Nitsche MA, Fricke K, Henschke U, Schlitterlau A, Liebetanz D, Lang N, Henning S, Tergau F, Paulus W (2003c) Pharmacological modulation of cortical excitability shifts induced by transcranial direct current stimulation in humans. J Physiol 553:293-301.

Nitsche MA, Liebetanz D, Schlitterlau A, Henschke U, Fricke K, Frommann K, Lang N, Henning S, Paulus W, Tergau F (2004c) GABAergic modulation of DC stimulation-induced motor cortex excitability shifts in humans. Eur J Neurosci 19:2720-2726.

Nitsche MA, Cohen LG, Wassermann EM, Priori A, Lang N, Antal A, Paulus W, Hummel F, Boggio PS, Fregni F, Pascual-Leone A (2008) Transcranial direct current stimulation: State of the art 2008. Brain Stimulation 1:206-223.

Nitsche MA, Seeber A, Frommann K, Klein CC, Rochford C, Nitsche MS, Fricke K, Liebetanz D, Lang N, Antal A, Paulus W, Tergau F (2005) Modulating parameters of excitability during and after transcranial direct current stimulation of the human motor cortex. The Journal of physiology 568:291-303.

O'Connell NE, Wand BM, Marston L, Spencer S, Desouza LH (2010) Non-invasive brain stimulation techniques for chronic pain. Cochrane Database Syst Rev 9:CD008208.

Okell TW, Chappell MA, Woolrich MW, Gunther M, Feinberg DA, Jezzard P (2010) Vessel-encoded dynamic magnetic resonance angiography using arterial spin labeling. Magn Reson Med 64:698-706.

Owen AM, Evans AC, Petrides M (1996) Evidence for a two-stage model of spatial working memory processing within the lateral frontal cortex: a positron emission tomography study. Cereb Cortex 6:31-38.

Owen DG, Bureau Y, Thomas AW, Prato FS, St Lawrence KS (2008) Quantification of pain-induced changes in cerebral blood flow by perfusion MRI. Pain 136:85-96.

Owen DG, Clarke CF, Ganapathy S, Prato FS, St Lawrence KS (2010) Using perfusion MRI to measure the dynamic changes in neural activation associated with tonic muscular pain. Pain 148:375-386.

Ozen S, Sirota A, Belluscio MA, Anastassiou CA, Stark E, Koch C, Buzsaki G (2010) Transcranial electric stimulation entrains cortical neuronal populations in rats. J Neurosci 30:11476-11485.

Paice JA (2003) Mechanisms and management of neuropathic pain in cancer. J Support Oncol 1:107-120.

Parazzini M, Fiocchi S, Rossi E, Paglialonga A, Ravazzani P (2011) Transcranial direct current stimulation: estimation of the electric field and of the current density in an anatomical human head model. IEEE Trans Biomed Eng 58:1773-1780.

Pascual-Leone A, Rubio B, Pallardo F, Catala MD (1996) Rapid-rate transcranial magnetic stimulation of left dorsolateral prefrontal cortex in drug-resistant depression. Lancet 348:233-237.

Passard A, Attal N, Benadhira R, Brasseur L, Saba G, Sichere P, Perrot S, Januel D, Bouhassira D (2007) Effects of unilateral repetitive transcranial magnetic

stimulation of the motor cortex on chronic widespread pain in fibromyalgia. Brain 130:2661-2670.

Paulus W (2004) Outlasting excitability shifts induced by direct current stimulation of the human brain. Suppl Clin Neurophysiol 57:708-714.

Petersen ET, Zimine I, Ho YC, Golay X (2006) Non-invasive measurement of perfusion: a critical review of arterial spin labelling techniques. Br J Radiol 79:688-701.

Petrides M, Pandya DN (1999) Dorsolateral prefrontal cortex: comparative cytoarchitectonic analysis in the human and the macaque brain and corticocortical connection patterns. The European journal of neuroscience 11:1011-1036.

Petrovic P, Kalso E, Petersson KM, Ingvar M (2002) Placebo and opioid analgesia--imaging a shared neuronal network. Science (New York, NY 295:1737-1740.

Peyron R, Garcia-Larrea L, Gregoire MC, Costes N, Convers P, Lavenne F, Mauguiere F, Michel D, Laurent B (1999) Haemodynamic brain responses to acute pain in humans: sensory and attentional networks. Brain 122 (Pt 9):1765-1780.

Ploghaus A, Tracey I, Gati JS, Clare S, Menon RS, Matthews PM, Rawlins JN (1999) Dissociating pain from its anticipation in the human brain. Science (New York, NY 284:1979-1981.

Ploner M, Schmitz F, Freund HJ, Schnitzler A (1999) Parallel activation of primary and secondary somatosensory cortices in human pain processing. J Neurophysiol 81:3100-3104.

Polania R, Nitsche MA, Paulus W (2010) Modulating functional connectivity patterns and topological functional organization of the human brain with transcranial direct current stimulation. Hum Brain Mapp.

Polania R, Paulus W, Antal A, Nitsche MA (2011) Introducing graph theory to track for neuroplastic alterations in the resting human brain: a transcranial direct current stimulation study. Neuroimage 54:2287-2296.

Poreisz C, Boros K, Antal A, Paulus W (2007) Safety aspects of transcranial direct current stimulation concerning healthy subjects and patients. Brain Res Bull 72:208-214.

Porro CA, Baraldi P, Pagnoni G, Serafini M, Facchin P, Maieron M, Nichelli P (2002) Does anticipation of pain affect cortical nociceptive systems? J Neurosci 22:3206-3214.

Price DD (2000) Psychological and neural mechanisms of the affective dimension of pain. Science 288:1769-1772.

Priori A, Hallett M, Rothwell JC (2009) Repetitive transcranial magnetic stimulation or transcranial direct current stimulation? Brain Simulation 2:241-245.

Priori A, Berardelli A, Rona S, Accornero N, Manfredi M (1998) Polarization of the human motor cortex through the scalp. Neuroreport 9:2257-2260.

Rainville P, Duncan GH, Price DD, Carrier B, Bushnell MC (1997) Pain affect encoded in human anterior cingulate but not somatosensory cortex. Science 277:968-971.

Raskin J, Pritchett YL, Wang F, D'Souza DN, Waninger AL, Iyengar S, Wernicke JF (2005) A double-blind, randomized multicenter trial comparing duloxetine with placebo in the management of diabetic peripheral neuropathic pain. Pain Med 6:346-356.

Rennefeld C, Wiech K, Schoell ED, Lorenz J, Bingel U (2010) Habituation to pain: further support for a central component. Pain 148:503-508.

Rodriguez-Raecke R, Niemeier A, Ihle K, Ruether W, May A (2009) Brain gray matter decrease in chronic pain is the consequence and not the cause of pain. J Neurosci 29:13746-13750.

Rowbotham MC, Davies PS, Fields HL (1995) Topical lidocaine gel relieves postherpetic neuralgia. Ann Neurol 37:246-253.

Rueckert D, Sonoda LI, Hayes C, Hill DL, Leach MO, Hawkes DJ (1999) Nonrigid registration using free-form deformations: application to breast MR images. IEEE Trans Med Imaging 18:712-721.

Ruff CC, Blankenburg F, Bjoertomt O, Bestmann S, Freeman E, Haynes JD, Rees G, Josephs O, Deichmann R, Driver J (2006) Concurrent TMS-fMRI and psychophysics reveal frontal influences on human retinotopic visual cortex. Curr Biol 16:1479-1488.

Ruscheweyh R, Stumpenhorst F, Knecht S, Marziniak M (2010) Comparison of the cold pressor test and contact thermode-delivered cold stimuli for the assessment of cold pain sensitivity. J Pain 11:728-736.

Sadleir RJ, Vannorsdall TD, Schretlen DJ, Gordon B (2010) Transcranial direct current stimulation (tDCS) in a realistic head model. NeuroImage 51:1310-1318.

Sampson SM, Rome JD, Rummans TA (2006) Slow-frequency rTMS reduces fibromyalgia pain. Pain medicine (Malden, Mass 7:115-118.

Sardashti M, Schwartzberg DG, Stomp GP, Dixon WT (1990) Spin-labeling angiography of the carotids by presaturation and simplified adiabatic inversion. Magn Reson Med 15:192-200.

Schmelz M, Schmid R, Handwerker HO, Torebjork HE (2000) Encoding of burning pain from capsaicin-treated human skin in two categories of unmyelinated nerve fibres. Brain 123 Pt 3:560-571.

Selemon LD, Goldman-Rakic PS (1988) Common cortical and subcortical targets of the dorsolateral prefrontal and posterior parietal cortices in the rhesus monkey: evidence for a distributed neural network subserving spatially guided behavior. J Neurosci 8:4049-4068.

Seminowicz DA, Mikulis DJ, Davis KD (2004) Cognitive modulation of pain-related brain responses depends on behavioral strategy. Pain 112:48-58.

Seminowicz DA, Wideman TH, Naso L, Hatami-Khoroushahi Z, Fallatah S, Ware MA, Jarzem P, Bushnell MC, Shir Y, Ouellet JA, Stone LS (2011) Effective treatment of chronic low back pain in humans reverses abnormal brain anatomy and function. J Neurosci 31:7540-7550.

Silva AC, Zhang W, Williams DS, Koretsky AP (1995) Multi-slice MRI of rat brain perfusion during amphetamine stimulation using arterial spin labeling. Magn Reson Med 33:209-214.

Sindrup SH, Gram LF, Brosen K, Eshoj O, Mogensen EF (1990) The selective serotonin reuptake inhibitor paroxetine is effective in the treatment of diabetic neuropathy symptoms. Pain 42:135-144.

Singer JR, Crooks LE (1983) Nuclear magnetic resonance blood flow measurements in the human brain. Science 221:654-656.

Smith SM (2002) Fast robust automated brain extraction. Hum Brain Mapp 17:143-155.

Smith SM, Nichols TE (2009) Threshold-free cluster enhancement: addressing problems of smoothing, threshold dependence and localisation in cluster inference. Neuroimage 44:83-98.

Smith SM, Jenkinson M, Johansen-Berg H, Rueckert D, Nichols TE, Mackay CE, Watkins KE, Ciccarelli O, Cader MZ, Matthews PM, Behrens TE (2006) Tract-based spatial statistics: voxelwise analysis of multi-subject diffusion data. Neuroimage 31:1487-1505.

Smith SM, Jenkinson M, Woolrich MW, Beckmann CF, Behrens TE, Johansen-Berg H, Bannister PR, De Luca M, Drobnjak I, Flitney DE, Niazy RK, Saunders J, Vickers J, Zhang Y, De Stefano N, Brady JM, Matthews PM (2004) Advances in functional and structural MR image analysis and implementation as FSL. Neuroimage 23 Suppl 1:S208-219.

Soler MD, Kumru H, Pelayo R, Vidal J, Tormos JM, Fregni F, Navarro X, Pascual-Leone A (2010) Effectiveness of transcranial direct current stimulation and visual illusion on neuropathic pain in spinal cord injury. Brain 133:2565-2577.

Speer AM, Kimbrell TA, Wassermann EM, J DR, Willis MW, Herscovitch P, Post RM (2000) Opposite effects of high and low frequency rTMS on regional brain activity in depressed patients. Biol Psychiatry 48:1133-1141.

Speer AM, Benson BE, Kimbrell TK, Wassermann EM, Willis MW, Herscovitch P, Post RM (2009) Opposite effects of high and low frequency rTMS on mood in depressed patients: relationship to baseline cerebral activity on PET. J Affect Disord 115:386-394.

Staahl C, Drewes AM (2004) Experimental human pain models: a review of standardised methods for preclinical testing of analgesics. Basic Clin Pharmacol Toxicol 95:97-111.

Stagg CJ, Nitsche MA (2011) Physiological basis of transcranial direct current stimulation. Neuroscientist 17:37-53.

Stagg CJ, O'Shea J, Kincses ZT, Woolrich M, Matthews PM, Johansen-Berg H (2009a) Modulation of movement-associated cortical activation by transcranial direct current stimulation. The European journal of neuroscience 30:1412-1423.

Stagg CJ, Best JG, Stephenson MC, O'Shea J, Wylezinska M, Kincses ZT, Morris PG, Matthews PM, Johansen-Berg H (2009b) Polarity-sensitive modulation of cortical neurotransmitters by transcranial stimulation. J Neurosci 29:5202-5206.

Steeds CE (2009) The anatomy and physiology of pain. Surgery 27:507-511.

Stucky CL, Gold MS, Zhang X (2001) Mechanisms of pain. Proc Natl Acad Sci U S A 98:11845-11846.

Sundgren PC, Petrou M, Harris RE, Fan X, Foerster B, Mehrotra N, Sen A, Clauw DJ, Welsh RC (2007) Diffusion-weighted and diffusion tensor imaging in fibromyalgia patients: a prospective study of whole brain diffusivity, apparent

diffusion coefficient, and fraction anisotropy in different regions of the brain and correlation with symptom severity. Acad Radiol 14:839-846.

Svendsen KB, Jensen TS, Bach FW (2004) Does the cannabinoid dronabinol reduce central pain in multiple sclerosis? Randomised double blind placebo controlled crossover trial. BMJ 329:253.

Takada M, Nambu A, Hatanaka N, Tachibana Y, Miyachi S, Taira M, Inase M (2004) Organization of prefrontal outflow toward frontal motor-related areas in macaque monkeys. Eur J Neurosci 19:3328-3342.

Takahashi E, Ohki K, Kim DS (2007) Diffusion tensor studies dissociated two fronto-temporal pathways in the human memory system. NeuroImage 34:827-838.

Talbot JD, Marrett S, Evans AC, Meyer E, Bushnell MC, Duncan GH (1991) Multiple representations of pain in human cerebral cortex. Science 251:1355-1358.

Taylor CP (2004) The biology and pharmacology of calcium channel alpha2-delta proteins. CNS Drug Rev 10:183-188.

Tekin S, Cummings JL (2002) Frontal-subcortical neuronal circuits and clinical neuropsychiatry: an update. J Psychosom Res 53:647-654.

Terney D, Bergmann I, Poreisz C, Chaieb L, Boros K, Nitsche MA, Paulus W, Antal A (2008) Pergolide increases the efficacy of cathodal direct current stimulation to reduce the amplitude of laser-evoked potentials in humans. J Pain Symptom Manage 36:79-91.

Torres L, Dunlop DD, Peterfy C, Guermazi A, Prasad P, Hayes KW, Song J, Cahue S, Chang A, Marshall M, Sharma L (2006) The relationship between specific tissue lesions and pain severity in persons with knee osteoarthritis. Osteoarthritis Cartilage 14:1033-1040.

Tracey I (2010) Getting the pain you expect: mechanisms of placebo, nocebo and reappraisal effects in humans. Nat Med 16:1277-1283.

Tracey I, Mantyh PW (2007) The cerebral signature for pain perception and its modulation. Neuron 55:377-391.

Tracey I, Becerra L, Chang I, Breiter H, Jenkins L, Borsook D, Gonzalez RG (2000) Noxious hot and cold stimulation produce common patterns of brain activation in humans: a functional magnetic resonance imaging study. Neuroscience letters 288:159-162.

Tracey I, Ploghaus A, Gati JS, Clare S, Smith S, Menon RS, Matthews PM (2002) Imaging attentional modulation of pain in the periaqueductal gray in humans. J Neurosci 22:2748-2752.

Treede RD, Kenshalo DR, Gracely RH, Jones AK (1999) The cortical representation of pain. Pain 79:105-111.

Treede RD, Jensen TS, Campbell JN, Cruccu G, Dostrovsky JO, Griffin JW, Hansson P, Hughes R, Nurmikko T, Serra J (2008) Neuropathic pain: redefinition and a grading system for clinical and research purposes. Neurology 70:1630-1635.

Tsubokawa T, Katayama Y, Yamamoto T, Hirayama T, Koyama S (1993) Chronic motor cortex stimulation in patients with thalamic pain. J Neurosurg 78:393-401.

Valet M, Sprenger T, Boecker H, Willoch F, Rummeny E, Conrad B, Erhard P, Tolle TR (2004) Distraction modulates connectivity of the cingulo-frontal cortex and the midbrain during pain--an fMRI analysis. Pain 109:399-408.

van der Werf YD, Sanz-Arigita EJ, Menning S, van den Heuvel OA (2010) Modulating spontaneous brain activity using repetitive transcranial magnetic stimulation. BMC Neurosci 11:145.

Wachter D, Wrede A, Schulz-Schaeffer W, Taghizadeh-Waghefi A, Nitsche MA, Kutschenko A, Rohde V, Liebetanz D (2011) Transcranial direct current stimulation induces polarity-specific changes of cortical blood perfusion in the rat. Exp Neurol 227:322-327.

Wager TD, Scott DJ, Zubieta JK (2007) Placebo effects on human mu-opioid activity during pain. Proceedings of the National Academy of Sciences of the United States of America 104:11056-11061.

Wager TD, Rilling JK, Smith EE, Sokolik A, Casey KL, Davidson RJ, Kosslyn SM, Rose RM, Cohen JD (2004) Placebo-induced changes in FMRI in the anticipation and experience of pain. Science (New York, NY 303:1162-1167.

Wagner T, Fregni F, Fecteau S, Grodzinsky A, Zahn M, Pascual-Leone A (2007) Transcranial direct current stimulation: a computer-based human model study. Neuroimage 35:1113-1124.

Wang J, Aguirre GK, Kimberg DY, Roc AC, Li L, Detre JA (2003) Arterial spin labeling perfusion fMRI with very low task frequency. Magn Reson Med 49:796-802.

Wang Y, Shima K, Sawamura H, Tanji J (2001) Spatial distribution of cingulate cells projecting to the primary, supplementary, and pre-supplementary motor areas: a retrograde multiple labeling study in the macaque monkey. Neurosci Res 39:39-49.

Wang Y, Saykin AJ, Pfeuffer J, Lin C, Mosier KM, Shen L, Kim S, Hutchins GD (2011) Regional reproducibility of pulsed arterial spin labeling perfusion imaging at 3T. Neuroimage 54:1188-1195.

Watson A, El-Deredy W, Iannetti GD, Lloyd D, Tracey I, Vogt BA, Nadeau V, Jones AK (2009) Placebo conditioning and placebo analgesia modulate a common brain network during pain anticipation and perception. Pain 145:24-30.

Wiech K, Tracey I (2009) The influence of negative emotions on pain: behavioral effects and neural mechanisms. NeuroImage 47:987-994.

Wiech K, Ploner M, Tracey I (2008a) Neurocognitive aspects of pain perception. Trends in cognitive sciences 12:306-313.

Wiech K, Farias M, Kahane G, Shackel N, Tiede W, Tracey I (2008b) An fMRI study measuring analgesia enhanced by religion as a belief system. Pain 139:467-476.

Williams DS, Detre JA, Leigh JS, Koretsky AP (1992a) Magnetic resonance imaging of perfusion using spin inversion of arterial water. Proc Natl Acad Sci U S A 89:212-216.

Williams DS, Detre JA, Leigh JS, Koretsky AP (1992b) Magnetic resonance imaging of perfusion using spin inversion of arterial water. Proc Natl Acad Sci U S A 89:212-216.

Williams DS, Grandis DJ, Zhang W, Koretsky AP (1993) Magnetic resonance imaging of perfusion in the isolated rat heart using spin inversion of arterial water. Magn Reson Med 30:361-365.

Woolf CJ (2010) What is this thing called pain? J Clin Invest 120:3742-3744.

Woolf CJ, Salter MW (2000) Neuronal plasticity: increasing the gain in pain. Science (New York, NY 288:1765-1769.

Woolrich MW, Jbabdi S, Patenaude B, Chappell M, Makni S, Behrens T, Beckmann C, Jenkinson M, Smith SM (2009) Bayesian analysis of neuroimaging data in FSL. Neuroimage 45:S173-186.

Wu WC, Fernandez-Seara M, Detre JA, Wehrli FW, Wang J (2007) A theoretical and experimental investigation of the tagging efficiency of pseudocontinuous arterial spin labeling. Magn Reson Med 58:1020-1027.

Yao J, Qin F (2009) Interaction with phosphoinositides confers adaptation onto the TRPV1 pain receptor. PLoS Biol 7:e46.

Ye FQ, Berman KF, Ellmore T, Esposito G, van Horn JD, Yang Y, Duyn J, Smith AM, Frank JA, Weinberger DR, McLaughlin AC (2000) H(2)(15)O PET validation of steady-state arterial spin tagging cerebral blood flow measurements in humans. Magn Reson Med 44:450-456.

Zambreanu L, Wise RG, Brooks JC, Iannetti GD, Tracey I (2005) A role for the brainstem in central sensitisation in humans. Evidence from functional magnetic resonance imaging. Pain 114:397-407.

Zhang W, Silva AC, Williams DS, Koretsky AP (1995) NMR measurement of perfusion using arterial spin labeling without saturation of macromolecular spins. Magn Reson Med 33:370-376.

Zhang Y, Brady M, Smith S (2001) Segmentation of brain MR images through a hidden Markov random field model and the expectation-maximization algorithm. IEEE Trans Med Imaging 20:45-57.

Zheng X, Alsop DC, Schlaug G (2011) Effects of transcranial direct current stimulation (tDCS) on human regional cerebral blood flow. Neuroimage.

Zubieta JK, Bueller JA, Jackson LR, Scott DJ, Xu Y, Koeppe RA, Nichols TE, Stohler CS (2005) Placebo effects mediated by endogenous opioid activity on mu-opioid receptors. J Neurosci 25:7754-7762.